Doctoral Dissertation

Numerical Assessment of Land Derived Nutrients and Their Seasonal Circulation Patterns in Harima Nada

PINTOS ANDREOLI Valentina

December 2023

Division of Sustainable Energy and Environmental Engineering

Graduate School of Engineering, Osaka University

Supervisor:
Professor **KONDO Akira**
Engineering for Assessing the Sustainable Environment
Division of Sustainable Energy and Environmental Engineering

Assistant Supervisors:
Professor **TOKAI Akihiro**
Environmental Management
Division of Sustainable Eneregy and Environmental Engineering

Associated Professor **SHIMADERA Hikari**
Engineering for Assessing the Sustainable Environment
Division of Sustainable Energy and Environmental Engineering

Acknowledgments

I want to acknowledge my supervisor, Professor Akira KONDO, for receiving me in his laboratory when I applied as a MEXT student and give me the opportunity to study at Osaka University. Kondo Sensei, thank you for your kindness and supervision during the past six years. I also want to thank and acknowledge my co-supervisor, Associate Professor Hikari SHIMADERA, for his help, research guidance, contributions, and all the time dedicated to answering my questions and emails. Hikari, I hope the future gives us the chance to become friends. My special thanks to Professor Akihiro TOKAI for accepting to be an assistant supervisor for my defense and my thesis paper.

I would also like to thank Kondo Laboratory staff Hisae MARUOKA and Assistant Professor Tomohito MATSUO for their support during my time in Kondo Lab. Maru Chan, thank you for being infinitely helpful and kind since I arrived at the laboratory. A special thanks to all the students I have met during my time at Osaka University, particularly my kouhai Hiroto YASUGA. Yasu kun, thank you for trying hard with the English and for working hard when I needed it. My special thanks to Yutaro KOGA, Motoharu SUZUKI, and all the staff and people from the Hyogo Prefecture Environmental Research Center for the opportunity to work there during the past four and a half years. I learned many things and always had an amazing time when going there.

Finally, I want to thank my family and my friends. Mamá, papá y Flavia, gracias por estar siempre de mi lado sin importar las circunstancias y respetar mis decisiones. Mamá y papá, saben que tengo mucho más “que un montón de palabras y rimas” en las manos y es en gran parte gracias a ustedes. Flafi, gracias por aguantar todo lo que pasó sola; si no lo hubieses hecho,quizás yo no hubiese terminado. My dear friends, the ones here in Japan and the ones that are at distance, thank you for becoming part of my soul family, find me when I got lost, share the happiness and the horrors with me, tolerate me, and be protagonists of all my memories during these past six years.

Abstract

Using numerical simulations, this study aimed to promote the comprehension of rivers' nutrient transport and the circulation patterns of discharged freshwaters in coastal areas. Characterizing river watersheds and coastal regions is fundamental for maintaining, recovering, and balancing human activities with natural ecosystems. The Kako River accounts for 40% of the freshwater and inland nutrients in Harima Nada, so its influence in the region is of considerable importance for all the biogeochemical processes in the coastal and marine surrounding areas. The Harima Nada region was chosen for its sustained oligotrophication processes during the past 25 years, the strong influence of rivers' discharges, and its socioeconomic importance in western Japan. All the research background and introduction are detailed in Chapter 1.

Chapter 2 of this work developed a general methodology to quantify nonpoint sources of total nitrogen (TN) and total phosphorous (TP) in the Kako River watershed using an approach that combines simulation and empirical tools for estimating export coefficients. This methodology is simple to implement, reduces the amount of observed data needed, and can be extended to any other river watershed or river catchment area of similar characteristics with minimum modifications. A Hydro-Chemical Model was tuned and validated in the study area, and export coefficients for TN and TP nonpoint source estimation were estimated and validated in the Kako River watershed.

Chapter 3 involved the development of an atmospheric-marine model coupling the WRF and ROMS components of the COAWST Model System to study the Kako River's seasonal circulation patterns and mean residence times in the sea as the starting point for the future development of a high-resolution coastal biogeochemical model. Atmospheric and marine variables were validated in Harima Nada and at different points of WRF and ROMS domains, and seasonal circulation patterns were studied by tracer experiments in the region.

In Chapter 4, the export coefficients methodology from the 1st part was used to estimate freshwater discharge and TN loads from all the ten rivers that discharge in the Harima Nada area and the Yoshino River, which discharges next to the southern-east border

of Harima Nada next to the Naruto Strait. The obtained results are expected to be added as forcing fields to the atmospheric-marine model to be used in the future development of the biogeochemical model for the area.

Finally, conclusions are summarized in Chapter 5 being among the most important ones, that the export coefficients performance for nonpoint source estimation of total nitrogen were validated and verified for the Kako River TN and TP loads between April 2010 and March 2012 using a physically distributed hydrochemical-transport model with very good results and high performance in describing the observations. The developed coupled atmospheric-marine model performed well at the studied horizontal resolutions in simulating the characteristics of West Japan and the Seto Inland Sea. It was found that circulation patterns in Harima Nada do not seem to vary much with depth, but they showed significant seasonal differences. The river's water distribution and mean residence times were also found to be seasonally affected, and the results agreed with the biomass production and growth rates of Harima Nada waters. The findings for freshwater discharge and total TN loads discharged showed that the Kako River is the most important contributor of nutrients and freshwater in the region, followed by the rivers of the northern coast in the Hyogo Prefecture. Additionally, it was found that the Yoshino River can export as much TN and freshwater into the sea as all the rivers of Harima Nada combined. To date, many efforts and research have been conducted in the entire Seto Inland Sea and its marine basins and Nadas to help in reverting and assessing the environmental problems that affect it. Still, most approaches have not used a coupled model of the presented characteristics. This work sets an antecedent for developing a biogeochemical model for the Harima Nada and the surrounding areas using online 2-way coupled high-resolution models that can help assess how to revert the environmental problems of one of Japan's most important coastal regions.

Contents

List of Tables

List of Figures

List of abbreviations

AMeDAS	Automated Meteorological Data Acquisition System
CFL	Courant-Friedrichs-Lewy ratio
CO	Chemical observatory
COAWST	Coupled Ocean-Atmospheric-Wave-Sediment-Transport Model System
DEM	Digital elevation map
DIN	Dissolved inorganic nitrogen
DIP	Dissolved inorganic phosphorous
EC	Export coefficient
ECM	Export coefficients model
GIS	Geographic information system
HIES	Hyogo Institute of Environmental Sciences
HYCOM	Hybrid Coordinated Ocean Model
IA	Index of agreement
IRLS	Iterative reweighted least squares method
JMA	Japan Meteorolgical Agency
MAD	Mean absolute deviation
MLIT	Ministry of Land, Infrastructure, Transport and Tourism of Japan
MLR	Multiple linear regression
MOEJ	Ministry of Environment of Japan
MSE	Mean square error
NSE	Nash-Sutcliffe efficiency
OLS	Ordinary least square regression

pBIAS	Percentage of bias
PS	Point source
R	Correlation coefficient
R^2	Coefficient of determination
RMSE	Root mean square error
ROMS	Regional Ocean Modeling System
RSR	RMSE – observed standard deviation ratio
SSH	Sea surface height
TN	Total nitrogen
TP	Total phosphorous
u-wind	Zonal wind component
v-wind	Meridional wind component
WRF	Weather Research and Forecasting Model

Research Achievements

Refereed Papers

Seasonal study of the Kako River discharge dynamics into Harima Nada using a coupled atmospheric-marine model, Pintos Andreoli, V., Shimadera, H., Yasuga, H., Koga, Y., Suzuki, M., Kondo, A.; *Water – Special Issue: Hydrodynamics in Coastal Areas;* submitted 2023 October 30th, currently under revised review

Inverse estimation of nonpoint source export coefficients for total nitrogen and total phosphorous in the Kako River basin; Pintos Andreoli, V., Shimadera H., Koga Y., Mori M., Suzuki M., Matsuo T., Kondo A.; *Journal of Hydrology*, 620-A, May 2023 (Early access 2023/04/23). https://doi.org/10.1016/j.jhydrol.2023.129395

Analysis of nitrogen and phosphorous load dynamics in Kako and Ibo river basins during flood events; Koga Y., Suzuki M., Pintos V.; *Journal of Japan Society of Hydrology and Water Resources*, 35-1, 32-40, 2022. (in Japanese, with English abstract) https://doi.org/10.3178/jjshwr.35.32

Numerical Assessment of Total Nitrogen (TN) Load Discharged from Rivers into Harima-Nada, the Seto Inland Sea, Using a Numerical Coupled Hydrological-Water Quality Model; Pintos Andreoli V., Mori M., Koga Y., Shimadera H., Suzuki M., Matsuo T., Kondo A.; *IOP Conference Series: Earth and Environmental Science*, 801, 012009, 2021. DOI: 10.1088/1755-1315/801/1/01200

Academic Conferences

Inverse estimation of nonpoint source export coefficients in the Kako River basin; September 03 – 06 2023; Dejima Messe, Nagasaki Prefecture; ***Japanese Society of Hydrogy and water/Japan Hydrological society – Annual meeting 2023*** (oral presentation, in English)

Numerical Assessment of Total Nitrogen (Tn) Load Discharged from Rivers into Harima-Nada, the Seto Inland Sea, Using A Numerical Coupled Hydrological - Water

Quality Model, (International conference) January 29-30, 2021 (virtual), ***11th International Conference on Future Environment and Energy*** (oral presentation, in English)

Estimation of Total Nitrogen Load Discharges from Rivers on Harimanada, Seto Inland Sea, March 16-18, 2020 (held in the journal), ***54th Japan Water Environment Annual meeting***, 3-A-10-4 (in English)

Chapter 1 - Introduction

1.1 Research background

1.1.1 General considerations on water pollution

The management of water resources has been historically one of the biggest problems in the history of humans. Water is necessary for the survival of all the species in the Animal and Plantae Kingdoms. It is also a source of uncountable resources and the inhabitant of extremely rich ecosystems. The deterioration of water resources and their ecosystems has anthropogenic causes (Vitousek et al., 1997), the reason why efficiently managing water resources, as well as solving water pollution issues, is one of the biggest challenges of modern societies (Arenas-Sánchez et al., 2016).

Freshwater represents less than 3% of the total water resources of the planet, and its accessibility is considerably restricted for humans. The ice of the polar regions and the glaciers, plus the underground aquifers, account for almost 99% of the planet's freshwater resources (Fig. 1). Because of this, surface waters availability and their security are essential for human life and the development of our societies. However, water is not only used for direct consumption; most human socio-economic activities are directly linked with it, from agriculture to manufacturing industries. On the other hand, seas and oceans are not only the home of extremely rich ecosystems but also a source of food and many other natural resources.

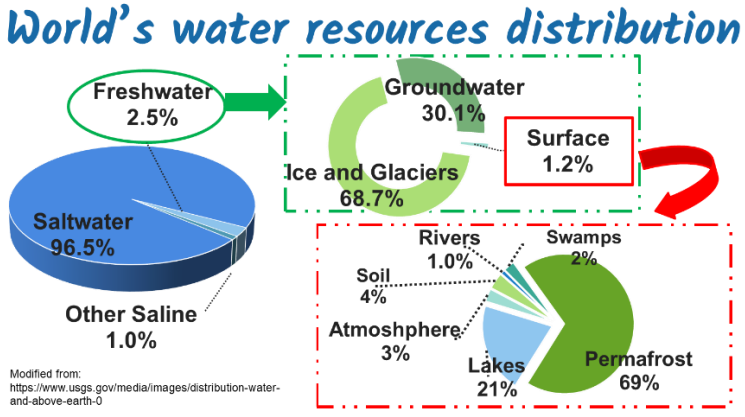

Fig. 1- Distribution of natural water resources in the World

The water reservoirs usually more affected by environmental and pollution problems are the superficial reservoirs (lakes, rivers), the shallow groundwater aquifers, and the estuaries and coastal areas, like harbors and ports. Depending on the extent of the pollution problems, they can provoke severe consequences in human health, the detriment of the biodiversity of a region, or the destruction of the natural ecosystems affected.

One of the most common and extensively used classifications for water pollutants (Moeller et al., 1980) is in:

- Toxic and harmful: all those substances that can harm humans and animals by causing disease or physical damage, like most of the heavy metals and carcinogenic organic substances.
- Indirectly harmful: they are non-poisonous substances that make water unpleasant to use or destroy ecosystems' "beauty", as sediments from industries or speeded up by human activities, oil spilled in accidents, high salt concentrations, etc.
- Oxygen depleting: substances that demand oxygen from the water and promote the anaerobic decay of organic matter and the death of living organisms; in this category are all the substances that are also major nutrients in terrestrial and aquatic ecosystems.

The first type is easy to identify because toxic substances can be easily tracked and are not a natural constituent of ecosystems, directly linking them to industrial activities. The second type is less easy to target since human activities can indirectly provoke it, but it is less potentially harmful and easy to revert in the short or mid-term. The third type of pollutant is the most challenging type to address, and its importance is from medium to high in superficial waters. Major nutrients like nitrogen or phosphorous are critical for maintaining ecosystems and are common constituents of agricultural fertilizers, sewage waters, and industrial waters, but their unbalance in natural waters has the potential to provoke severe environmental problems like eutrophication or oligotrophication processes (Conley et al., 2009; Fuhrer et al., 1999).

Water pollution can also be classified from the source of pollutant into:

- Point source (PS) pollution
- Nonpoint source pollution

The first one was defined by Carpenter et al. (1998) as the type of pollution that can be easily tracked because its characteristics make it easy to identify and quantify (e.g., toxic and harmful substances). On the contrary, nonpoint source pollution is a diffuse type of pollution, impossible to particularly identify, driven by human activities and changes in land use (Novotny, 2003). Pollution driven by indirectly harmful pollutants and most oxygen-depleting substances (e.g., sediments, nutrients) is considered mostly nonpoint source pollution.

Because nonpoint source pollution is difficult to estimate, many strategies have been developed to help with its determination. Watershed modeling is one of the most used tools for assessing environmental issues and solving water environmental problems, including the transport of pollutants and their estimation. Export coefficients are numerical relations to quantify the amount of pollutant (in concentration or load) that a particular land use can "export" per unit of extension and time to a water body by runoff mechanisms, which makes them the core of many numerical models for nonpoint source estimation of pollutants at the basin or catchment area level. Johnes (1996) proposed and tested the effectivity of the Export Coefficient Model (ECM) under the idea that nutrient loads are the sum of individual sources in a basin, an idea extended later as a part of more complex hydrological and physical models. The usage of export coefficients has many limitations, most closely related to their determination and the extent of their validity, which is why much effort has been put into improving their estimation in the past decades.

Because water supply is vital for human life and economic development, governments usually put big efforts into developing combined management strategies for conserving and restoring water resources and securing freshwater supplies. Among the multiple tools that governments and contemporary societies use for "handling" the water pollution problems are: the control of the socio-economic activities in an area, the development of strict laws and environmental policies, the design and construction of

monitoring networks, the development of restoration plans for affected areas, and the education of their inhabitants. Still, identifying pollution sources is usually not a simple task, and the weight or the extent to which these tools can be effectively applied depends not only on how severe the environmental problems are but also on the economic development and resources of a country or region. This makes finding solutions to address water pollution environmental issues not general and difficult in most cases since the problems can be very similar, but the solutions are necessary, local, and particular.

1.1.2 The Seto Inland Sea and the Harima Nada region

The Seto Inland Sea is the biggest and most important of all the enclosed seas of Japan. With an area of approximately 22.200 km^2, 30% of the Japanese population living in its surrounding and coastal regions, and 1/3 of Japanese manufacturing industries, it is one of Japan's most environmentally affected regions(Yanagi, 2015). It is located in west Japan and connects with the Sea of Japan on the northern west side by the Kanmon Strait and with the Pacific Ocean by the Bungo Channel on the southern west side and the Kii Channel in the southeast. It allocates over 700 islands, straits, and basins/nadas of all sizes on its waters (Yanagi, 2015).

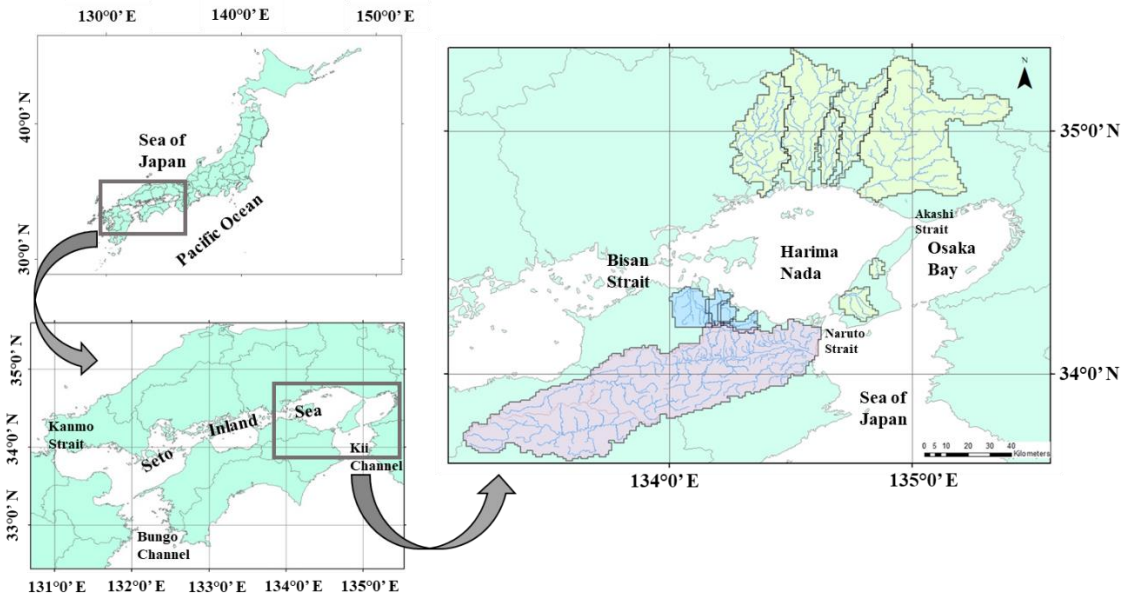

Fig. 2 - Geographic location of the study area

The Seto Inland Sea is a shallow sea with an average depth of 40 to 45 meters, except for the channels that connect it with the Pacific Ocean. Because of its enclosed geography and mountainous shoreline, the area has special climatological conditions responsible for a high and rich biodiversity. In addition, numerous rivers that transport essential nutrients from the inland to the sea surround its coasts and are responsible for the historically high productivity per unit of area of fishery products and seaweed. However, this situation has been changing during the past three decades due to the environmental issues the region has faced since the late ‘60s when the Japanese economy rapidly grew and reconverted.

The rapid development of numerous and large industrial areas in the region, plus the reclamation and sand mining activities that occurred during the ‘70s, rapidly contributed to the deterioration and destruction of many ecosystems all around the Seto Inland Sea (Abo et al., 2018; Yanagi, 2015). During that period, the lack of strong environmental policies and controls for wastewater discharges or sediments disposition into the rivers and the sea promoted the rapid deterioration of the region’s environmental conditions. Between the end of 1960 and 1990, eutrophication problems were the most significant environmental issue in the Seto Inland Sea, with a continued increase of nutrients and organic matter in the waters that led to an excessive enrichment of the existent ecosystems. The number of individuals in the ecosystems considerably grew, benefiting fishery and seaweed production during this period until the peak of production was reached in 1980 (Fig. 3) (Abo & Yamamoto, 2019; Yanagi, 2015).

With the uncontrolled increase of nutrients, red tide problems started becoming more common and severe around the region, particularly in places where the population was considerably large, like Osaka Bay, Hiroshima Bay, Fukuoka coasts, etc. This caused the establishment and development of some special laws from 1973, that derived in the year 1979 in the Law Concerning Special Measures for Conservation of the Environmental of the Seto Inland Sea, a general law that intended to regulate the nutrients discharge in the region (Abo & Yamamoto, 2019; Yanagi, 2015). However, the implementation of the law was not enough to revert the damage to the ecosystems and their imbalance, and the concentration of nutrients became inhibitory for many species of algae and phytoplankton during the following years.

Those species with a better adaptability to high nutrients concentration became predominant, and their uncontrolled growth was responsible for continuous red tide events, hypoxia conditions in many areas, and the aggravation of the biodiversity loss between the '80s and '90s. The severe environmental problems led to the reinforcement of environmental policies and existent laws to remediate the situation. Since the mid-'90s and due to the reasons above, the concentration of nutrients and organic matter started decreasing in a sustained manner in the entire Seto Inland Sea.

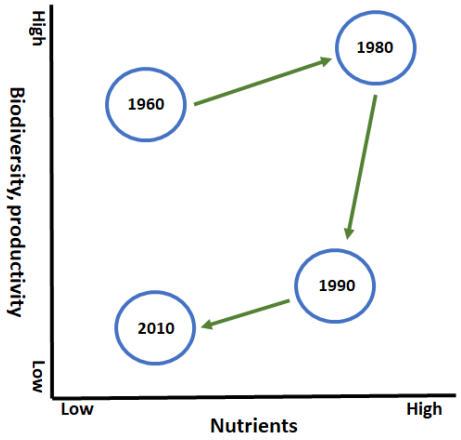

Fig. 3 – History of Eutrophication and oligotrophication in the Seto Inland Sea

In the past three decades, many areas were restored with the reduction of nutrients discharge, but others started suffering from oligotrophication problems. With oligotrophication, a new change in the algae and phytoplankton populations occurred, which affected fishery, seaweed production, and other related socio-economic activities (Abo et al., 2018; Yanagi & Tanaka, 2013). The oligotrophication processes occurred in many areas of the Seto Inland Sea at a different extent, but the most problematic areas were identified in the south of Osaka Bay and Harima Nada, where the sustained decrement of dissolved inorganic nitrogen (DIN) per year reached values of 0.2 µM from the late'90s to nowadays (Abo & Yamamoto, 2019; Yanagi, 2015).

Harima Nada is located on the eastern side of the Seto Inland Sea. Its limits are the Bisan Strait in the west, Osaka Bay in the east on the Akashi Strait, and the Kii channel on the southern east side on the Naruto Strait (Fig. 1). The northern and eastern shorelines belong

to the Hyogo Prefecture and are densely populated and industrialized due to its proximity to Osaka, the 2nd biggest city in Japan. On the other hand, the southern shoreline corresponds with the northeast part of Shikoku Island, where the Kagawa and Tokushima Prefectures are located. This area is less populated and industrialized, and the main activities are related to the primary sector.

The enclosed geography of the region, a shallow bathymetry (average of 30 m), and eleven rivers of different watershed and streamflow sizes directly discharging on its waters are responsible for some unique characteristics in Harima Nada. Rivers are the link between inland activities and the sea by transporting pollutants, nutrients, and sediments in their waters, and the larger they are, the more important their influence is. All the biogeochemical processes of the area are dependent on rivers' water and nutrients load distribution, and are strongly linked with the water circulation patterns in Harima Nada (Abo & Yamamoto, 2019; Yanagi, 2015), the reason why its understanding is essential to assess on solutions for the environmental issues of the region.

The most important among all the rivers that discharge into Harima Nada is the KaKo River, located in the center of the northern coast in Hyogo Prefecture. The Kako River, with approximately 1730 km^2 of catchment area, is one of the largest rivers of western Japan. It is the most important contributor of freshwater and land-derived nutrients to the region (Harada & Tanda, 2011; Yoshida et al., 2010), particularly during spring and summer (March to September) when the rainy and typhoon seasons occur in Japan. The Kako River is the representative river of Harima Nada, and this work aimed to help describe and clarify its watershed and discharge dynamics.

For those above, the region's waters have historically been a source of seafood and seaweed production due to their high productivity, with fish farming and nori cultivation the oldest and most important activities. Since the mid-'90s, the situation started shifting, and a continuous decrease in fish catchment has affected the region and its productivity (Fig. 4-a). Additionally, many seaweed farms have seen their production affected by discoloration problems. As a result, much research has been conducted by prefectural and the Japanese

National Government to elucidate which phenomena or processes are affecting the Harima Nada waters. Most of those research findings pointed at the decrement of DIN in the region and changes in the ratio DIN – dissolved inorganic phosphorous (DIP), as well as changes in the ratio total nitrogen (TN) – total phosphorous (TP), as the main causes for the present situation (Abo et al., 2018; Abo & Yamamoto, 2019; Naito et al., 2011; Nishikawa et al., 2010, 2011; Yanagi, 2015).

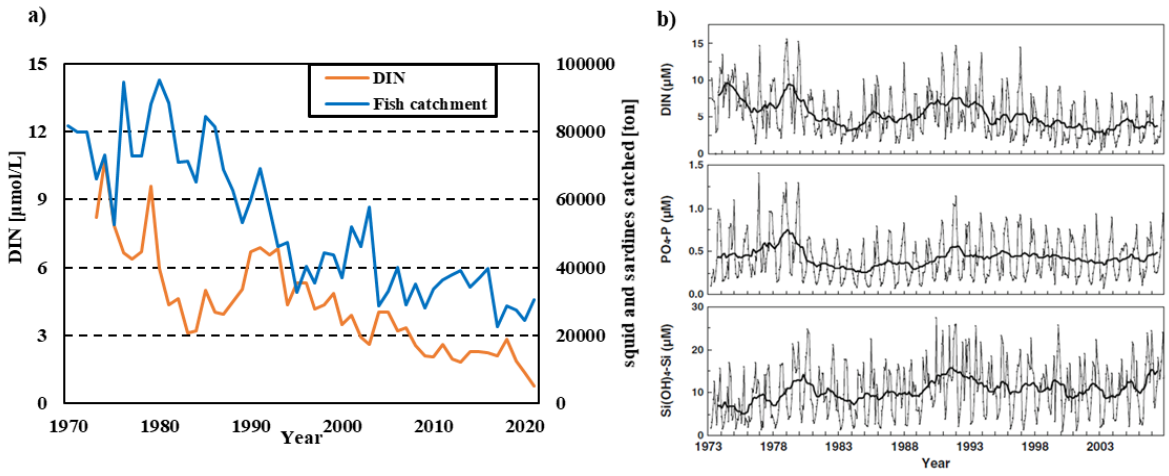

Fig. 4 - Historical DIN concentration and fish catchment tons in Harima Nada waters (a) and evolution of DIN, phosphorous (PO_4 - P), and silicic acid ($Si(OH)_4$ - Si) concentrations and their averages in Harima Nada (b, from Nishikawa et al., 2010)

Fig. 4 – b shows the time series evolution of DIN, phosphorous (PO_4-P), and silicic acid ($Si(OH)_4$ – Si) in Harima Nada. DIN concentration reached its peak during the years that promoted the severe oligotrophication of the entire Seto Inland Sea (‘70s and ‘80s), stabilized during the ‘90s, and started decreasing since the reinforcement of environmental policies and controls from the year 2000 (Fig 1 - a and 1- b). Phosphorous concentration did not vary considerably after remediation measures were taken, which shows that it is not the cause of the oligotrophication problems since its availability is not limiting biomass production. On the other hand, silicic acid concentrations have grown in the past decades. The changes in the silicic acid concentration and its more recent accumulation were studied by Nishikawa et al. (2010) and attributed to changes in the silicon cycle in Harima Nada. Changes in phytoplankton species of the area and the reduction of biomass production due to episodes of limiting nitrogen availability have caused the accumulation of silicic acid that goes out of

the ecosystem cycles and accumulates in the water as another sign of oligotrophication problems and loss of biodiversity (Naito et al., 2011; Nishikawa et al., 2010, 2011).

1.2 Research objectives

The main objective of this work is to help with the numerical assessment of land-derived nutrients from the inland into the sea and the clarification of the seasonal dynamics of the Kako River discharge in Harima Nada as the 1st step in the development of a high-resolution biogeochemical model for the region.

To achieve the main objective, this research was divided into the following three secondary goals:

1) The development of a methodology to improve export coefficients determination and nonpoint source estimation of nutrients at the river basin level in the Kako River, the most representative river of the Harima Nada and one of the most important rivers of western Japan.
2) The development, configuration, and validation of a coupled atmospheric-marine model and the study of the Kako River dynamics to help determine biogeochemical parameters and processes as the 1st antecedent for a future high-resolution biogeochemical model for the study area.
3) The estimation of the TN and TP loads from all the rivers of the study region by extending the methodology applied to the Kako River to quantify freshwater and inland nutrient loads into the sea.

1.3 Research extent

This research aims to help clarify the processes that led to oligotrophication problems affecting the Harima Nada region and many other recovered/remediated coastal areas in Japan and worldwide using numerical tools.

To accomplish the three main objectives, first, an improvement on one of the general methodologies for nonpoint source nutrient estimation was developed and validated in one of the most important rivers of West-Japan to enhance land-derived nutrients estimation at

the river basin level. For doing so, a river watershed physically-distributed hydrological model was coupled with a chemical transport model, tuned and validated for nutrient loads and streamflow in the Kako River, and its results were used in combination with observed data to estimate nutrients general export coefficients.

Secondly, a coupled atmospheric-marine model was proposed and validated to allow the reproduction of the study area conditions. This sets a precedent for the Harima Nada area, where most of the developed numerical models use offline atmospheric assimilated data. The coupled approach improves the quality of the results by avoiding some of the scaling problems that assimilated datasets have for small areas, giving the proposed model a better definition and more realistic significance. The obtained results in the 1st part for the Kako River were forced in the atmospheric-marine model, and the circulation patterns of the river's waters and nutrients distribution were seasonally studied and analyzed for the study region.

Lastly, the developed methodology for estimating riverine nutrient loads was extended to all the rivers that discharge in the Harima Nada region to calculate the total nutrient loads and the discharged freshwater in the sea. The results confirmed the importance of the Kako River in Harima Nada, and can be used to complete the rivers' water circulation and nutrients study in the region, and unfinished task in this work due to the lack of time.

Numerical simulations have the advantage of helping and assessing the characterization of river watersheds and coastal regions at a relatively fast and "low" cost. Understanding coastal dynamics is fundamental for maintaining, recovering, and balancing human activities with natural ecosystems. To date, many efforts and research have been conducted in the entire Seto Inland Sea and its marine basins and Nadas to help in reverting and assessing the environmental problems that affect it. This work aimed to cover the first steps in developing a biogeochemical model for the Harima Nada and the surrounding areas that can help assess how to reduce the environmental problems of one of Japan's most important coastal regions.

References – Chapter 1

Abo, K., Satoshi, A., Kazuhiro, H., Yoshiki, N., Hayashi, H., Murata, K., Wanishi, A., Ishikawa, Y., Masui, T., Nishikawa, S., Yamada, K., Noda, M., & Tokumitsu, S. (2018). Long-Term Variations in Water Quality and Causal Factors in the Seto Inland Sea , Japan. *Bulletin on Coastal Oceanography (in Japanese, English Abs.)*, *55*(2), 2101–2111.

Abo, K., & Yamamoto, T. (2019). Oligotrophication and its measures in the Seto Inland Sea , Japan. *Bulletin of Japan Fisheries Research and Education Agency*, *49*, 1–6. http://www.fra.affrc.go.jp/bulletin/bull/bull49/49-0504.pdf

Arenas-Sánchez, A., Rico, A., & Vighi, M. (2016). Effects of water scarcity and chemical pollution in aquatic ecosystems: State of the art. *Science of the Total Environment*, *572*, 390–403. https://doi.org/10.1016/j.scitotenv.2016.07.211

Carpenter, S. R., Caraco, N. F., Correll, D. L., Howarth, R. W., Sharpley, A. N., & Smith, V. H. (1998). NONPOINT POLLUTION OF SURFACE WATERS WITH PHOSPHORUS AND NITROGEN. In *Ecological Applications* (Vol. 8, Issue 3).

Conley, D. J., Paerl, H. W., Howarth, R. W., Boesch, D. F., Seitzinger, S. P., Havens, K. E., Lancelot, C., & Likens, G. E. (2009). Ecology - Controlling eutrophication: Nitrogen and phosphorus. *Science*, *323*(5917), 1014–1015. https://doi.org/10.1126/science.1167755

Fuhrer, G. J., Gilliom, R. J., Hamilton, P. A., Morace, J. L., Nowell, L. H., Rinella, J. F., Stoner, J. D., & Wentz, D. A. (1999). *The quality of Our Nation's Waters : Nutrients and Pesticides - U.S. Geological Survey*, *Circular 1225*. U.S. Department of the Interior. https://doi.org/10.3133/cir1225

Harada, K., & Tanda, M. (2011). Influence of the changes of the load inflow total nitrogen (TN) from rivers of Harima area in Hyogo Prefecture to the dissolved inorganic nitrogen (DIN) in Harima-nada. *Bull. Hyogo Pref, Tech. Cent Agr. Forest. Fish. (Fish. Sec) (in Japanese)*, *42*, 87–91.

Johnes, P.J. (1996). Hydrology Evaluation and management of the impact of land use change on the nitrogen and phosphorus load delivered to surface waters: the export coefficient modelling approach. *Journal of Hydrology 183*, 323–349. https://doi.org/https://doi.org/10.1016/0022-1694(95)02951-6

Moeller, T., Bailar, J. C., Kleinberg, J., Guss, C. O., Castellion, M. E., & Metz, C. (1980). *13- WATER AND THE HYDROSPHERE, Chemistry With Inorganic Qualitative Analysis*. https://doi.org/https://doi.org/10.1016/B978-0-12-503350-3.50018-4

Naito, K., Tanabe, A., Itakura, S., Yamaguchi, M., & Imai, I. (2011). Evaluation of major nutrients regulating the growth of diatoms in Harima-Nada, the Seto Inland Sea, Japan. *Bulletin of Fisheries Sciences, Hokkaido University*, *61*(1), 5–12.

Nishikawa, T., Hori, Y., Nagai, S., Miyahara, K., Nakamura, Y., Harada, K., Tada, K., & Imai, I. (2011). Long time-series observations in population dynamics of the harmful diatom Eucampia zodiacus and environmental factors in Harima-Nada, eastern Seto inland Sea, Japan during 1974-2008. *Plankton and Benthos Research*, *6*(1), 26–34. https://doi.org/10.3800/pbr.6.26

Nishikawa, T., Hori, Y., Nagai, S., Miyahara, K., Nakamura, Y., Harada, K., Tanda, M., Manabe, T., & Tada, K. (2010). Nutrient and phytoplankton dynamics in Harima-Nada, eastern Seto Inland Sea, Japan during a 35-year period from 1973 to 2007. *Estuaries and Coasts*, *33*(2), 417–427. https://doi.org/10.1007/s12237-009-9198-0

Novotny, V. (2003). *Water Quality Diffuse Pollution and Watershed Management* (2nd Edition). John Wiley & Sons.

Vitousek, P. M., Mooney, H. A., Lubchenco, J., & Melillo, J. M. (1997). Human domination of Earth's ecosystems. *Science*, *277*(5325), 494–499. https://doi.org/10.1126/science.277.5325.494

Yanagi, T. (2015). Oligotrophication in the Seto Inland Sea. In *Eutrophication and Oligotrophication in Japanese Estuaries – The present status and future tasks* (pp. 39–67). Springer Netherlands.

Yanagi, T., & Tanaka, T. (2013). Origins of Phosphorus and Nitrogen in the Seto Inland Sea, Japan. *Reports of Research Insitute for Applied Mechanics, Kyushu University*, *144*, 13–18.

Yoshida, M., Nakagawa, N., & Umemoto, S. (2010). *Variation of nutrient salt concentration in rivers water flowing into Osaka Bay and Harima-Nada (in Japanese)*. http://www.eco-hyogo.jp/files/1813/8182/2580/notes201203.pdf

Chapter 2 - Inverse estimation of nonpoint source export coefficients for total nitrogen and total phosphorous in the Kako River basin

2.1 Introduction

Phosphorous and nitrogen are major elements in the living cycle of animals and plants as natural constituents of terrestrial and aquatic ecosystems, soils, and sediments. They are also connected with human activities and settlements because of their presence in sewage and industrial waters, fertilizers, wastes, etc. These two elements are essential for life, but their excess in nature leads to severe environmental problems, particularly for superficial and shallow groundwaters. Because of their natural presence and sources, phosphorous and nitrogen pollution sources are hard to identify and are classified as nonpoint source pollutants.

Export coefficients (EC) are an easy-to-implement and valuable tool for estimating nonpoint source pollutant loads by numerical models, but their determination usually entails many challenges. Many theoretical and practical considerations need to be addressed for their estimation because they are not "multipurpose" coefficients, and their estimation is linked with the conditions in time for the place they are estimated and their direct application. Some of the biggest challenges in the obtention of ECs are: obtaining long series of observed water quality and mainstream discharge in many points along the area of interest, the isolation of the water catchments from each land use, and scaling the coefficients for an entire basin or area of interest (Shrestha et al., 2008). Because the conditions of their determination influence them, their generalization and scaling are difficult, representing one of this method's most significant limitations. Identifying pollution sources, their weight, and the representability of the resultant ECs remains challenging despite all the efforts and strategies suggested over the past decades.

There are three main approaches to determining EC: empirical, physical-based, or a mix of both. With the necessity of better EC values for a better watershed and superficial waters management and the development of more powerful computational tools, the initial EC Model proposed by Johnes (1996) has considerably evolved. Shrestha et al. (2008) proposed a methodological framework using routine quality data in the mainstream to empirically estimate EC and their integration in water catchment modeling. The effect of precipitation and terrain heterogeneities to reduce the scaling problems and give a more

generalized EC was proposed by Ding et al. (2010). Hua et al. (2019) studied and identified individual agricultural nonpoint sources at the sub-basin level, and Wang et al. (2020) proposed the use of dynamic EC to represent watershed heterogeneities and reduce the scaling problems that global ECs have. Regardless of the above, ECs determination requires large amounts of observed data to reduce uncertainties, and the mathematical expressions of the empirical models that link variables are relatively complex.

Hodge & Armstrong (1993) proposed that there is a direct relationship between stormwaters, land use, EC, and concentration of a nonpoint source pollutant in the mainstream. Their main idea is that pollutant loads can be estimated from river streamflow, land runoff discharge, and pollutant concentrations at any mainstream point as a function of the land use and the water catchment area upstream of the observation point.

In this work, the idea proposed by Hodge & Armstrong (1993) was modified, and the incidence of rain events was added to consider the strong correlation between rainfall and nutrients in the mainstream (Haygarth et al., 2004; X. Yang et al., 2017). Using a combination of observed datasets for water quality and streamflow in the mainstream near the estuary with river direct runoff simulations discretized per rain even, a multiple linear regression (MLR) was constructed to estimate the EC of the entire Kako River watershed. Direct runoff was defined as the water that runs over the first 30 cm of soil after rain or snowmelt. The MLR was constructed by applying a robust regression method to avoid data transformations and excessive data filtering of outliers originated from long periods of rain or heavy rainfall (rainy season and typhoon events) that are characteristic in east and southeast Asia.

2.2 Methods

2.2.1. Study site

For this work, the Kako River, located in the center of Hyogo Prefecture, west Japan, was chosen (Fig. 5). As was previously mentioned, the Kako River is one of the most important rivers in western Japan, and its estuary is located in Harima Nada, the Seto Inland Sea, a region of environmental interest. The Kako River watershed has an area of approximately 1730 km^2 and a land use distribution of more than 60% mountainous forests.

The land use in the basin was divided into five classes according to the geographic information from the Ministry of Land, Infrastructure, Transport, and Tourism of Japan (MLIT - 1). ECs were estimated for the following five classes of land use: mountain (66.4%), paddy fields (18.7%), city (111.3%), farm (1.0%), and water bodies (2.6%).

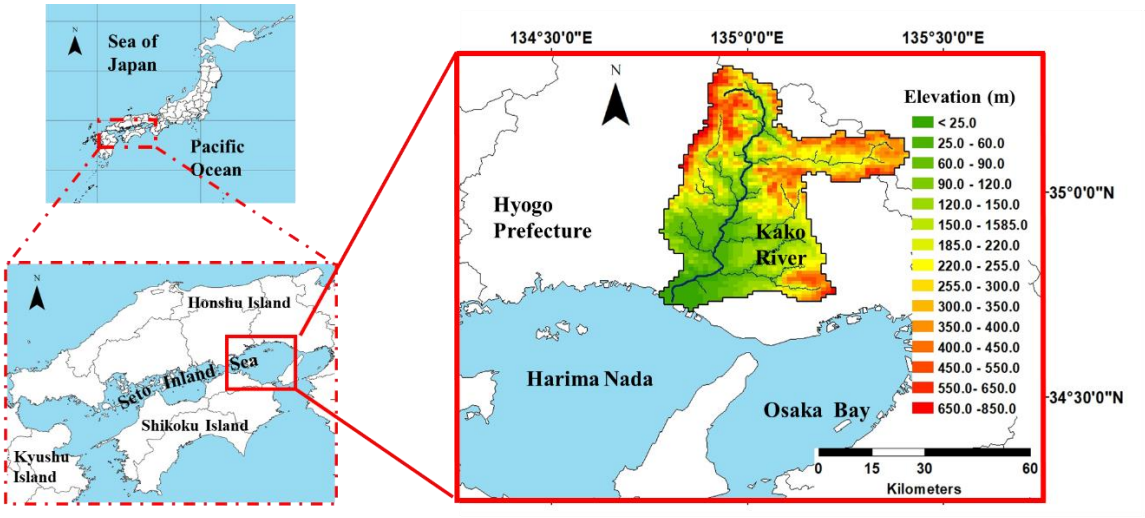

Fig. 5 – Location of the study site

2.2.2. Computational domain framework and datasets

The Kako River basin was represented as a mesh of 1x1 km cells. Geographic information system (GIS) datasets for digital elevation maps (DEM), land use, watershed boundaries, and river channels from the National Land Numerical Information System of MLIT were used in this work (MLIT - 1). Forestation datasets were obtained from the Biodiversity Center of Japan. Fig.6 shows the location of the different observatories used in this work (a) and the land use distribution of the four classes chosen to estimate the ECs.

Streamflow observatories' location and datasets correspond to the Water Information System (MLIT - 2), which collects and monitors mainstream discharge and water levels hourly. Because of data availability during the study period, only observatories D2 and D3 (Fig. 6 - a) were used for tuning and validating the hydrological model. Observed river concentration for total nitrogen (TN) and total phosphorous (TP) used corresponded to the chemical observatory (CO in Fig. 6 – a). This point is close to the river estuary, receiving

more than 90% of the watershed waters and integrating nutrients from the entire basin to a similar extent. From the observed data, it was found that the average rain event concentration on the mainstream of the Kako River was 1.0 mg/L for TN and 0.10 mg/L for TP, with a standard deviation of 0.2 and 0.04 mg/L, respectively, for the entire study period.

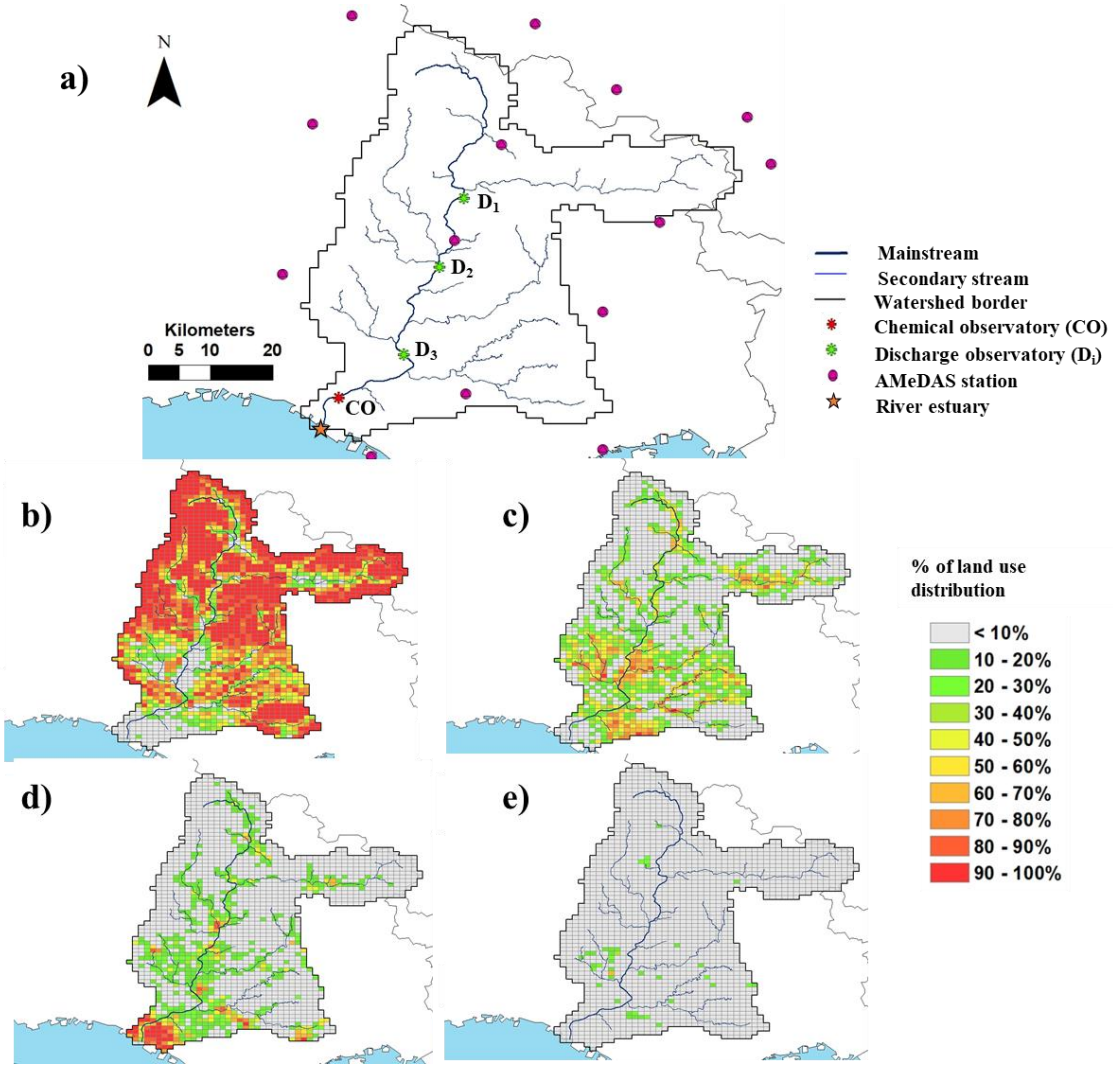

Fig. 6 - Mainstream discharge and chemical observatory stations in the Kako River watershed (a), and % of occupation of the four land use types, mountain (b), paddy fields (c), city (d), and farm (e) used in the hydrogeochemical model

Water samples in the CO were collected daily and analyzed by the Hyogo Institute of Environmental Sciences (HIES) from April 2010 to March 2012. The sampling and analysis

techniques were conducted following the "Examination Plan to Restore Materials Circulation in Sea Areas - Study in the Northeastern Harima Nada" (2013).

Atmospheric and meteorological datasets for atmospheric pressure, precipitation, solar irradiance, temperature, water vapor pressure, and wind speed datasets from the Meteorological Observatories and Automated Meteorological Data Acquisition System (AMeDAS) (Japan Meteorological Agency (JMA)) were used to force simulations and in the formal data analysis. Meteorological variables were gridded by interpolating them in the river basin using the Thiessen polygon method. All the dataset information is summarized in Table 1.

To handle the differences in altitude that the Kako River watershed has (more than 60% was classified as mountainous regions) and consider the orographic influence of rain and temperature (Goovaerts, 1999), corrections for temperature and precipitations were made on each cell according to the DEM. Equations 2.1 and 2.2 were used to correct temperature and precipitation. In Eq. 2.1, T_j accounts for the temperature in the j^{th} cell (K), T_{v0} is the observed temperature at the corresponding station (K), Γ is the lapse rate (K m^{-1}), and z is the difference in altitude between the elevation of the cell and the observatory station (m). For Eq. 2.2, precipitation in the j-cell r_j (mm) was estimated by adding to the observed precipitation value at the station r_{s0} (mm), an extra term for correction using the coefficient c_γ (m^{-1}) multiplied by the difference in altitude z (m).

$$T_j = T_{v0} - \Gamma * z \qquad \text{(Eq. 2.1)}$$

$$r_j = r_{s0}(1 + c_\gamma * z) \qquad \text{(Eq. 2.2)}$$

Table 1 Information on the input datasets used in the model simulation

	Dataset	Resolution	Source
Hydrological Module	Elevation	1 km	MLIT-a
	Land use	1 km	MLIT-a
	River channel	*	MLIT-a
	Forestation	1 km	Biodiversity Center of Japan
	Precipitation	Hourly	Hourly data at AMeDAS stations (JMA)
	Air temperature, wind speed, water-vapor pressure, atmospheric pressure, solar irradiance	Hourly	Data from meteorological observatories and AMeDAS stations (JMA)
Regression Model	Precipitation	Hourly	Hourly data at meteorological observatories and AMeDAS stations (JMA)
	Discharged water (total and from each land use)	Hourly	Result from the hydrological model
	TN / TP concentration	Daily	HIES
Chemical Module	Land use	1 km	MLIT-a
	Export coefficients	Yearly	Result from the regression model
Model Validation	Freshwater flow	Hourly	MLIT-b
	TN / TP concentration	Daily	HIES

(* - does not correspond)

2.2.3. Study period and rainfall events discretization

The 24 months between April 2010 and March 2012 were used in this study. To evaluate differences in the annual rainfall patterns and validate the EC coefficients performance using simulation, the observed datasets were split into two subsets of 12 months each for TN and TP. Year I correspond to the 1st 12 months of the period (April 2010 – March 2011), and Year II to the rest (April 2011 – March 2012). For the case in which ECs were calculated using Year I TN and TP series (CASE I), Year II subsets were used to validate the results, and when ECs were calculated from Year II subset (CASE II), Year I observations were used in the validation.

Firstly, annual cumulative precipitation and the average for the area were checked to evaluate if significant differences in rainfall patterns existed between 2006 and 2015 (Fig. 7 – a). Additionally, total cumulated monthly precipitation was estimated for Year I and Year

II and compared with the monthly average for the same period (Fig. 7 – b). This analysis found that for Year I, total precipitation was 1470 mm, a value very similar to the annual average in the Kako River watershed area (1510 mm/year). For the Year II, the situation was considerably different. Annual cumulated precipitation in Year II was approximately 30% higher than the average (1924 mm), an outlier for the region in the ten years evaluated. The analysis of monthly deviations between Year I and II found that the months with higher precipitation in Year II corresponded with May (rainy season) and September (typhoon season), which pointed to the occurrence of more extreme meteorological events during that year. These observations reinforced the idea of separately studying CASE I and II to evaluate the incidence of rainfall in the ECs coefficients and test the proposed methodology's robustness.

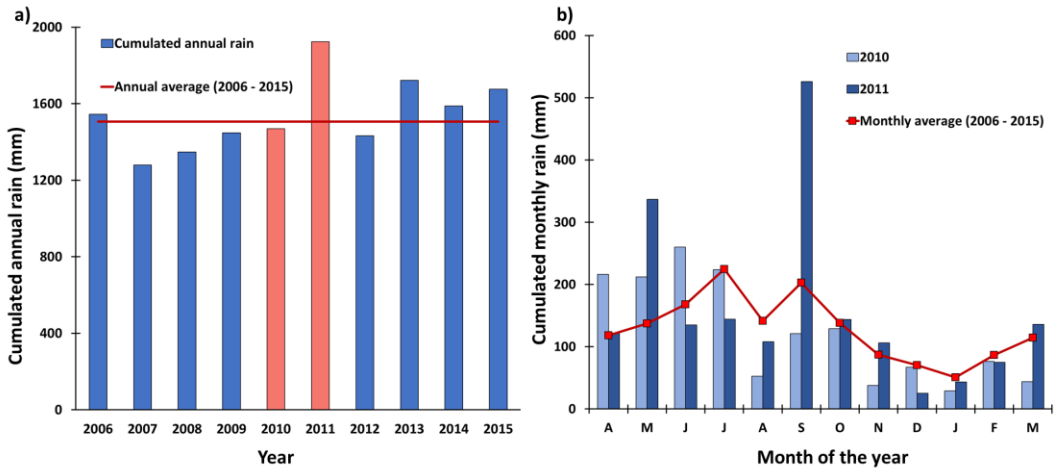

Fig. 7 - Annual and averaged cumulated precipitation (Apr. – March) between 2006 and 2015 (a), and monthly cumulated rainfall and ten years average for years I and II (b) in the Kako River watershed

The construction of the MLRs needed to estimate direct runoff contribution from each land use per rain event in the entire basin as regression variables since it adds rain duration and intensity to the current model approach. To do this, the hourly weighted average value of precipitation on the entire basin was calculated, and rain events were defined from the 1st hour of precipitation (average value ≠0) until the previous hour of rainfall started again. The intensity and duration of the identified rain events were calculated as the summation of the rain mm and the duration hours of each event. Using this approach, a total of 821 rain events

were identified in the 24 months of this analysis, 399 during Year I and 422 in Year II. The hourly direct runoff from each land use was discretized using these rain events and regressed in the MLR.

2.2.4. Linearization and ECs model

2.2.4.1 Data handling

The direct runoff from each land use was hourly estimated in the point CO (Fig. 6 – a) by simulations. The methodology used for this was to add (posterior to the validation of the physically distributed hydrological model) an inert tracer to each land use, and the tracer load in the control point was estimated and correlated with the water contribution of that particular land use. Total direct runoff contribution into the mainstream was calculated hourly in the CO, and monthly results per land use and the ratio contribution can be seen in Fig. 8.

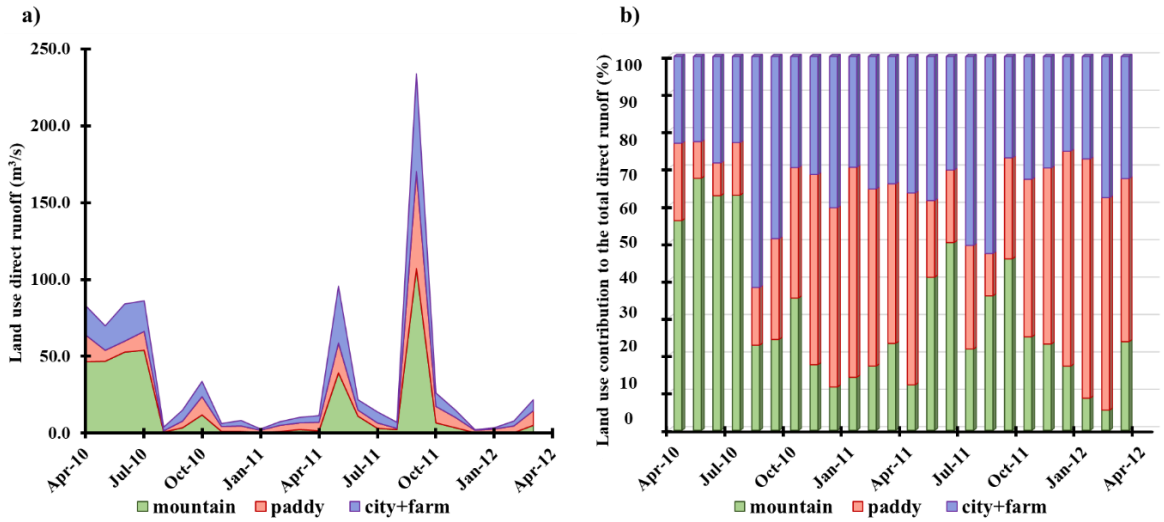

Fig. 8 - Estimated monthly total direct runoff in the chemical observatory (a) and ratio contribution per land use (b) in Year I and Year II

As previously mentioned, land use direct runoff was discretized per rain event and used as a regression variable of the MLR models to obtain the ECs. The stochastic nature of rain events and their chaotic distribution in intensity and duration breaks the most important hypothesis for constructing a linear model: the variance distribution of the variables is not homogeneous. The heteroscedasticity problem is very common when linearizing natural variables with random distributions and strong outliers in the data population. To address this

problem and avoid unnecessary data transformations that make difficult the understanding and significance of the regression coefficients, a robust regression method was chosen.

Daily values of observed TN and TP concentration in the mainstream were interpolated hourly to smooth the hourly loads for the rain event discretization. The linear relationship between nutrient load and discharged water per rain event was verified by plotting the average total load of TN and TP in the mainstream vs. the total direct runoff from each rainfall event between April 2010 and March 2012 (Fig. 9). The obtained results validated the linearity of the relationship between the chosen variables to regress in the MLR without the necessity of any data transformation.

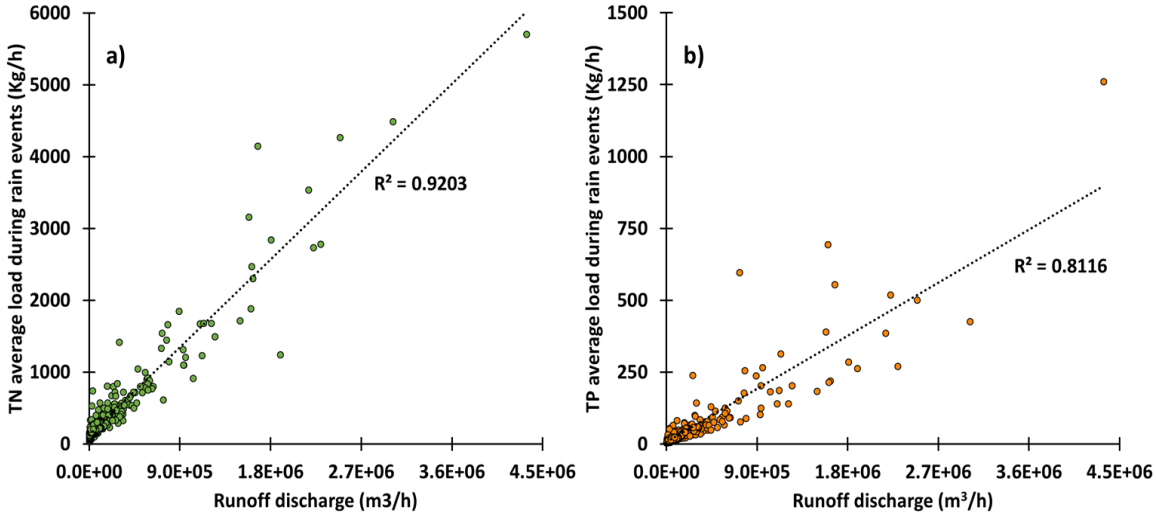

Fig. 9 - Verification of the linearity assumption between the rain event's nutrient load in the river and total direct runoff for TN (a) and TP (b) at the chemical observatory

2.2.4.2 Robust Regression model – Iterative Reweighted Least Squares Method (IRLS)

Because of the particularities of the Japanese climate and the seasonal occurrence of particular extreme rainfall events during rainy and typhoon seasons (from April until the end of October every year), a good estimation of ECs necessarily needed to consider as many "outliers" as possible, to describe the watershed's conditions the most accurately possible.

The IRLS was chosen in this work because, like all the robust regression methods, it can handle unequal variance distributions, buffering outliers' strong effect on the intercept and the slope of the MLR (Kutner M.H et al., 2005). In addition, it is one of the methods that can be used in multivariate systems. The method's main idea is to evaluate residuals and normalize their distribution by calculating an estimated weight from the entire population distribution. Its implementation requires the usage of two combined weight functions, the Huber and the bisquare functions, to adjust the regression weights and increase sensibility (Fig. 10). The weight functions' tunning values were chosen to provide a 95% efficiency of the regression estimator (1.345 for the Huber function and 4.685 for the bisquare function).

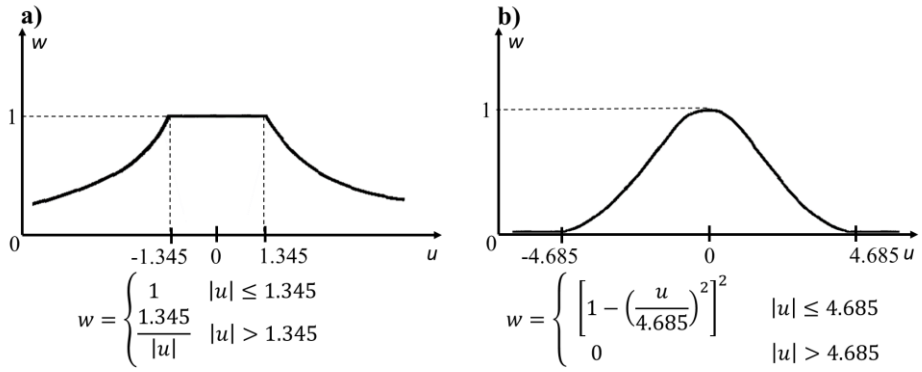

Fig. 10 - Huber (a) and bisquare (b) weight functions for 95% efficiency of the regression estimator (w= weight, u=scaled residual)

The first step of the method's implementation is constructing an ordinary least square regression (OLS) to obtain its first set of scaled residuals. The weight functions are designed to be used with scaled or studentized residuals, but to scale the residuals, it is needed to estimate the terms $s\{e_i\}$ and h_{ii}. (Eq. 2.4 and Eq. 2.5). In this work, it was chosen to use scaled studentized residuals to increase fitting sensitivity from the direct runoff outliers.

The term $s\{e_i\}$ accounts for the standard deviation of the i^{th}-residual. Because the mean square error (MSE) is not a robust estimator of the error term in the presence of strong outliers or when the distribution is far from normal, the median absolute deviation (MAD) was used to scale the studentized residuals (Eq. 2.9 and Eq. 2.10). The usage of the MAD to calculate $s\{e_i\}$ increases the method's robustness and the regression's sensitivity to the outliers, mainly when the leverage is significant in the x values (Kutner et al., 2005). The

constant 0.6745 in Eq. 2.9 provides an unbiased estimator of the error for independent observations from a normal distribution when calculating the MAD. The value h_{ii} corresponds with the i^{th}-element in the diagonal of the hat matrix and represents the leverage of the i^{th}-observation to the entire pool of observations. It can be calculated from Eq. 2.6 using the matrix of Eq. 2.7 and the design matrix $\boldsymbol{X}$ (Eq. 2.8) or directly extracted from the diagonal of the hat matrix $\boldsymbol{H}$ ($\boldsymbol{H} = \boldsymbol{X}(\boldsymbol{X}'\boldsymbol{X})^{-1}\boldsymbol{X}'$).

The iterative process was conducted in this work until the MLR coefficients for the j^{th} and (j^{th}+1) iteration steps had a difference of less than 5%. All the equations for the method implementation are summarized in Table 2, and Fig. 11 shows the flowchart of the method implementation.

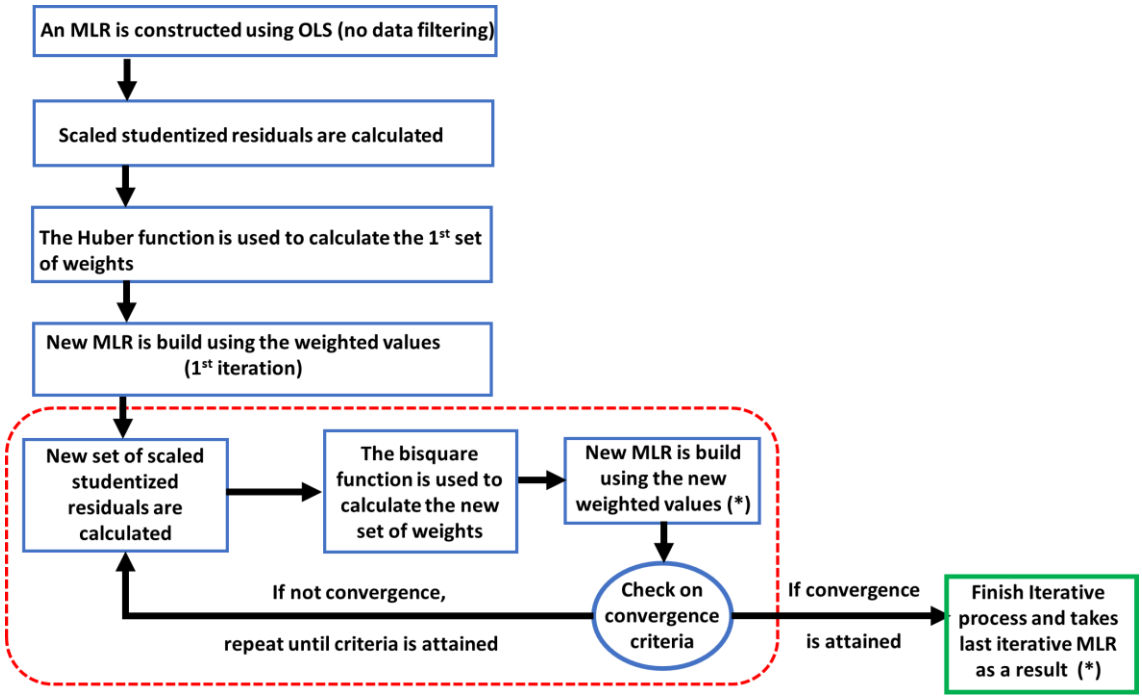

Fig. 11 - Implementation flowchart for the IRLS

Table 2 – Parameters and equations used to implement IRLS

Parameter	Equation	
Residual	$e_i = Y_i - \hat{Y}_i$	(Eq. 2.3)
Studentized residual	$r_i = \frac{e_i}{s\{e_i\}}$	(Eq. 2.4)
	$s\{e_i\} = \sqrt{MSE(1-h_{ii})}$	(Eq. 2.5)
	$h_{ii} = \boldsymbol{X_i'}(\boldsymbol{X'X})^{-1}\boldsymbol{X_i}$	(Eq. 2.6)
	$\boldsymbol{X_{i}}_{p\text{x}1} = \begin{bmatrix} 1 \\ x_{i\,1} \\ \vdots \\ x_{i\,p-1} \end{bmatrix}$	(Eq. 2.7)
	$\boldsymbol{X} = \begin{pmatrix} 1 & x_{11} & \cdots & x_{1\,p-1} \\ 1 & x_{21} & \cdots & x_{2\,p-1} \\ \vdots & \vdots & & \vdots \\ 1 & x_{n1} & \cdots & x_{n\,p-1} \end{pmatrix}$	(Eq. 2.8)
Scaled studentized residuals	$u_i^* = \frac{e_i}{s^*\{e_i\}}$	(Eq. 2.9)
	$s^*\{e_i\} = \sqrt{MAD(1-h_{ii})}$	(Eq. 2.10)
	$MAD = \frac{1}{0.6745}\, median\{\lvert e_i - median\{e_i\}\rvert\}$	(Eq. 2.11)

2.2.4.3 The MLR definition and construction

Hodge & Armstrong's (1993) assumption described by Eq. 2.12, in which the total load of pollutant in the mainstream TL (kg s^{-1}) can be estimated as the summation of each of i land use types contributions (m: mountain, p: paddy, c: city, and f: farm), calculated as the pollutant concentration from the i^{th} land use α_i (kg m^{-3}) multiplied for the runoff discharge QS_i (m^3 s^{-1}) from that land use during the the k^{th} rainfall event was modified to define the MLR models developed in this work as in Eq. 2.13. The intercept PS accounts for other contributions (point source, runoff erosion contribution, etc.), and ε is the error term.

$$TL_k = \sum_i \alpha_i QS_{i_k} \qquad \text{(Eq. 2.12)}$$

$$\mathrm{TL_k} = (\alpha_\mathrm{m}\overline{\mathrm{QS_m}} + \alpha_\mathrm{p}\overline{\mathrm{QS_p}} + \alpha_{\mathrm{c+f}}(\overline{\mathrm{QS_c}} + \overline{\mathrm{QS_f}}))_\mathrm{k} + \mathrm{PS} + \varepsilon \qquad \text{(Eq. 2.13)}$$

To validate the assumption that the relationship between the average nutrient load in the mainstream and the direct runoff from each land use $\left(\overline{QS}_{i_k}\right)$ was linear per rain event, plots were made for TN and TP (Fig. 12). Additionally, a scatter plot matrix for the direct

runoff variable was made to check if there were internal correlations between the variables, and if the MLR coefficients were independent between them (Fig. 13). The predictor variables were shown to be linearly correlated with nutrient's load, as well as no significant trends were found in the scatter plot matrix, validating the selected approach.

Initially, land use was classified into four major sources of TN and TP in this approach, but because of the small basin percentage that farm land use represents in the entire watershed (only 1%), the overlap of city and farm land uses in the same regions, and the small occupation ratio of farms in the cells they are distributed (see Fig. 6 – d and 6 – e) it was chosen to collapse both variables in the construction of the MLR, and jointly estimate a unique EC for representing them. The extent of this assumption, considering that farming activities are minimal and do not represent one of the main activities of the study area, reduced the error in estimating regression coefficients and, consequently, improved the ECs for the entire watershed. The combined variable's direct runoff was expressed as the summation of the direct runoff from each land use.

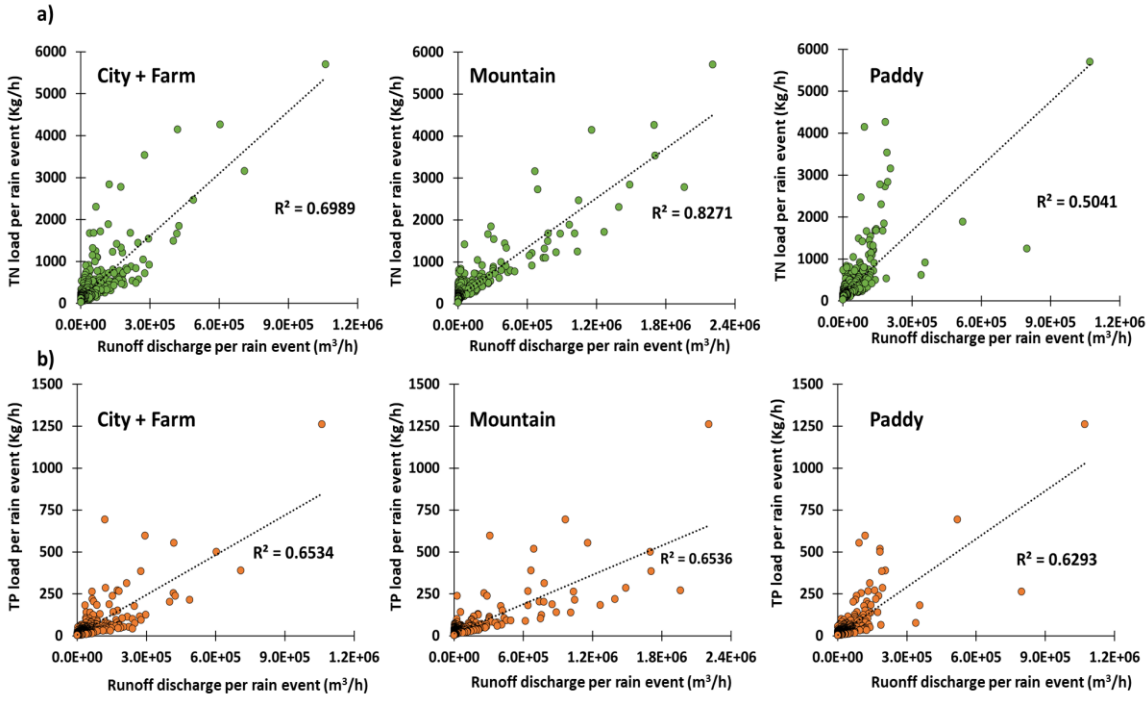

Fig. 12 - TN (a) and TP (b) average load in the mainstream vs. direct runoff discharge from each land use of the MLR per rain event at the chemical observatory to verify the linearity assumption

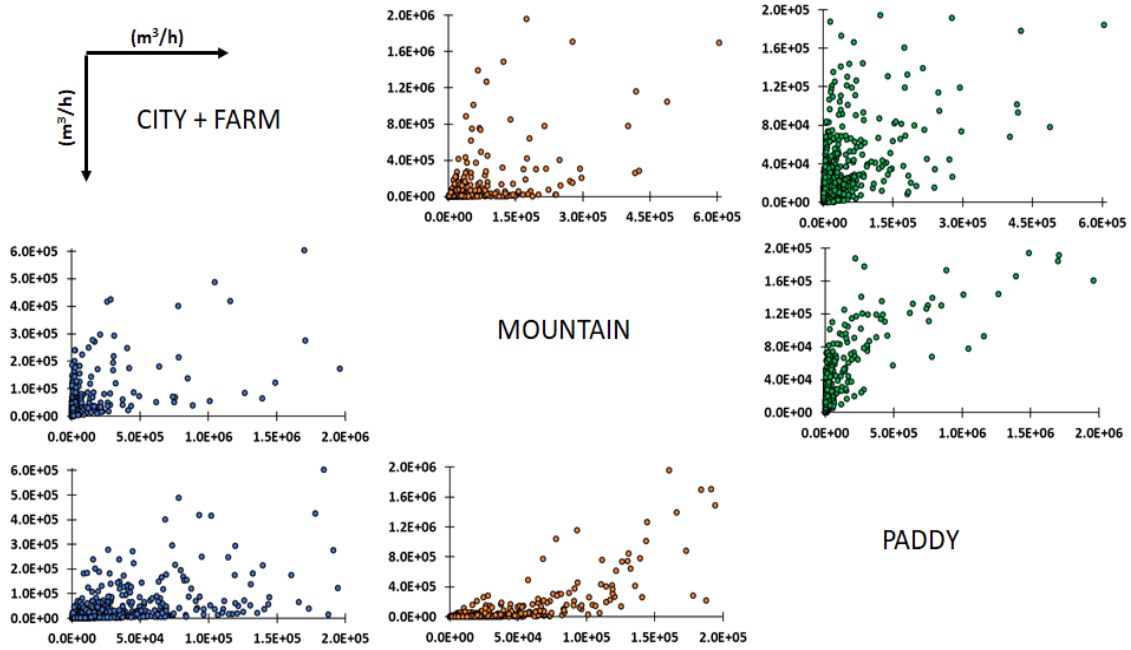

Fig. 13 - Scatter plot matrix of average direct runoff discharge at the chemical observatory per rain event from each land use for years I and II

Two MLRs and sets of regression parameters α_i were obtained for each nutrient; one pair of MLRs was constructed by regressing the data subsets from Year I, and the other one corresponded to Year II. From the α_i coefficients, annual ECs were calculated as in Eq. 2.14. The EC of the i^{th} land use W_i (kg ha-1 y-1), was estimated as the annual summation of the hourly nutrient load from the the i^{th} land use ($\alpha_i * QS_i$ (kg h-1)) divided by the total area A_i of the i^{th} land use in the basin (ha).

$$W_i = \frac{1}{A_i}\sum_h \alpha_i \times QS_i(h) \qquad \text{(Eq. 2.14)}$$

2.2.4.4 Model performance and results evaluation tools

Model performance and results were evaluated using the statistics recommended by Moriasi et al. (2007) for hydrological simulations. The coefficient of determination (R^2), Nash-Sutcliffe efficiency (NSE), root mean square error – observation standard deviation ratio (RSR), and the percentage of bias (pBIAS) were selected and are summarized in Table 3. R^2 helps evaluate the variance distribution between observations and calculated values.

NSE is a dimensionless statistic that measures how good the plot 1:1 for observed values is. pBIAS is an error index used to evaluate how far apart simulation results are from the observations and can be positive (underestimation) or negative (overestimation). Finally, RSR is also an error index that standardizes the root mean square error (RMSE) by using the observed data's standard deviation; lower values of RSR correlate with a better reproduction of the observations.

There are extensive recommendations for the model's performance statistical parameters evaluation, mainly reported for monthly or yearly time resolutions. Because of differences in the bibliographic recommendations, the monthly benchmarks for model performance evaluation were taken from Moriasi et al. (2007).

Table 3 – Statistics used for evaluating the river model's performance

$$R^2 = \left[\frac{\sum_n (O_t - \bar{O})(P_t - \bar{P})}{\sqrt{\sum_n (O_t - \bar{O})^2}\sqrt{\sum_n ((P_t - \bar{P})^2)}}\right] \quad \text{(Eq. 2.15)}$$

$$NSE = 1 - \frac{\sum_n (P_t - O_t)^2}{\sum_n (O_t - \bar{O})^2} \quad \text{(Eq. 2.16)}$$

$$pBIAS = \left[\frac{\sum_n \left(\frac{(O_t - P_t)}{O_t} * 100\right)}{n}\right] \quad \text{(Eq. 2.17)}$$

$$RMSE = \sqrt{\frac{\sum_n (P_t - O_t)^2}{n}} \quad \text{(Eq. 2.18)}$$

$$RSR = \frac{RMSE}{STDEV_{obs}} = \left[\frac{\frac{\sqrt{\sum_n (P_t - O_t)^2}}{n}}{\frac{\sqrt{\sum_n (O_t - \bar{O})^2}}{n}}\right] \quad \text{(Eq. 2.19)}$$

$\boldsymbol{P_t}$= Predicted value at t time, $\boldsymbol{O_t}$= Observed value at t time, $\bar{\boldsymbol{O}}$= Mean of observed values, $\bar{\boldsymbol{P}}$= mean of predicted values, $\boldsymbol{n}$= number of values considered

2.3 The Simulation Models

Numerical and simulation models have become, in the past decades, a trustable tool for evaluating and assessing many environmental problems. The accessibility to a wide

variety of meteorologic and geographic datasets with high-resolution (DEM, GIS datasets, etc.), complemented with the interest of national governments and agencies of sharing time series of meteorological observations, land use, population distribution, etc., gives to the obtained results practical use and significance. In this work, a physically distributed model based on the Hydrological River Basin Environment Assessment Model (Hydro-BEAM) developed by Kojiri (2006) was coupled to a chemical transport model to estimate nutrients concentration in the CO near the river estuary. The layout of the Hydro-Chemical Model is represented in Fig. 14.

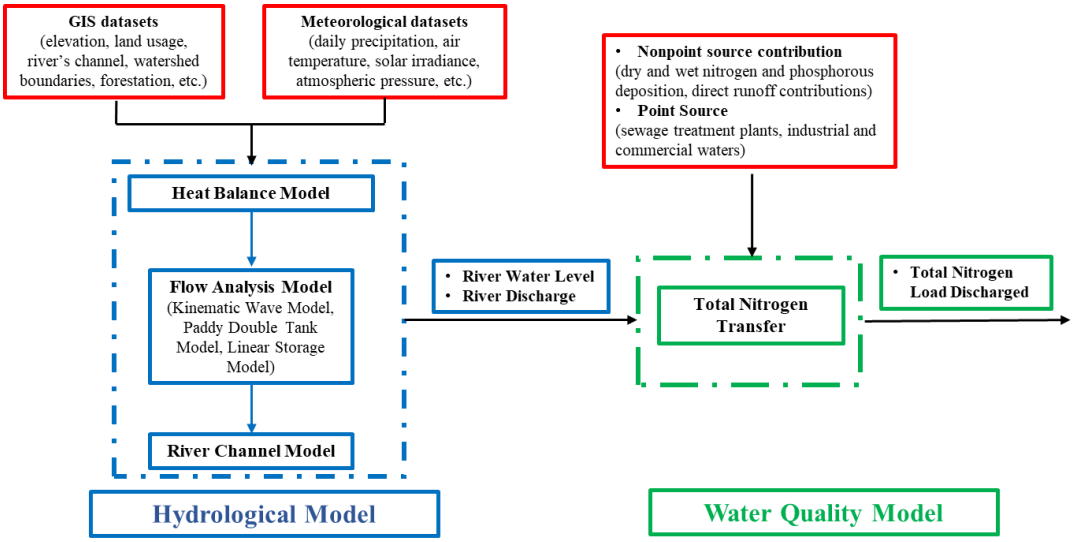

Fig. 14 - General layout of the Hydro-Chemical Model used

2.3.1 Hydrological Model

Kojiri's (2006) model was developed to estimate water quantity and quality by combining GIS and meteorological data. It is a four-layered runoff model in which the river watershed is divided into cells representing two different water processes: soil hydraulics and river channel hydraulics. Each cell is represented with a straight inner water channel, whose direction is defined by the DEM. The soil hydraulics depend on the land uses and are determined by weighting land use occupation ratios to estimate their infiltration values (Kojiri et al., 2008).

Fig. 15 shows a layout of the cell design and the representation of the four layers (A to D). Direct runoff only occurs in layer A (first 30 cm). There is horizontal flux into the cell river channel from layers A to C. The vertical exchange is possible between the four layers, but the bottom of layer D marks the non-flux frontier of the model. The model additionally contemplates each cell's evapotranspiration, snow-fall and snow-melting process, intake/release flux in the channel, heat transfers, etc.

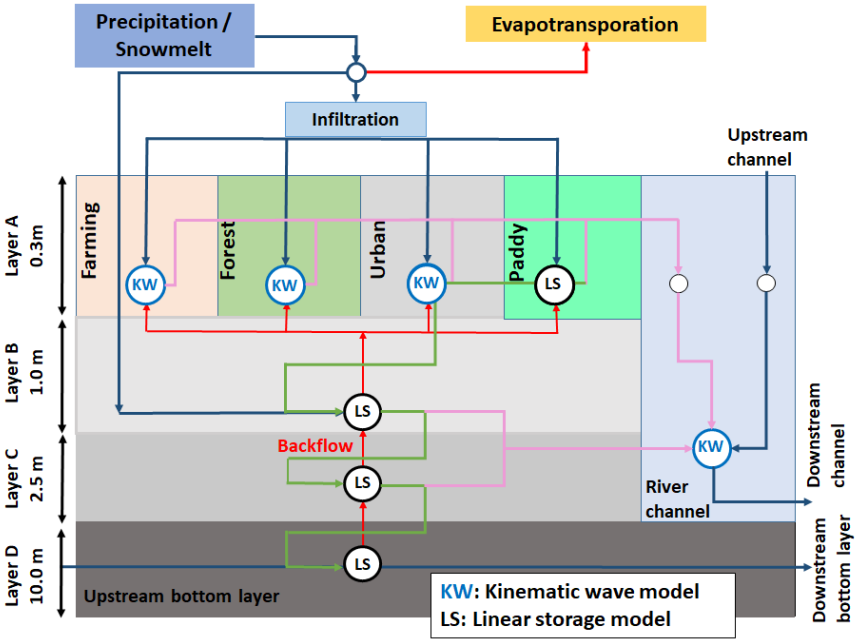

Fig. 15 - Layout of the hydrological model

The runoff processes from mountains, urban areas, farms, and paddy fields are modeled using the Kinematic Wave Model, and a Linear Storage Model is used for the vertical exchanges between all the underground layers (Kojiri & Park, 2002). Paddy fields are modeled separately using a Tank Model approach because of their particular operating conditions. The paddy model consists of a double tank model with three holes connecting it with the rest of the system at different depths. The upper hole represents the surface direct runoff discharges; the second hole is the link between the base flow in the upper layer of the hydrological model, and the bottom one represents the exchange flow with the groundwater layers (Fig. 15). All the equations describing the physical process in the model are presented in Appendix 1.

2.3.2 Nutrients Load Model

The nutrients model is a modification of the transport model developed by Ikenoue et al. (2020). It allows the conservative estimation of nutrient loads by using a method that integrates advection, diffusion, emission, and lateral runoff processes derived from the terrain slope and information from the DEM. This model does not contemplate chemical reactions or physicochemical processes like absorption or adsorption in soils or sediments during transport. The physical transport processes are represented in Eq. 2.20, where A_r is the cross-section area of the river channel (m^2), C_{TN} accounts for nutrient concentration in the river channel (g m^{-3}), U is the average cross-sectional flow speed (m s^{-1}), D_{TN} is the diffusivity coefficient of the nutrients (m^2 s^{-1}), and f_{TN} is the lateral nutrient inflow from the terrain slope (g $m^{-1}s^{-1}$).

$$\frac{\partial}{\partial t}(A_r C_{TN}) + \frac{\partial}{\partial x}(A_r U C_{TN}) = \frac{\partial}{dx}\left(A_r D_{TN}\frac{\partial C_{TN}}{\partial x}\right) + f_{TN} \qquad \text{(Eq. 2.20)}$$

The term f_{TN} is responsible for the surface load in the river watershed, accounting for the surface runoff contribution from each land use. Its calculation is performed on each cell j^{th} of the domain and added to the entire watershed mesh, and it is represented by Eq. 2.21. ω_i is the average exported concentration from each i^{th} land use (g m^{-3}), QS_i accounts for the direct runoff from each land use (m^3 s^{-1}), and bl is a geometrical parameter that corresponds to the length of the river channel in each cell. Concentration values ω_i were calculated from the ECs calculated using the MLRs results described by Eq. 2.22. The EC value of the i^{th} land use W_i (g $m^{-1}s^{-1}$), was divided between the quotient of dividing the total direct runoff discharged in a year from the i^{th} land use (m^3 s^{-1}) and the total area A_i occupied in the entire basin for that land use (m^2).

$$f_{TN} = \frac{\sum_j \left(\omega_m QS_m(j) + \omega_p QS_p(j) + \omega_c QS_c(j) + \omega_f QS_f(j)\right)}{bl} \qquad \text{(Eq. 2.21)}$$

$$\omega_i = \frac{W_i}{\left(\frac{QS_{i_{year}}}{A_i}\right)} \qquad \text{(Eq. 2.22)}$$

2.4 Results and Discussion

2.4.1 Discharged water simulations

The Hydrological model was previously tuned and validated before estimating mainstream and land use direct runoff. For its validation, two observatories located in the mainstream of the Kako River (D2 and D3 Fig. 6 – a) were used from April 2010 to December 2011 (observed datasets for the observatory D1 were not continuous, and for the year 2012 were not available in any point). Daily, weekly, and monthly average streamflow on the mainstream were calculated from the MLIT (MLIT - 2) hourly dataset at the selected points.

Table 4 – Mainstream discharge performance in stations D2 and D3 at different time resolutions

April 2009 – Dec 2011	R^2	NSE	pBIAS	RSR
D2				
Daily	0.85	0.82	-14.8	0.42
Weekly	0.96	0.94	-15.4	0.25
Monthly	0.97	0.92	-14.7	0.21
D3				
Daily	0.81	0.77	-8.36	0.48
Weekly	0.94	0.91	-8.96	0.30
Monthly	0.94	0.91	-8.34	0.22

Performance rating (Moriasi et al., 2007)
Very good: **RSR**≤0.50, 0.75<**NSE**≤1.00, **pBIAS**≤±10 (streamflow) **pBIAS**≤±25 (nutrients)
Good: 0.50<**RSR**≤0.60, 0.65<**NSE**≤0.75, ±10<**pBIAS**≤±15 (streamflow) ±25<**pBIAS**≤±40 (nutrients)
Satisfactory: 0.60<**RSR**≤0.70, 0.50<**NSE**≤0.65, ±15<**pBIAS**≤±25 (streamflow) ±40<**pBIAS**≤±70 (nutrients)

Table 4 summarizes the results of the statistics used for evaluating performance and the benchmark values proposed by Moriasi et al. (2007), and Fig. 16 shows the hyeto-hydrographs for daily, weekly, and monthly observed data and simulation results between April 2010 and December 2012. Results showed that the model has very good performance for all the evaluated statistics in both observatories at all the studied time resolutions. NSE values are in all the cases higher than 0.75, showing that simulation results are in high agreement with the observations. pBIAS values are negative in both observatories, showing a tendency to slightly overestimate streamflow discharge more significantly in D2 than in D1. RSR values are smaller at weekly and monthly resolutions, indicating that the value of the error in the estimation is buffered for the average.

The obtained results validated the usage of the hydrological model and showed that model setup and tunning effectively reproduce the Kako River streamflow for the study period.

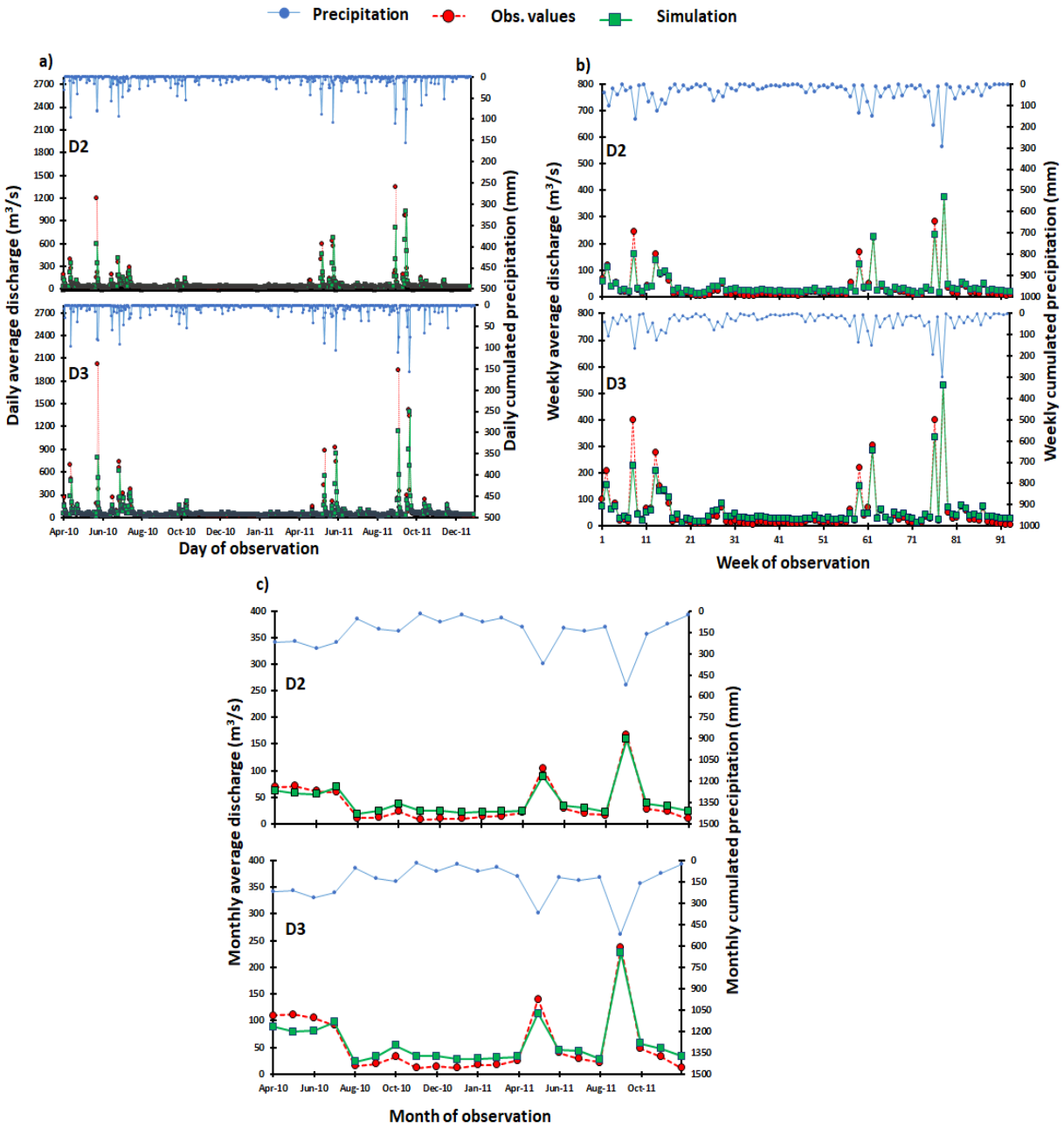

Fig. 16 - Hyeto-hydrograph of daily (a), weekly (b), and monthly (c) average observed and simulated mainstream discharge in stations D2 and D3 from April 2010 to December 2011

2.4.2 MLR and export coefficient analysis

The current approach calculates ECs from direct runoff, so they depend on rain. According to Eq. 2.14, and under the consideration that land uses did not vary their corresponding area during the time of this study, changes in the values of the ECs can be only caused by changes in the annual direct runoff over the land uses. Because of the significant difference in rain patterns observed between Year I and Year II (Fig. 7), the variability of the ECs values and their performance to describe the Kako River watershed in conditions slightly different than those corresponding to their calculation could be studied. CASE I and II (defined in 2.2.3) were used to discuss, compare, and visualize the results obtained.

2.4.2.1 TN export coefficients

The construction of the MLR using the IRLS method for CASE I and CASE II converged in both cases in the 3rd iteration step, filtering five rain events over 399 in CASE I and three rain events in 422 in CASE II. These results showed that the chosen method could effectively handle the differences in data variance and avoid excessive filtering for the selected discretization.

Table 5 summarizes the obtained ECs, the regression coefficients from the MLR models, and the intercept values for TN and TP in the Kako River basin. Table 6 does the same for the contribution ratio per land use on the mainstream for each nutrient. It was found that ECs for mountain and city-farm land uses positively correlate

with their values for Year I and Year II. Also, the regression coefficients maintain their values almost unchanged for these two land uses, besides the behavior of the ECs. In the case of mountain land use, the magnitude of the ECs remained practically constant, while for the city-farm land use, the corresponding value for Year II was double that for Year I. This difference in the ECs for city-farm land use can indicate a substantial difference in the direct runoff from this land use during Year II.

Variations between both study cases were also found for the regression and ECs of the paddy land use. In this case, there was also a positive correlation between years, but the

magnitude of the change was 4:1 for the regression and 2:1 for the ECs between Year I and Year II. It is reported that the value of paddy ECs can be easily affected by rain in East Asia, particularly during the fertilization period (May to June). Large amounts of rainfall during this period can quickly stabilize nutrient concentration inside the paddy field or provoke the leaching of nutrients into superficial waters (Liao et al., 2021; J. Wang et al., 2015). During Year II, abnormally high precipitations occurred (Fig. 7 – b) in the fertilization months, which can explain the differences found. As an additional point, because of paddy's special operating conditions and the differences in the hydraulic model used to represent it, it is expected that the correlation with rain events will have differences in other land uses.

The annual TN load was found to be 20% higher during Year II than in Year I, but the corresponding ratios followed the same trend in contribution per land use (city-farm > mountain > paddy) (Table 6). Still, besides the trend in contribution remained the same, important differences in the values of TN exported from each land use were observed. For Year II, mountain and paddy land use contribution was reduced by approximately 24% and 55%, respectively, while an increase of 65% was found in the corresponding city-farm land use in the same year.

The values of the MLRs' intercept also showed differences (100.4 and 115.5 kg h^{-1} for Year I and Year II, respectively), but their contribution ratio remained constant (Table 6). Because the intercept of the MLR accounts for other types of nutrient load contribution, considerable changes between years were not expected since the economic and demographic conditions during the study period did not change in the area of the Kako River watershed. The 15% difference between years could be produced, among other things, for an increment of the nitrogen wet deposition in the area and the soil runoff and fertilizers leaching due to the additional 30% extra precipitations registered for that year.

Table 5 - MLR regression and export coefficients (W_i) for TN and TP

TN				
Export coefficients Wi (kg ha-1 y-1)	**Wm**	**Wp**	**Wc+f**	
Year I	4.597	8.798	22.896	
Year II	4.182	4.712	42.141	
TN regression	**αm** (kg m^{-3})	**αp** (kg m^{-3})	**αc+f** (kg m^{-3})	**α0**(kg h^{-1})
Year I	1.25×10^{-3}	1.77×10^{-3}	2.24×10^{-3}	100.36
Year II	1.11×10^{-4}	4.82×10^{-4}	2.54×10^{-3}	115.45
TP				
Export coefficients Wi (kg ha-1 y-1)	**Wm**	**Wp**	**Wc+f**	
Year I	0.510	0.519	3.460	
Year II	0.696	0.659	3.646	
TP regression	**αm** (kg m^{-3})	**αp** (kg m^{-3})	**αc+f** (kg m^{-3})	**α0**(kg h^{-1})
Year I	1.39×10^{-4}	1.05×10^{-4}	3.38×10^{-4}	6.73
Year II	1.84×10^{-4}	16.73×10^{-4}	2.20×10^{-4}	10.63

Table 6 - TN and TP contribution ratio from each land use and other sources

TN					
	Total averaged input (kg h^{-1})	**Mountain** (%)	**Paddy** (%)	**City -Farm** (%)	**Other sources** (%)
Year I	263.2	25.2	13.6	23.1	38.1
Year II	313.8	19.2	6.10	37.9	36.8
TP					
	Total averaged input (kg h^{-1})	**Mountain** (%)	**Paddy** (%)	**City -Farm** (%)	**Other sources** (%)
Year I	25.3	28.9	8.30	36.3	26.5
Year II	33.0	30.3	8.20	29.4	32.1

2.4.2.2 TP export coefficients

In the case of TP, MLR models converged on the 7th iteration in both cases, and ten rain events were filtered for each data subset. Fewer variations were found among the obtained ECs and the contribution ratios per land between years I and II than for TN (Tables 5 and 6). The ECs for mountain and paddy showed a 30% increase in Year II to Year I, whereas the city-far land use values remained practically unchanged. These results indicated that the magnitude of the direct runoff had to have increased per land use to maintain the ECs

values constant. When comparing the values of the MLR coefficients, a 30% increase was found for the mountain land use, and a decrease of the same extent for the paddy and city-farm was observed during Year II. These observations can be associated with a higher availability of phosphorous sources because of soil runoff in the mountain land use provoked by the additional precipitations during Year II. On the other hand, soil runoff may not be so important for paddy and city-farm land because of the type of coverage.

As for TN, the contribution trend remained the same for TP (city-farm > mountain > paddy) between years. An increase of 30% in the total TN load exported from land was found for Year II, but the contribution ratios varied to a lesser extent than for TN between years. The mountain and paddy land uses contribution ratios remained almost constant in Year II (+5% and -1.4%), but there was a 20% reduction in the city-farm land use contribution ratio over the total.

Same as for TN, it was expected that the intersect of the MLR models did not change substantially for phosphorous because point source contributions and chemical availability are more limited than in the case of TN, but the results showed that the intercept increased by 40% for Year II. This change in the intercept value was correlated with 20% more contribution from other sources over the TP load exported, which evidenced the presence of soil runoff and other mechanisms that affect the amount and intensity of TP loads in the Kako River basin with rain. Phosphorous wet deposition values are in the order of 20 to 30 times smaller than for TN (Anderson & Downing, 2006; He et al., 2011), so its contribution is insignificant to explain the differences found. On the contrary, soil runoff and dry deposition are significant in evaluating TP contribution to superficial water bodies (He et al., 2011; Riemersma et al., 2006; Y. Y. Yang & Toor, 2018). In the case of the Kako River watershed, more than 60% of the land use corresponds to steep mountains that can be easily affected by soil runoff and erosion for extreme rainfall events, which can easily increase the availability of phosphorous species and their transport into the mainstream. Additionally, the concentration of TP in rivers can be affected by damn operation during rainy and summer seasons in East Asia (Bao et al., 2020; Nukazawa et al., 2017). The most important dam of

the Kako River is closely located upstream from the CO, which could have affected the TP on the mainstream, pulling the intercept of the MLR in Year II to higher values.

2.4.3 ECs performance and nutrients model validation

2.4.3.1 TN performance

The calculated ECs for TN showed good and very good performance in simulating TN load in the mainstream for the twelve months of verification and validation in CASE I and CASE II. The benchmark scores were also referred to Moriasi et al. (2007). At daily resolution, the NSE and RSR for CASE I values were in the satisfactory benchmark for the validation period, indicating that the ECs perform better at weekly or higher time resolutions when rainfall conditions substantially differ from those they were estimated. For CASE II statistics, it was observed that at daily resolution during the verification period, the NSE value was lower in comparison (good performance benchmark), but it was less of a problem than for CASE I. However, the performance was very good for the validation period and at weekly and monthly time resolutions.

The performance on simulating average magnitudes (pBIAS) was found to be very good in both cases at all the time resolutions for TN estimation. Nonetheless, the absolute values of pBIAS were higher in CASE I, and their positive sign showed the tendency to underestimate average TN loads in the mainstream. On the contrary, for CASE II, the pBIAS sign was negative, and showed the tendency to overestimate values during the validation period, which can be easily seen in Fig. 17. Fig. 17 also shows the high correlation between observed and simulated data for the time series, and the strong relationship between total rainfall and TN load in the Kako River basin at all the time resolutions. In Fig. 17, daily resolution graphs are not shown because their resolution due to the large amount of points represented is not good. These graphs were added together with the TP daily charts in Appendix II.

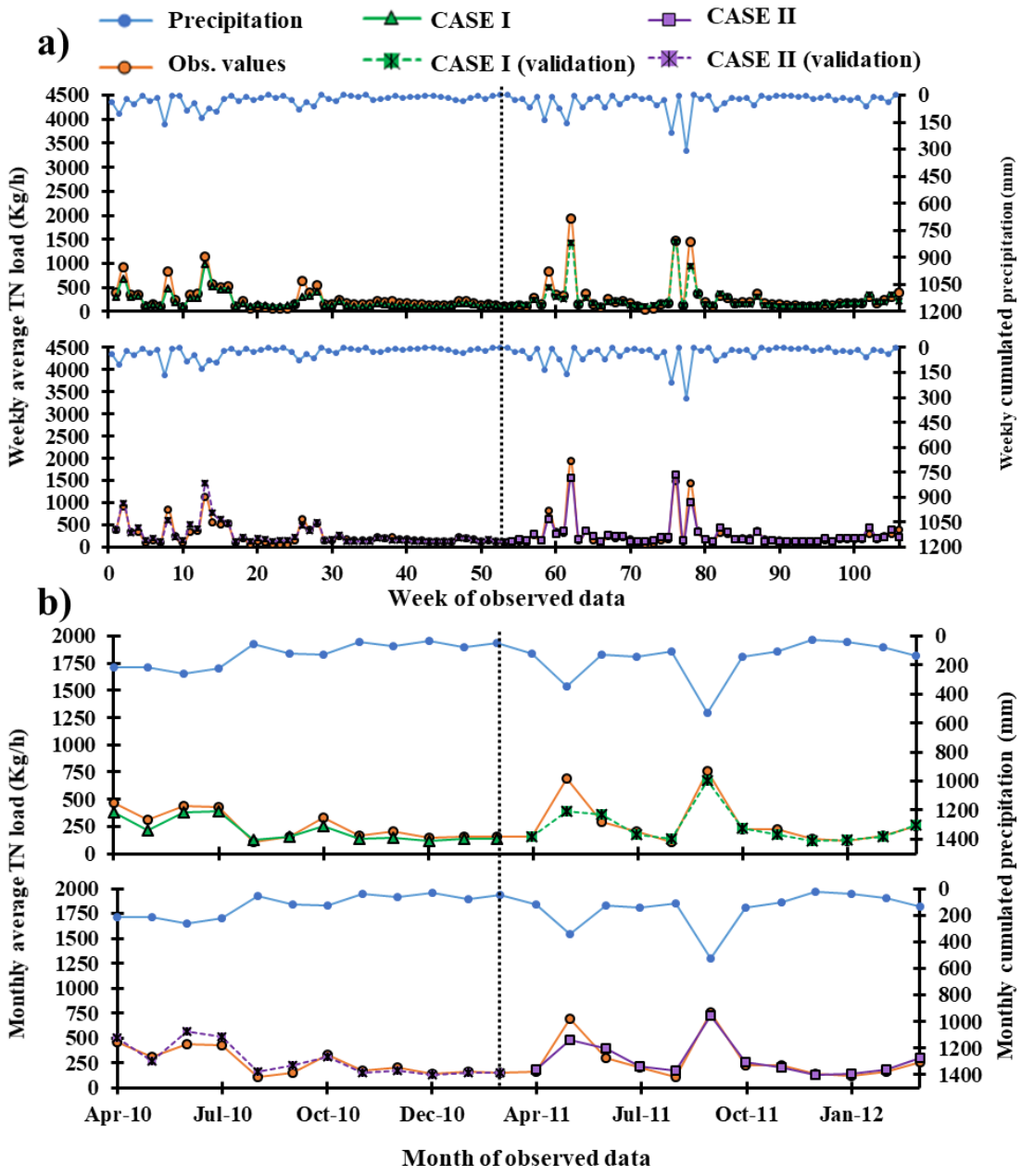

Fig. 17 - - Hyeto-load graphs of weekly (a) and monthly (b) average TN load under cases I and II in the chemical observatory for the 24 months of data collection. The vertical dashed line separates years I and II, and the validation period for each case is represented using colored dashed lines

Table 7 - Export coefficients verification and validation at different time resolutions

TN	Verification				Validation			
	R^2	**NSE**	**pBIAS**	**RSR**	**R^2**	**NSE**	**pBIAS**	**RSR**
CASE I	April 2010 – March 2011				April 2011 – March 2012			
Daily	0.92	0.81	+18.1	0.43	0.80	0.61	+10.6	0.63
Weekly	0.83	0.85	+16.1	0.39	0.97	0.89	+12.3	0.33
Monthly	0.95	0.83	+15.6	0.39	0.9	0.79	+11.4	0.43
CASE II	April 2011 – March 2012				April 2010 – March 2011			
Daily	0.82	0.66	-1.93	0.28	0.89	0.88	-7.60	0.34
Weekly	0.97	0.92	+0.03	0.28	0.91	0.87	-8.10	0.35
Monthly	0.94	0.87	-1.38	0.34	0.90	0.80	-8.45	0.43
TP								
	R^2	**NSE**	**pBIAS**	**RSR**	**R^2**	**NSE**	**pBIAS**	**RSR**
CASE I	April 2010 – March 2011				April 2011 – March 2012			
Daily	0.84	0.83	+12.4	0.41	0.79	0.62	-30.5	0.61
Weekly	0.88	0.86	+13.1	0.37	0.92	0.69	+29.5	0.55
Monthly	0.92	0.92	+5.55	028	0.94	0.68	+29.3	0.54
CASE II	April 2011 – March 2012				April 2010 – March 2011			
Daily	0.78	0.70	+7.74	0.54	0.85	0.84	-14.5	0.40
Weekly	0.91	0.81	+6.50	0.43	0.89	0.85	-14.0	0.40
Monthly	0.94	0.86	+6.43	0.36	0.92	0.88	+12.5	0.34

2.4.3.2 TP performance

For TP, the calculated ECs showed less annual variation with rainfall, but the contribution from other sources substantially increased. The statistical evaluation for CASE I showed a very good performance during the verification period at all the considered time resolutions, but the performance was lower for the validation, with daily time resolution showing to be the one with higher associated errors and deviations from the observations (satisfactory benchmark). During the validation time, weekly and monthly results showed that the model is good at reproducing trends (higher value of NSE) and reducing residual variations (smaller RSR results). The ECs from CASE II also performed very well in the verification and validation period at all the time resolutions (Table 7). The same was true for TN. It was found that the ECs perform better at weekly or higher time resolutions.

Higher values of pBIAS were obtained for TP load estimation in CASE I, in which the model underestimated TP loads in the mainstream by up to around 30%. This was less of a problem for the ECs from CASE II, where the differences were minor and a slight

overestimation in TP loads occurred (negative sign of pBIAS, see Fig. 18). The main performance for CASE II showed that observed values are better reproduce with the ECs calculated from Year II subset data at weekly and monthly time resolutions. Still, significant differences between observations and simulation results can be appreciated in the peaks of the time series, which indicates that other processes not considered in this work affect TP load in the mainstream. Daily resolution charts are presented in Appendix II.

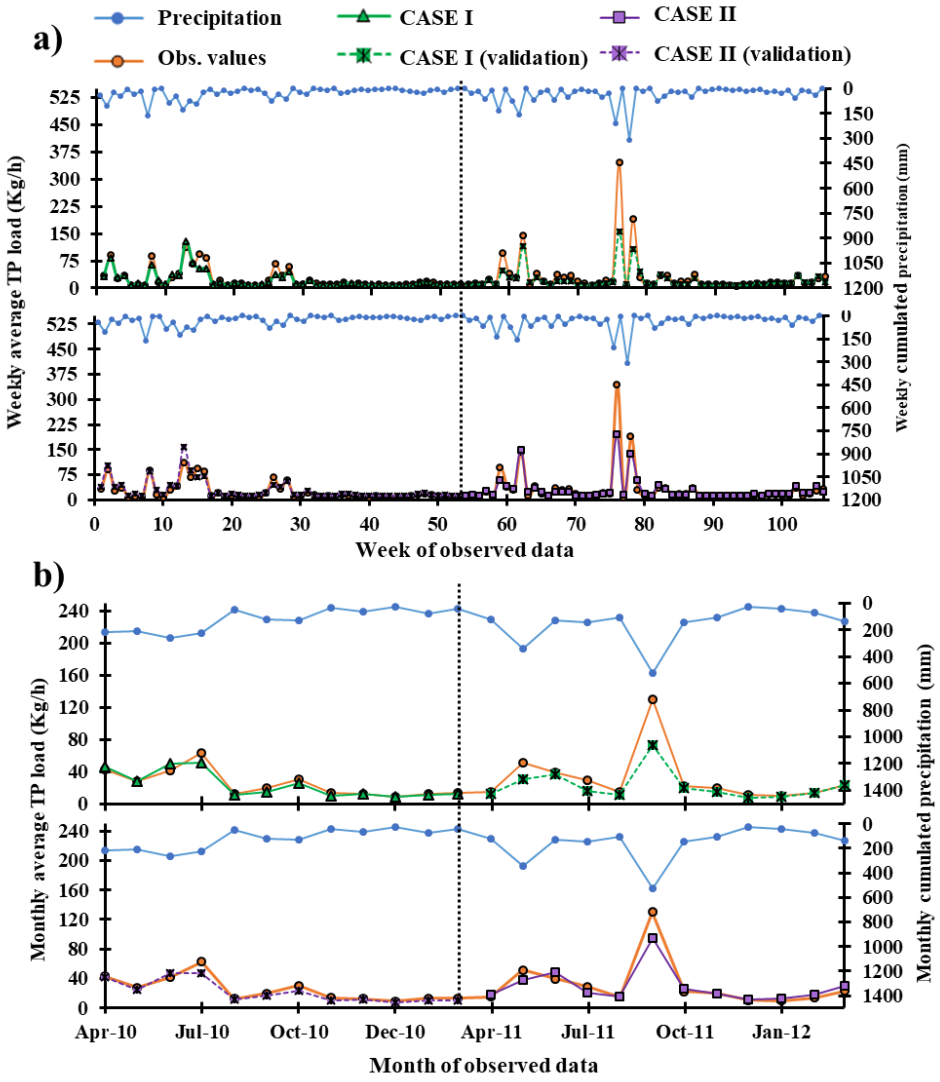

Fig. 18 -Hyeto-load graphs of weekly (a) and monthly (b) average TP load under cases I and II in the chemical observatory for the 24 months of data collection. The vertical dashed line separates years I and II, and the validation period for each case is represented using colored dashed lines

2.4.4 General considerations on the MLR model performance and its limitations

Extreme rainfall events, such as those that occur during typhoons or significant rainfall episodes during the rainy season in Japan, are responsible for substantial peaks of runoff and nutrient loads in the mainstream driven by multiple mechanisms. During these episodes, soil dynamics change for oversaturation, and the complex processes of soil runoff and erosion occur. Only these two processes have particular physical mechanisms that vary depending on the type of soil and coverage, which are out of this work's scope but can strongly affect the performance of any numerical model. In addition, the dynamics of nutrients availability in soils depend on the aqueous solution properties of the involved substances, which makes them complex and multivariant-dependent. This phenomenon was not considered in this work to keep the MLR approach as simple as possible because of the lack of observed data to account for soil runoff in the transport model or the MLR. The obtained results showed that without this consideration, the model and the estimated ECs could efficiently reproduce the Kako River watershed exported nutrients without problems and considerably small errors. However, the methodology and the model may need to be adjusted before their application in areas where conditions are different.

The use of a robust regression for constructing the MLR models and, in particular, the IRLS method applied for that also need some considerations in their application. The selected method normalizes the residual distribution by weighting the regression variables against the entire data population. Weights are assigned from 1 (mean of the population distribution) to 0 depending on the leverage of the outlier. In constructing the MLRs, around 1% and 2.5% of the rain events presented a leverage high enough to be considered outside the linearity conditions of the linear model. The IRLS method is good at maximizing the points used in the regression but pulls down the regression coefficients to normalize the distribution of the regressed variable, an effect that can be undesired if its extension is too large because the model tends to underestimate outliers to a similar extent as the weight of their relative leverages.

The application of this methodology has some additional limitations related to the simplifications of the approach. Its use can be extended to similar-sized river basins or river catchments to the one of the Kako River, but the estimation of fixed ECs can be unsuitable and needs to be revised. Fixed ECs calculated using a single point near the estuary may not be representative of large river basins with well-defined catchment areas and significant differences in their land uses that vary with time (W. Wang et al., 2020). Additionally, basins or catchment areas with clustered land uses need more observation points and a rigorous definition of the water catchments. Higher resolution GIS datasets are required to categorize the sources of particular land uses and differentiate special contributions, a point not considered in this approach.

Lastly, because ECs strongly depend on the selected approach to estimate them, their application is restricted, and the quality of their assessment can substantially vary. It was observed that those ECs calculated in a year of abnormally high precipitation (Year II) showed a better performance in reproducing nutrients export in years of average rainfall, but they tend to slightly overestimate the nutrient loads in the mainstream (Table 7). On the contrary, ECs estimated under average precipitation conditions have lower performance, particularly for TP estimations. In this work, it was observed that an increase in rainfall affects the values of the ECs and their performance, but to evaluate the extent of this observation, it would be necessary to extend the study to dry years, a task that could not be accomplished in this instance because of the lack of observed datasets.

2.5 Conclusions

A hydrological model was effectively tuned and validated to calculate the Kako River's mainstream and direct runoff discharges. TN and TP nonpoint source ECs were estimated and validated in the study site for the four primary land uses. By combining observed quality datasets and simulation results, it was possible to reduce the number of observation points to only one near the river estuary. The application of a robust regression method was tested to be suitable for avoiding data transformations and the excessive filtering of the outliers, giving more significance to the regression model and its coefficients. High

reproducibility was found to estimate mainstream nutrient loads with the obtained ECs using numerical simulations, particularly for time resolutions of weeks or higher. Special considerations must be taken when applying the present methodology in places significantly different climatologically, geologically, and geographically since modifications may be needed. Differences in rainfall of more than 30% significantly downgrade the performance of the ECs obtained, underestimating nutrient loads to a greater extent depending on the chosen time resolution.

References – Chapter 2

Anderson, K. A., & Downing, J. A. (2006). Dry and wet atmospheric deposition of nitrogen, phosphorus and silicon in an agricultural region. *Water, Air, and Soil Pollution*, *176*(1–4), 351–374. https://doi.org/10.1007/s11270-006-9172-4

Bao, L., Li, X., & Su, J. (2020). Alteration in the potential of sediment phosphorus release along series of rubber dams in a typical urban landscape river. *Scientific Reports*, *10*(1), 2–11. https://doi.org/10.1038/s41598-020-59493-3

Biodiversity Center of Japan. http://www.biodic.go.jp/dload/mesh_vg.html

Ding, X., Shen, Z., Hong, Q., Yang, Z., Wu, X., & Liu, R. (2010). Development and test of the Export Coefficient Model in the Upper Reach of the Yangtze River. *Journal of Hydrology*, *383*(3–4), 233–244. https://doi.org/10.1016/j.jhydrol.2009.12.039

Examination plan to restore materials circulation in sea areas - Study in the northeastern Harima Nada (in Japanese). (2013). https://www.env.go.jp/content/900542060.pdf

Goovaerts, P. (1999). Using elevation to aid the geostatical mapping of rainfall erosivity. *Catena*, *34*(3–4), 227–242.

Haygarth, P., Turner, B. L., Fraser, A., Jarvis, S., Harrod, T., Nash, D., Halliwell, D., Page, T., & Beven, K. (2004). Temporal variability in phosphorus transfers: Classifying concentration-discharge event dynamics. *Hydrology and Earth System Sciences*, *8*(1), 88–97. https://doi.org/10.5194/hess-8-88-2004

He, J., Balasubramanian, R., Burger, D. F., Hicks, K., Kuylenstierna, J. C. I., & Palani, S. (2011). Dry and wet atmospheric deposition of nitrogen and phosphorus in Singapore. *Atmospheric Environment*, *45*(16), 2760–2768. https://doi.org/10.1016/j.atmosenv.2011.02.036

Hodge, T. A., & Armstrong, L. J. (1993). Use of a linear regression model to estimate stormwater pollutant loading. *New Techniques for Modeling the Management of Stormwater Quality Impacts*, 201–214. https://doi.org/10.14796/JWMM.R175-09

Hua, L., Li, W., Zhai, L., Yen, H., Lei, Q., Liu, H., Ren, T., Xia, Y., Zhang, F., & Fan, X. (2019). An innovative approach to identifying agricultural pollution sources and loads by using nutrient export coefficients in watershed modeling. *Journal of Hydrology*, *571*, 322–331. https://doi.org/10.1016/J.JHYDROL.2019.01.043

Ikenoue, T., Shimadera, H., & Kondo, A. (2020). Impact of soil erosion potential uncertainties on numerical simulations of the environmental fate of radiocesium in the Abukuma River basin. *Journal of Environmental Radioactivity*, *225*(April), 106452. https://doi.org/10.1016/j.jenvrad.2020.106452

Japan Meteorological Agency (JMA). (n.d.). *Meteorological Observatories and Automated Meteorological Data Acquisition System (AMeDAS)*. https://www.data.jma.go.jp/gmd/risk/obsdl/

Johnes, P. J. (1996). Hydrology Evaluation and management of the impact of land use change on the nitrogen and phosphorus load delivered to surface waters: the export coefficient modelling approach. *Journal of Hydrology*, *183*, 323–349. https://doi.org/https://doi.org/10.1016/0022-1694(95)02951-6

Kojiri, T. (2006). Hydrological River Basin Environment Assessment Model (Hydro-BEAM). In V. Singh & D. K. Frevert (Eds.), *Watershed Models* (pp. 613–626). Taylor & Francis Group.

Kojiri, T., Hamaguchi, T., & Ode, M. (2008). Assessment of global warming impacts on water resources and ecology of a river basin in Japan. *Journal of Hydro-Environment Research*, *1*(3–4), 164–175. https://doi.org/10.1016/j.jher.2008.01.002

Kojiri, T., & Park, J. H. (2002). Integrated river basin environment assessment on water quantity and quality by considering utilization processes. *Proceedings of the International Conference on Water Resources and Environment Research*, 397–401.

Kutner M.H, Nachtseim C.J., Neter J., & Li W. (2005). Chapter 11 Building the Regression Model III: Remedial Measures. In *Applied Linear Statistical Models* (5th Edition, pp. 421–480). McGraw Hill Irwin.

Liao, Y., He, J., Su, B., Dou, J., Xu, Y., & Li, L. (2021). Validation of an in-situ observation method for nonpoint source pollution in paddy fields: A case study of a Beijing paddy field. *Water (Switzerland)*, *13*(22). https://doi.org/10.3390/w13223235

Ministry of Land Infrastructure Transport and Tourism of Japan (MLIT). (MLIT - 1). *National Land-Numerical Information System*. https://nlftp.mlit.go.jp/ksj/index.html

Ministry of Land Infrastructure Transport and Tourism of Japan (MLIT). (MLIT - 2). *Water Information System*. http://www1.river.go.jp/

Moriasi, D. N., Arnold, J. G., Van Liew, M. W., Bingner, R. L., Harmel, R. D., & Veith, T. L. (2007). Model Evaluation Guidelines for Systematic Quantification of Accuracy in Watershed Simulations. *Transactions of the ASABE American Society of Agricultural and Biological Engineers*, *50*(3), 885–900. https://doi.org/10.13031/2013.23153

Nukazawa, K., Kihara, K., & Suzuki, Y. (2017). Negligible contribution of reservoir dams to organic and inorganic transport in the lower Mimi River, Japan. *Journal of Hydrology*, *555*, 288–297. https://doi.org/10.1016/j.jhydrol.2017.10.020

Riemersma, S., Little, J., Ontkean, G., & Moskal-Hebert, T. (2006). Phosphorus sources and sinks in watersheds: A review. In *Alberta Soil Phosphorus Limits Project Volume 5: Background information and reviews* (Vol. 5). https://www1.agric.gov.ab.ca/$department/deptdocs.nsf/all/sag11864/$FILE/vol-5-watershed-review.pdf

Shrestha, S., Kazama, F., Newham, L. T. H., Babel, M. S., Clemente, R. S., Ishidaira, H., Nishida, K., & Sakamoto, Y. (2008). Catchment scale modelling of point source and nonpoint source pollution loads using pollutant export coefficients

determined from long-term in-stream monitoring data. *Journal of Hydro-Environment Research*, *2*(3), 134–147. https://doi.org/10.1016/j.jher.2008.05.002

Wang, J., Shao, J., Wang, D., Ni, J., & Xie, D. (2015). Simulation of the dissolved nitrogen and phosphorus loads in different land uses in the Three Gorges Reservoir Region - Based on the improved export coefficient model. *Environmental Sciences: Processes and Impacts*, *17*(11), 1976–1989. https://doi.org/10.1039/c5em00380f

Wang, M., Chen, L., Wu, L., Zhang, L., Xie, H., & Shen, Z. (2022). Review of Nonpoint Source Pollution Models: Current Status and Future Direction. In *Water (Switzerland)* (Vol. 14, Issue 20). MDPI. https://doi.org/10.3390/w14203217

Wang, W., Chen, L., & Shen, Z. (2020). Dynamic export coefficient model for evaluating the effects of environmental changes on nonpoint source pollution. *Science of the Total Environment*, *747*. https://doi.org/10.1016/j.scitotenv.2020.141164

Yang, X., Tan, L., He, R., Fu, G., Ye, J., Liu, Q., & Wang, G. (2017). Stochastic sensitivity analysis of nitrogen pollution to climate change in a river basin with complex pollution sources. *Environmental Science and Pollution Research*, *24*(34), 26545–26561. https://doi.org/10.1007/s11356-017-0257-y

Yang, Y. Y., & Toor, G. S. (2018). Stormwater runoff driven phosphorus transport in an urban residential catchment: Implications for protecting water quality in urban watersheds. *Scientific Reports*, *8*(1), 1–10. https://doi.org/10.1038/s41598-018-29857-x

Chapter 3 - Seasonal Study of the Kako River discharge dynamics into Harima Nada using a coupled atmospheric-marine model

3.1 Introduction

All human activities have some environmental influence in coastal areas, regardless of whether they are performed inland or on the shoreline (Powell et al., 2019; Stein et al., 2013), but the most significant deterioration issues are closely related to the economic growth and development of a country or region (Elliff & Kikuchi, 2015; Horstman et al., 2009; Stein et al., 2013). For this reason, during past decades, extensive efforts in preventing, remediating, and promoting good practices for river watershed management and coastal protection have developed worldwide (Barbier et al., 2008; Bayraktarov et al., 2016; Powell et al., 2019).

As was previously detailed in Chapter 1, Harima Nada is a shallow basin of the Seto Inland Sea with present oligotrophication problems and is easily affected by river discharges. The Kako River is the major contributor of fresh water and inland nutrients to the entire region (Harada & Tanda, 2011; Pintos Andreoli et al., 2021; Yoshida et al., 2010) as it was shown in Chapter 3, one of the reasons why a better understanding of its dynamics is essential to define the biogeochemical process that affect Harima Nada.

In this chapter, to numerically evaluate the Kako River dynamics and nutrient distribution in Harima Nada, a coupled atmospheric-marine model was developed using the Coupled Ocean-Atmospheric-Wave-Sediment-Transport (COAWST) Modeling System developed by the United States Geological Survey (Warner, Armstrong, et al., 2010; Warner et al., 2008). The atmospheric (WRF – Weather Research and Forecasting Model) and ocean (ROMS – Regional Ocean Modeling System) components of COAWST were coupled to reproduce the conditions in the entire Seto Inland Sea. Several inert tracer simulations were forced from the Kako River estuary to study seasonal water distribution and circulation patterns, mean residence times, and surface water age in Harima Nada as the first step in determining essential parameters to define and characterize the biogeochemical processes of the region necessary for the development of a high-resolution biogeochemical model of these characteristics for the area.

3.2 Methodology

3.2.1 The models

The COAWST model system was developed to help with the assessment of coastal processes and changes derived from natural disasters or extreme meteorological events (Warner et al., 2008, 2010), and it combines multiple high-resolution models and tools that allow the user to develop single or coupled applications. This work used ROMS v 3.9 (Rutgers), WRF Model v 4.2.2, and the Model Coupling Tool (MCT) v 2.6.0 distributed with version 3.7 of COAWST. Additionally, to simulate the Kako River discharge in the estuary, results from the hydrological model described in Chapter 2, section 2.3.1 were used.

3.2.1.1 The Atmospheric Model

The WRF Model (Skamarock et al., 2005) is a 3D terrain-following model widely used for atmospheric research and weather forecast applications because of its extensive range of horizontal and vertical resolutions. WRF applications can be configured and personalized to predict atmospheric variables such as wind momentum components, dew point, air temperature, relative humidity, long and shortwave radiative fluxes, etc., on a sigma-pressure coordinated grid. The WRF Model distributed with COAWST has a modified algorithm for bottom roughness when computing bottom stress over the ocean to include the effect of waves (Warner, Armstrong, et al., 2010).

3.2.1.2 The Marine Model

ROMS is a free-surface terrain-following model system based on using a combination of specially adjusted time-stepping algorithms for solving the 3D Reynolds-averaged Navier-Stokes equations by hydrostatic approximations (Haidvogel et al., 2008; Shchepetkin & Mcwilliams, 1998; Shchepetkin & McWilliams, 2003, 2005). ROMS allows the personalization of many model options for boundary conditions, turbulence models, advection scheme algorithms, biological models, etc., and has an adjoint model for computing model inverses and data assimilation. Like the WRF Model, the ROMS version distributed with COAWST is modified to allow grid refinement based on a composed grid

formulation approach (Warner, Armstrong, et al., 2010; Warner, Rockwell Geyer, et al., 2010).

3.2.2 Model configuration and data sets

The period of the simulations was from March 2010 to February 2011, and it was seasonally split as: March–May (Spring), June-August (summer), September -November (autumn), and December – February (winter). Spin-up lasted eight months for WRF and ROMS models and twelve months for river simulations.

WRF's domain was designed to cover Central and West Japan with a horizontal resolution of 6.0 km and a grid that extended 120 cells N-S and W-E, respectively (Fig. 19 - a). The physic options were defined the same as in Chatani et al. (2020), and 30 sigma-pressure coordinated layers were chosen from the surface to 100 hPa. Boundary conditions and forcing data used corresponded to ERA5, the fifth-generation European Center for Medium-Range Weather Forecast (ECMWF) reanalysis (Hersbach et al., 2023).

The ROMS domain was chosen to cover the entire Seto Inland Sea, and it was extended around 60 km from the Bungo Channel into the Pacific Ocean. ROMS' domain was centered in the WRF Model domain, 32 layers were defined in the vertical direction, and a horizontal resolution of 3.0 km, covering 100 cells in the N-S direction and 200 in the E-W, was chosen (Fig. 19 – a). Three-dimensional momentum, temperature, and salinity were configured to follow a nudged-open boundary condition following the radiation approach proposed by Orlanski (1976). Datasets from the Hybrid Coordinate Ocean Model (HYCOM)(Metzger et al., 2017; Naval Research Laboratory, 2021) were used to define 3D boundary conditions, initial conditions, and climatological fields. The 2D tidal boundary conditions were estimated by extracting the harmonic components from the barotropic tide model TPXO9 Atlas v.5 (Egbert & Erofeeva, 2002) for the entire Seto Inland Sea. Because of the chosen coupled configuration, the additional meteorological fields needed to force ROMS were forced from WRF Model results.

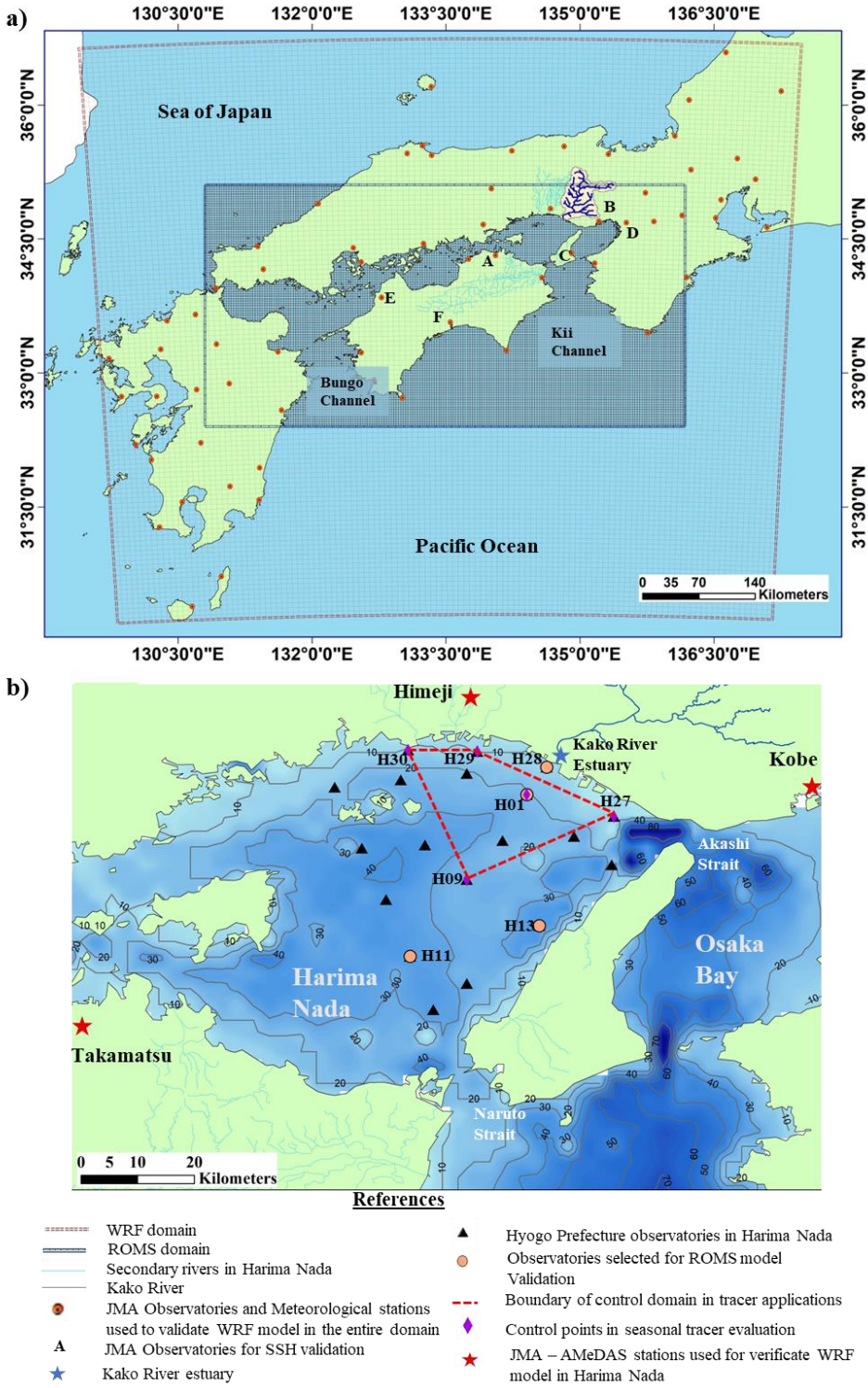

Fig. 19 - Calculation domains for WRF and ROMS (a) and Harima Nada region. JMA stations selected for sea surface height (SSH) evaluation are A) Takamatsu, B) Kobe, C) Sumoto, D) Osaka, E) Matsuyama, and F) Kochi

Ten rivers directly discharge into Harima Nada waters, and the most important river from Shikoku Island, the Yoshino River, is next to the region's southern border, the Naruto Strait (Fig. 19 – b). Using the results obtained in Chapter 2 for river discharge and TN load in the Kako River, the river estuary was forced into ROMS using a vertical influx algorithm to avoid Courant-Friedrichs-Lewy ratio (CFL) violations derived from high velocities in the discharge during the rainy or typhoon seasons in Japan. In addition, because the Harima Nada region has a shallow bathymetry, and the Kako River estuary is in a shallow area (~ 10 m depth), temperature, salinity, and TN concentration were uniformly distributed in all the vertical river column.

In order to study seasonal water distribution, mean residence times, and concentration patterns in Harima Nada, two types of tracer experiments were performed. In the first experiment, an inert tracer was injected into the Kako River for the entire simulation period (including spin-up months) to study water distribution patterns. Tracer concentration was chosen for this experiment as the average Kako River TN concentration of the corresponding year (1.0 kg m^{-3}). For the second analysis, to estimate seasonal mean residence times and concentration distribution, an inert tracer with a concentration of 5.0 kg m^{-3} was injected for 24 hours during the 1st day of each season and followed for 60 days in a particular control domain. Tracer concentration was observed in the points that delimited the control domain (H09, H27, H29, and H30) and in a point in front of the estuary H01 (see Fig. 19 – b). For this analysis, it was defined that the tracer totally flushed out from the control domain when its concentration became lower than $1x10^{-6}$ kg/m^3 (three orders of magnitude smaller than the maximum concentration value discharged), which occurred for all the seasons during the first 30 – 35 days after the injection.

Seasonal mean residence times were estimated using the water age method developed by Zhang et al. (2010), which refers to the constituent-oriented age and residence time theory (Deleersnijder et al., 2001; E. Delhez et al., 2003; E. J. M. Delhez, 2006; E. J. M. Delhez et al., 1999; É. J. M. Delhez et al., 2004; É. J. M. Delhez & Deleersnijder, 2006), and uses two tracer released together to estimates the mean age of the water in a targeted area.

Table 8 – WRF and ROMS models' setup and summary of the river forcing and tracer experimental conditions

WRF model	
Analysis period	March 2010 – February 2011
Spin-up	8 months (June 2009 – February 2010)
Horizontal grid cells (X x Y)	120 x120
Horizontal resolution	6.0 km
Vertical layers	30
Time step	25 seconds
Boundary and initial conditions	ERA5
ROMS model	
Analysis period	March 2010 – February 2011
Spin-up	8 months (June 2009 – February 2010)
Horizontal grid cells (X x Y)	200 x 100
Horizontal resolution	3.0 km
Vertical layers	32
Baroclinic time step	60 seconds
Boundary and initial conditions	HYCOM
Tidal boundary conditions	TPXO9 Atlas v.5
Rivers in the domain	11 (5 northern coasts, 2 center, 4 in the southern coast)
Rivers considered for calculation	1 (Kako River, largest freshwater contribution)
River input algorithm	Volume vertical influx
River and tracer experimental conditions	
Analysis period	March 2010 – February 2011
Spin-up	12 months (March 2009 – February 2010)
Horizontal resolution	1 km
River discharge temporal resolution	1 hour
Vertical levels of the estuary	32 layers
River vertical fractional distribution (Temperature, salinity, tracer)	Homogeneous
River temperature	15 °C, constant for the entire period
River salinity	0.0 PSU
Tracer concentration	- 0.1 kg/m3 (for seasonal distribution analysis) - 0.5 kg/m3 (for mean residence time seasonal analysis)
Tracer discharge injection	- Entire period for seasonal distribution analysis - 24 hours for mean residence time in seasonal analysis

The concept of water age was chosen in this work because its significance is more critical in estimating and defining parameters for biogeochemical models than the usual residence time approach, which is more important for ecological studies. The method computes the meant tracer age by estimating the mass-weight arithmetic average time since

the tracer left the source point and the mean residence time, defined as the time needed for the tracer to leave the control domain of interest. The mean residence time is determined by this method as the relationship between the mean age of the water in a location x (α_x) and tracer concentration at the same location (C_x), as shown in Eq. 3.1. The mean residence times estimated by this method agree with the residence time (Zhang et al., 2010) despite the physical significance and calculation differences.

$$\bar{\tau} = \frac{\alpha_x}{C_x} \qquad \text{Eq. 1}$$

The model's validation and performance were evaluated using observed datasets for the period of March 2010-February 2011. Atmospheric fields were validated with AMeDAS datasets from the observatories contained in the WRF domain (JMA). The marine model was validated for sea surface temperature and salinity using monthly observed datasets from the observatories of the Hyogo Prefecture in Harima Nada (Hyogo Prefectural Technology Center for Agriculture). The sea surface height (SSH) value was also verified at some points using biweekly information from coastal observatories of the JMA (see points A, B, C, D, E, and F in Fig. 19 – a). Table 8 summarizes the WRF and ROMS models setup, river forcing, and tracers' experimental conditions used in this study.

3.3 Results and Discussion

3.3.1 Models validation

3.3.1.1 Atmospheric model validation

The location of the WRF stations used to validate the simulation results is shown in Fig. 19 – a. Because the area of interest is relatively small compared to the entire extension of the WRF model, it was chosen to separately validate the whole domain from the study area. The comparison was punctual for validating the entire domain, and datasets from different stations across it were compared with the simulation results at the same geographic point. In the case of the Harima Nada area, observed datasets from the three AMeDAS

observatories shown in Fig. 19 – b were averaged and compared with the average of the simulation results for the region.

Because of the chaotic nature of atmospheric and ocean systems, the non-linear characteristics of the processes that represent them, and the broad time scale of the processes involved in their forecasting ("Encyclopedia of Applied and Computational Mathematics," 2015), statistical analysis of the results needs some extra considerations. In the scale of time of this work, variables like temperature or atmospheric pressure can be well described by normal distributions, but others like wind direction, rain, waves, or SSH have a higher random probability distribution, and their determination is affected by more significant errors. Because of this, a set of generalized statistics was selected for the validation, and only those more suitable for the particular variable were used. The bibliography's benchmarks for wind components, temperature, and relative humidity (Emery et al., 2001; WRAP, 2013) were extended to other variables that behave similarly to assess the model's performance.

Fig. 20 shows the observed and simulated average time series for zonal (u) and meridional (v) wind components, surface pressure, temperature, and relative humidity in the Harima Nada region. High reproducibility was found for the region's zonal wind components (u-wind), temperature, relative humidity, and surface pressure. On the other hand, the model showed lower performance in simulating the meridional wind component (v-wind) and wind speed, which can be associated with the complex geography of the study area.

Table 9 – Statistical results for WRF's validated variables in the Harima Nada area

	Observed average	Simulated average	R	pBIAS	MAE	RMSE	IA
u-wind (m/s)	0.74	0.92	0.96	---	0.49	0.62	0.93
v-wind (m/s)	-0.26	-0.41	0.72	---	1.05	1.31	0.62
Wind speed (m/s)	2.9	3.2	0.80	---	0.53	0.73	0.83
Surface pressure(hPa)	1010.3	1010.5	1.0	<0.1	0.37	0.50	1.0
Temperature (°C)	---	---	0.97	0.3	0.65	0.82	0.99
Relative humidity (%)	---	---	0.97	4.1	0.48	0.64	0.99

R: Correlation; pBIAS: Percentage of BIAS; MAE: Mean absolute error; RMSE: Root mean square error; IA: Index of agreement

Benchmarks: Wind – RMSE< 2.0; 0.6 < IA
Temperature - $|pBIAS| \leq 1.0$; MAE < 2.0; 0.8 < IA
Relative humidity - |MAE| < 2.0; 0.6 < IA

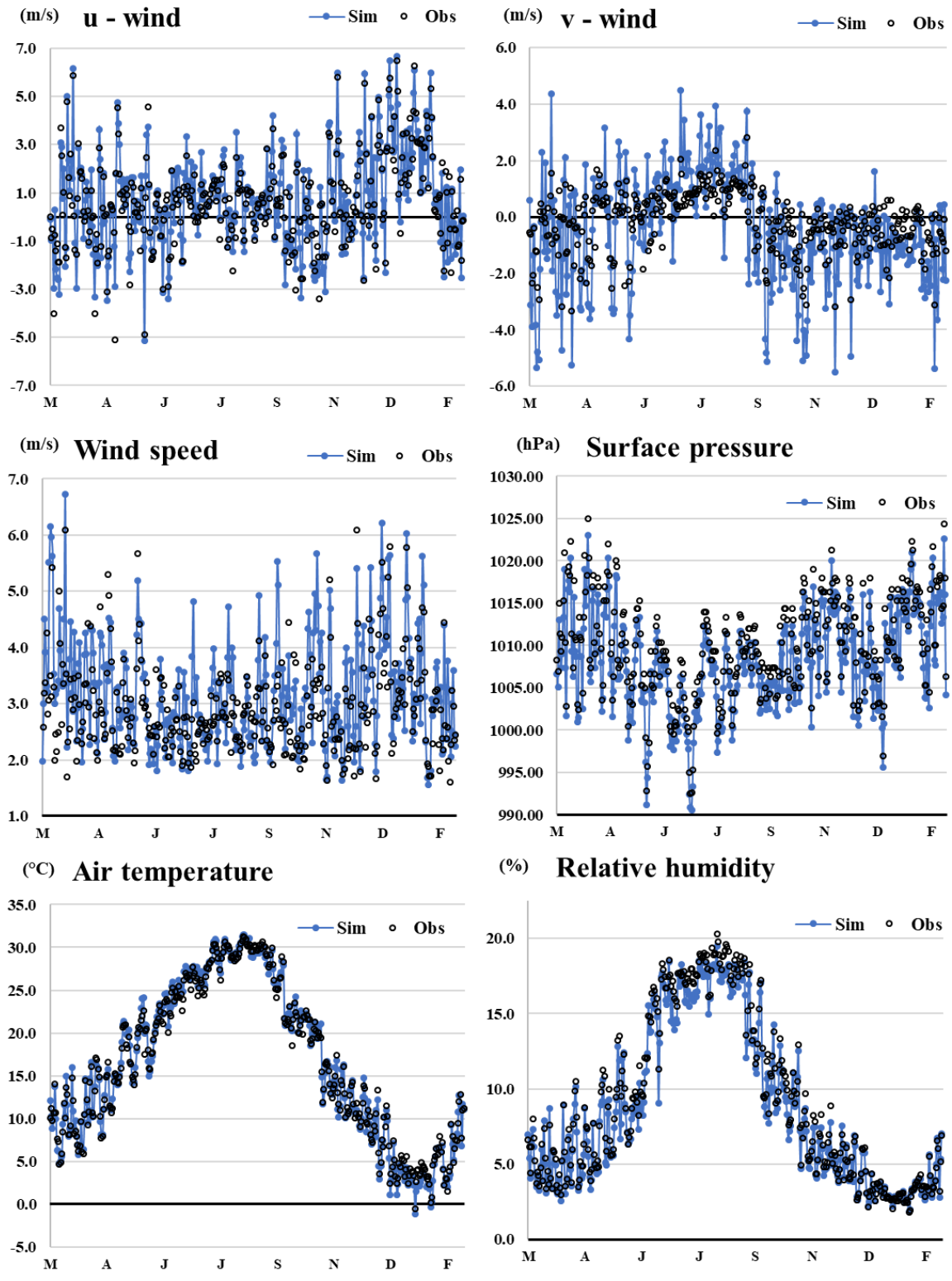

Fig. 20 - Calculated and observed meteorological average values for the Harima Nada area

In Table 9 are presented the results of the statistics used for evaluating performance and validating the WRF Model results, as well as the literature benchmarks for those variables that have them reported. For all of the selected variables (that are part of the atmospheric set of variables that force the ROMS Mosel System), good reproducibility and agreement with the reported benchmarks were found, which validated the proposed atmospheric model for the region. Monthly punctual validation for some of the stations shown in Fig. 19 - a is presented in Appendix III.

3.3.1.2 Marine model validation

Monthly and biweekly datasets were used for the marine model because of their availability. This time resolution may be unsuitable for efficiently evaluating some of the ocean variables, particularly those with high temporal variability or those strongly associated with other physical variables. In addition, the same considerations for validating the atmospheric model were taken in this case.

Validation was made punctually in the observatory stations H28, H01, H11, and H13 of the Hyogo Prefecture in Harima Nada (Fig. 19 - b). These points were selected among all the observatories because of their location and because they have time series at three different levels of depth, while for the rest of the cases observations corresponded only to the surface layer. The depth of the layers varies from point to point because of differences in the bathymetry of the region (see Table 10), and it was used as given in the observations for the comparison (Hyogo Prefectural Technology Center for Agriculture). Points H01 and H28 were selected because of their proximity to the estuary, while H11 and H13 are both far from the coast and located in the deepest area of Harima Nada.

The statistical performance results for water temperature and salinity are presented in Table 10. Regarding water temperature, the model showed high performance in reproducing the observations. Correlation coefficients and the agreement indexes were found to be close to 1 at the three depths for all the observatory stations that were considered.

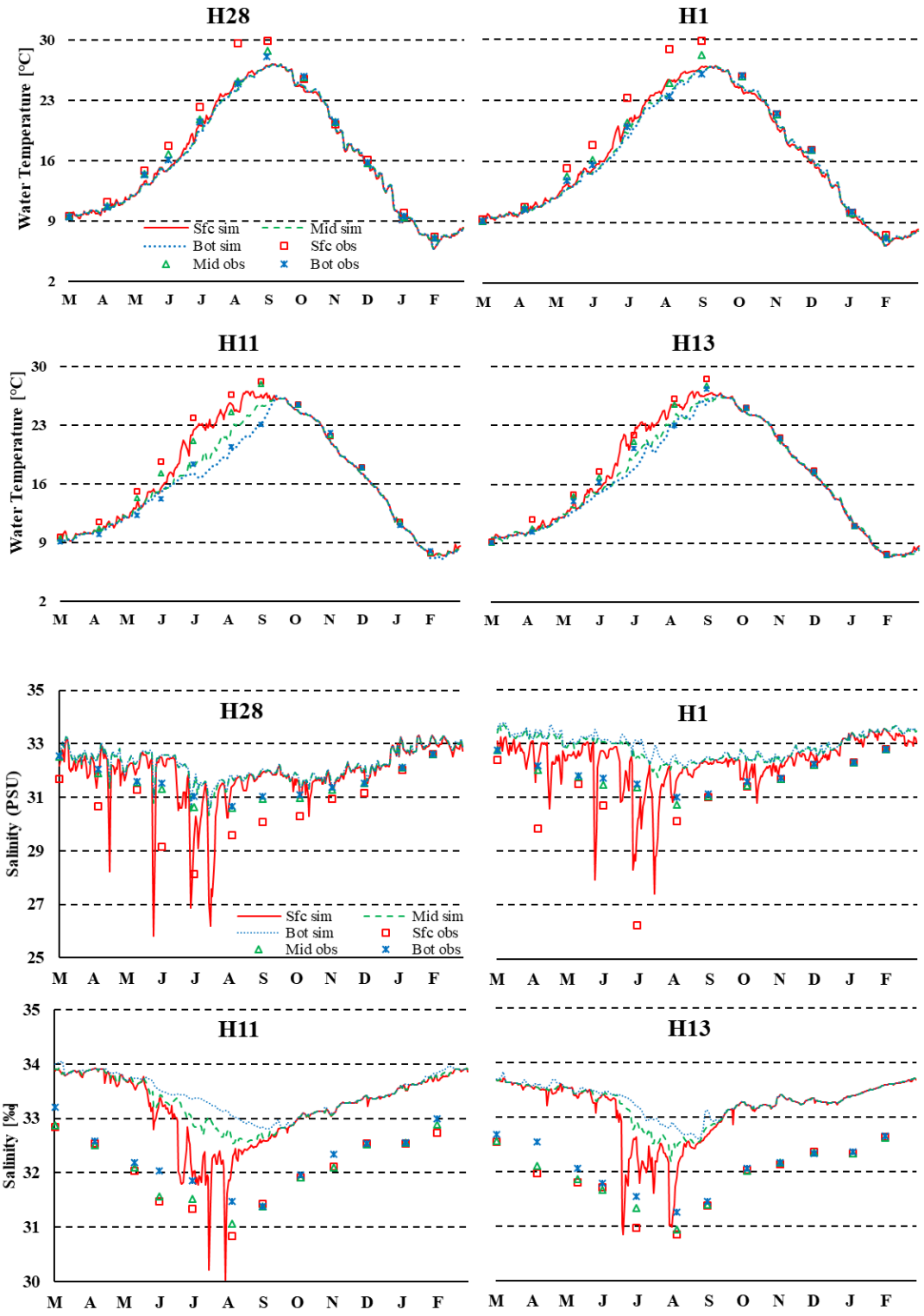

Fig. 21 - salinity and temperature at four different observatories in the Harima Nada

Positive values of pBIAS for temperature comparison showed that the model tended to underestimate water temperature, particularly in the surface layer and in the points closer to the coast during the summer months (Fig. 21), which may be a consequence of the selected model setup in the conditions for the river forcing (see Table 8). These differences were not so pronounced in the center of Harima Nada, indicating that river discharge effects are more critical and have a higher impact on the processes of the area near the shoreline.

For salinity results, the model did not show substantial problems in describing the observations, but some extra considerations in the model setup should be taken to improve the model's performance. The very enclosed geography of the study area makes it very sensitive to freshwater discharges, particularly during spring and summer (March to September) when rainy and typhoon seasons occur. The Kako River is the most important freshwater contributor to the region (Abo et al., 2018; Abo & Yamamoto, 2019), but it is not the only one, and the salinity results confirmed the importance of the other river discharges in Harima Nada. The higher variations between simulation and observations were found to be, the same as for water temperature in the surface layer, while the middle and bottom layers showed not to considerably vary and seem not to be seasonally affected, particularly in the center region (points H11 and H13), were both time series overlap.

The model overestimates salinity in the region (negative values of pBIAS and positive values of MAE) during all the seasons. The overestimation is percentage-wise small and in the order of 1 to 2 PSU units (Fig. 21), occurring more significantly in the central region (points H11 and H13), where the influence of the Kako River waters seems not to reach. These results reinforced the idea of larger amounts of freshwater (or with lower salinity) entering the study region and affecting salinity in the central part. Correlation values were good at all the observatories, indicating that the trends are well reproduced at the considered levels. The agreement indexes showed to be acceptable near the coast (H01 and H28), but the performance and reproducibility are lower in the central area, where the differences between observations and simulation results are more prominent due to the reasons previously mentioned.

Table 10 – Statistical results for ROMS' validated variables in the Harima Nada area

Temperature

		R	pBIAS	MAE	RMSE	IA
H01	sfc (~0.5 m)	0.99	9.4	-1.71	2.05	0.98
	mid (~10.0 m)	1.00	6.1	-1.04	1.48	0.99
	bott (~20.0 m)	1.00	4.2	-0.70	0.88	1.00
H28	sfc (0.5 m)	0.99	8.6	-1.54	1.97	0.98
	mid (~5.0m)	1.00	5.3	-0.90	1.09	0.99
	bott (~10.0m)	1.00	4.3	-0.72	0.86	1.00
H11	sfc (~0.5m)	1.00	5.4	-0.98	1.24	0.99
	mid (~10.0m)	0.99	6.5	-1.13	1.49	0.99
	bott (~32.0m)	0.99	1.6	-0.25	0.71	1.00
H13	sfc (0.5m)	0.99	3.5	-0.62	0.97	0.99
	mid (~10.0m	1.00	4.4	-0.76	1.08	0.99
	bott (~32.0m)	0.99	3.7	-0.63	1.02	0.99

Salinity

		Observed average (PSU)	Simulated average (PSU)	R	pBIAS	MAE	RMSE	IA
H01	sfc (~0.5 m)	31.0	32.3	0.90	-4.2	1.30	1.62	0.71
	mid (~10.0 m)	31.8	32.9	0.83	-3.4	1.07	1.48	0.61
	bott (~20.0 m)	31.9	33.0	0.78	-3.4	1.07	1.12	0.56
H28	sfc (0.5 m)	30.6	31.8	0.76	-3.9	1.20	1.44	0.71
	mid (~5.0m)	31.5	32.2	0.82	-2.2	0.71	0.81	0.71
	bott (~10.0m)	31.6	32.2	0.81	-2.0	0.63	0.73	0.72
H11	sfc (~0.5m)	32.0	33.2	0.84	-3.6	1.16	1.21	0.54
	mid (~10.0m)	32.1	33.3	0.86	-3.9	1.24	1.27	0.50
	bott (~32.0m)	32.3	33.5	0.83	-3.7	1.19	1.23	0.48
H13	sfc (0.5m)	31.9	33.2	0.91	-4.0	1.27	1.29	0.47
	mid (~10.0m	31.9	33.4	0.89	-4.5	1.45	1.48	0.41
	bott (~32.0m)	31.0	31.0	0.87	-4.0	1.28	1.31	0.40

R: Correlation; pBIAS: Percentage of BIAS; MAE: Mean absolute error; RMSE: Root mean square error; IA: Index of agreement
Average values for water temperature are not shown for their strong seasonal variability

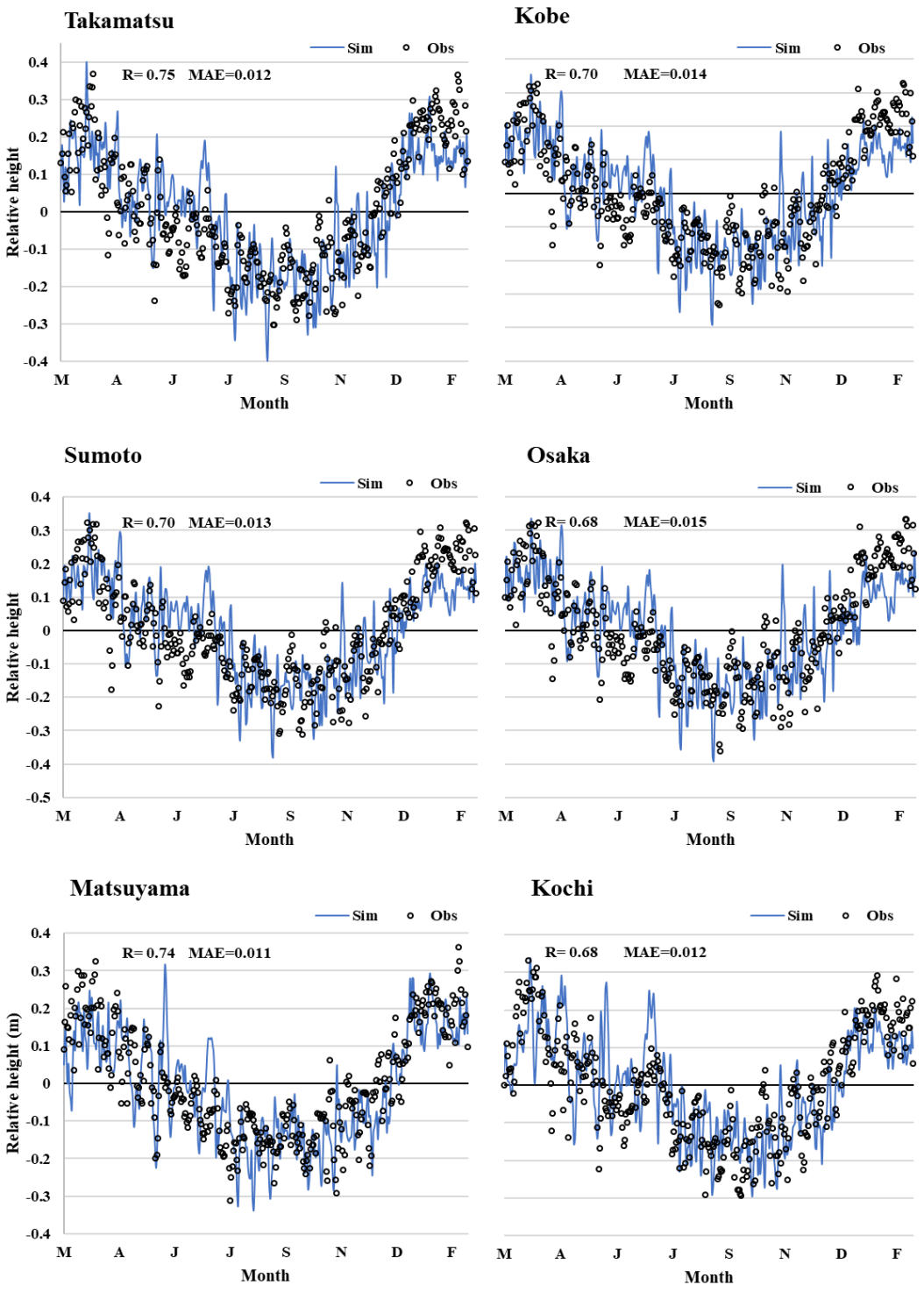

Fig. 22 - Comparison of relative SSH values with respect to the annual average and their correlation(R) and mean average errors (MAE) in different JMA coastal observatories inside the ROMS domain

The analysis of the relative SSH was conducted in the stations from A to F, shown in Fig. 19 – a. The comparison showed that the model and its configuration can effectively reproduce trends for the area (R~0.7) with errors that are in the order of 10 to 15%. The simulation of waves has implicit difficulties because of the geophysical processes involved, and it is strongly dependent on the geography or the study site, which is extremely complex in this case. For this reason, performance was considered sufficiently good in this first approach at the horizontal resolution of the study.

3.3.2 The Kako River discharge dynamics

Fig. 26 shows the seasonal averages of concentration and horizontal velocity in the Harima Nada region obtained from the first tracer simulations at the surface and 10m depth. Daily concentration and horizontal velocity component values are presented in Fig. A3.1 in Appendix III. The results agreed with the global water circulation of the Seto Inland Sea and the study area (W-E), showing that water enters into Harima Nada mostly from the Bisan Starit, and the outflux occurs mainly in the Akashi Strait (towards Osaka Bay), and the Naruto Strait (towards the Kii Channel).

Significant seasonal differences were found in the water distribution and the circulation patterns in Harima Nada. These differences are substantially more noticeable in the central region of Harima Nada, where the maximum average values for the magnitude of the speed occur during summer (Fig. 23 – B1 and Fig. A3.1 – H09), reaching values as high as 0.3 m/s, while in the rest of the months is around 20% lower. In the rest of Harima Nada, the magnitude of the speed does not seem to vary much seasonally. The most noticeable changes in circulation patterns seem to occur in summer and winter for the entire study area, when the highest and lowest river discharges occur, respectively. During summer, the high velocities and the circular patterns that occur in the central area promote vertical mix at all the levels to a more considerable extent than the rest of the seasons (Fig. 23). During the months of winter, the circulation is strongly driven from W-E in the entire area, particularly the northern coast, where during the other seasons tends to be E-W.

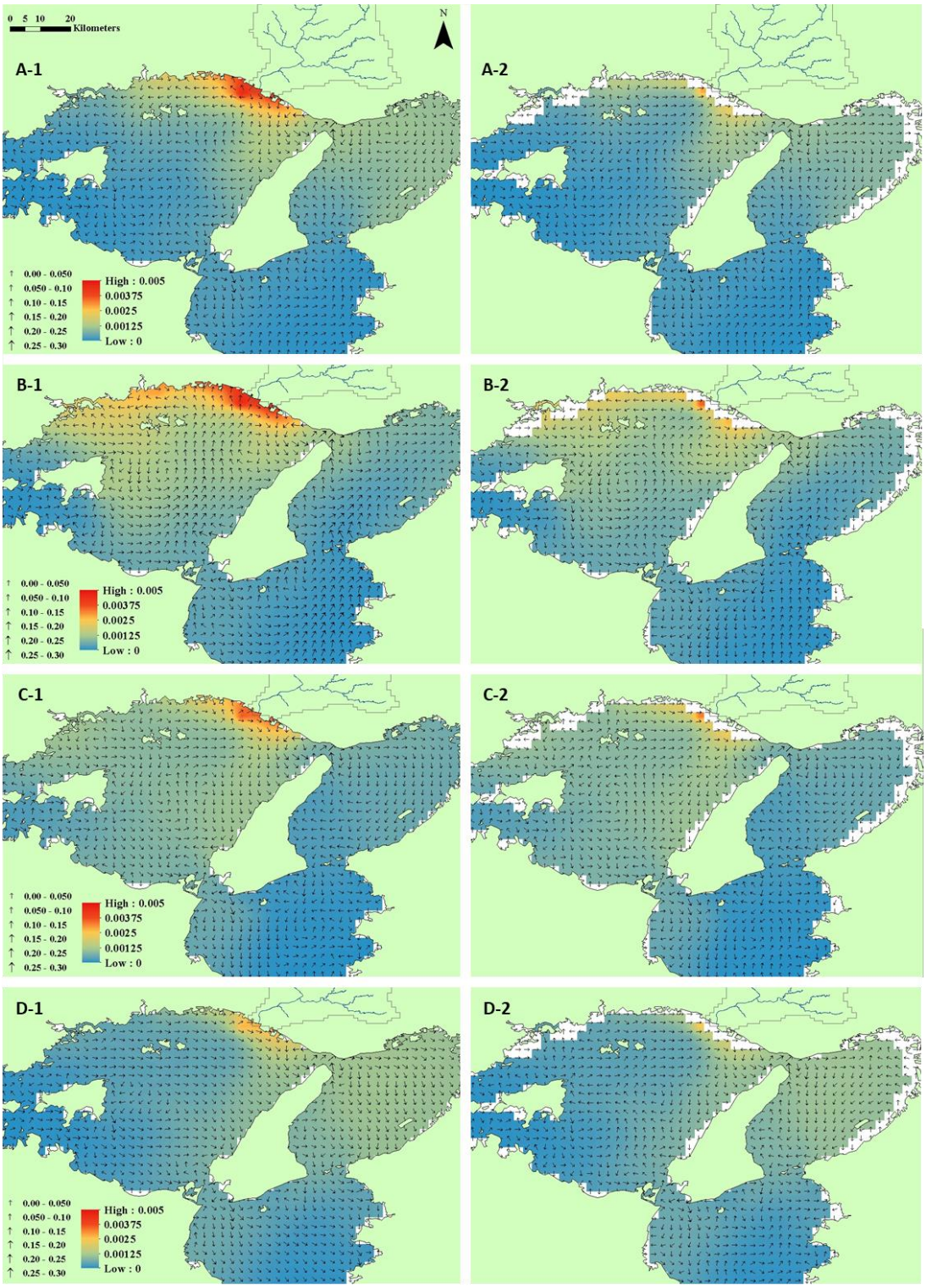

Fig. 23 - Seasonal tracer distribution and average horizontal velocity in Harima Nada at the surface (1) and 10 m layers (2). The white areas in the 10 m layer correspond to places of lower bathymetry

The tracer tends to distribute from the Kako River towards the west-northern coasts from spring to fall, following the global pattern of the horizontal velocities. The maximum dispersion occurs the same as the more noticeable changes in the circulation pattern during the months of summer and winter. This seasonal tracer distribution agrees with the observed data analysis of many environmental variables monitored in the region, which shows that the higher concentrations of nutrients and biomass production seasonally occur over the west-northern area during spring and summer (Japanese Ministry of Environment). During spring, tracer distributes primarily centered in the Kako River estuary on the direction of the coast, but in summer, the divergence of horizontal velocities promotes its dispersion and mix towards the center and the west-northern shoreline. In autumn, when the differences in water temperature seem to promote convection mechanisms, the tracer tends to distribute more homogeneously, and its concentration becomes lower than for the rest of the seasons in the entire Harima Nada. This situation changes in winter again, when the river discharge is the lowest, and the Kako River waters are dispersed towards Osaka Bay.

The same analysis at 10 m depth (second column in Fig. 23) found that the trend in circulation patterns and tracer distribution was mainly maintained. Concentration values and the magnitude of the horizontal speed decreased from one layer to the other. While in the surface layer concentration has a maximum value of 5x10-3 kg/m^3, at 10 m depth, the maximum values were in the order of 30% lower. Regarding the magnitude of the horizontal speed, values were found to be around 20% lower at 10 m than on the surface.

In Fig. 24, the daily concentration and remaining tracer fraction results from the second type of tracer experiments were seasonally plotted on the points that define the control domain and H01. Table 11 summarizes the results of the seasonal mean residence times, the maximum values for concentration, the location in the control domain, and the days necessary to reach the peak in concentration. The results showed that the calculated mean residence times correspond with the tracer's temporal distribution (Fig. 24). The higher mean residence times occur during spring and winter (28 and 25 days, respectively) when the water temperature is lower and circulates slower (see Fig. 21 and Fig. A3.1). The mean residence time in summer is 20 days (30% lower than in spring), and it was found to be 12 days (the

lowest) in autumn. It was found that the lower peaks in concentration also occur during spring and winter. In summer, the concentration peak becomes the highest due to a more significant load of tracer discharged because of the increase in rivers' streamflow. Also, the changes in the circulation pattern promote horizontal mixing and the dispersion of Kako River waters towards the west-northern coast and the entire Harima Nada. In autumn, vertical mechanisms promote the faster dilution of the tracer, which is also accompanied by surface winds of E-S direction, contributing to the horizontal dispersion in the entire area.

Table 11 – Results of 60 days of seasonal tracer simulations in Harima Nada at the surface layer

	Spring	Summer	Fall	Winter
Mean residence time (days)	28	20	12	25
Maximum concentration (kg/m3)	2.4 $x10^{-3}$	5.0 $x10^{-3}$	4.4 $x10^{-3}$	3.3 $x10^{-3}$
Location and days where the concentration peak is reached last	H09 9 days	H09 23 days	H30 8 days	H09 Never

From the results presented in Fig. 24, it was found that for the points located in the eastern and central part of Harima Nada (H27 and H09, respectively), the concentration of tracer was the lowest at all the seasons in around one order of magnitude when comparing it with the western points of the control domain (H29 and H30), which can also be seen in the seasonal distribution patterns of Fig.23. The tracer concentration was the lowest at all the seasons in the central part of Harima Nada (H09), with concentrations that vary in the range of $1x10^{-4}$ kg/m^3 during summer, to a minimum of 0.0 kg/m^3 in winter. It was also observed for point H09 that the maximum seasonal concentrations have a range of time distributions from five to ten days in fall and spring to twenty days in summer, while no tracer is detected in winter. At point H27, on the eastern side of Harima Nada, the maximum concentration occurred in winter. This point also showed the higher time distribution for the remaining fraction of tracer during winter, confirming that it is the season in which more river waters reach the area. In addition, maximum concentration peaks appeared between the 4^{th} and 7^{th} day in all the seasons, and the concentration and ratio contribution patterns have a similar trend for the seasons of cold (winter and spring) and warm (summer and fall) waters.

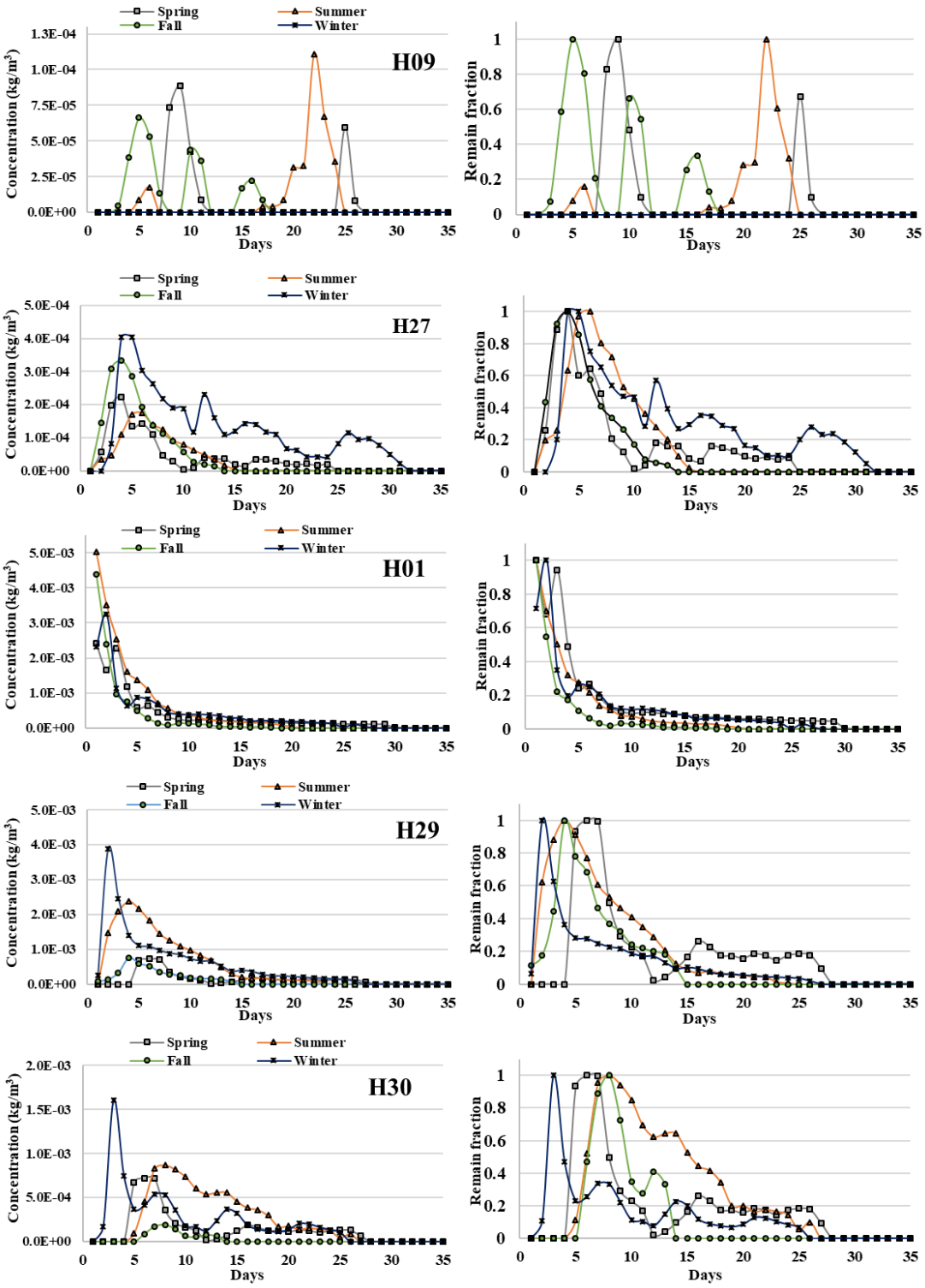

Fig. 24 - Tracer concentration and remain fraction values at the surface layer for different points of the control domain

For the point located next to the river estuary (H01), the higher concentrations tend to occur in summer and fall (~5.0x10-3 kg/m^3). At this point, the maximum concentration peaks are reached in one to two days, and the remaining tracer fractions showed the shortest seasonal time distribution. The western boundary points of the control domain (H29 and H30) reached the peaks of higher concentration in winter (two to three days). Concentration patterns were found to have the same trend in cold and warm water seasons, same as for point H27, but for the farther point from the Kako River estuary H30, the concentration showed to be in the order of three times smaller than for H29. The time distribution of the remaining tracer fraction was also found to be broader in H30 than in H29 for all the seasons except autumn.

3.4 Conclusions

A coupled atmospheric-marine model based on COAWST was successfully developed for the Seto Inland Sea region. The model showed high performance in reproducing atmospheric variables punctually and for the area of Harima Nada and was successfully validated. In the case of the marine model, performance was also evaluated, and showed to be good in reproducing water temperature, salinity, and SSH, but model setup conditions need to be adjusted to increase the model's performance, particularly at the surface layer. Results showed that the developed model could effectively describe the regional circulation patterns in the Seto Inland Sea and Harima Nada, and they adjust to the seasonal biomass production of the study area. Seasonal differences were found in circulation patterns and the distribution of Kako River waters in Harima Nada. These differences also extended to the seasonal mean residence times, ranging from a month in spring, to less than two weeks in autumn. No significant differences were found in water distribution and circulation patterns with depth, which can be a consequence of the shallow bathymetry of the region.

References – Chapter 3

Abo, K., Satoshi, A., Kazuhiro, H., Yoshiki, N., Hayashi, H., Murata, K., Wanishi, A., Ishikawa, Y., Masui, T., Nishikawa, S., Yamada, K., Noda, M., & Tokumitsu, S. (2018). Long-Term Variations in Water Quality and Causal Factors in the Seto Inland Sea , Japan. Bulletin on Coastal Oceanography (in Japanese, English Abs.), 55(2), 2101–2111.

Abo, K., & Yamamoto, T. (2019). Oligotrophication and its measures in the Seto Inland Sea , Japan. Bulletin of Japan Fisheries Research and Education Agency, 49, 1–6. http://www.fra.affrc.go.jp/bulletin/bull/bull49/49-0504.pdf

Barbier, E. B., Koch, E. W., Silliman, B. R., Hacker, S. D., Wolanski, E., Primavera, J., Granek, E. F., Polasky, S., Aswani, S., Cramer, L. A., Stoms, D. M., Kennedy, C. J., Bael, D., Kappel, C. V., Perillo, G. M. E., & Reed, D. J. (2008). Coastal ecosystem-based management with nonlinear ecological functions and values. Science, 319(5861), 321–323. https://doi.org/10.1126/science.1150349

Bayraktarov, E., Saunders, M. I., Abdullah, S., Mills, M., Beher, J., Possingham, H. P., Mumby, P. J., & Lovelock, C. E. (2016). The cost and feasibility of marine coastal restoration. Ecological Applications, 26(4), 1055–1074. https://doi.org/10.1890/15-1077

Chatani, S., Shimadera, H., Itahashi, S., & Yamaji, K. (2020). Comprehensive analyses of source sensitivities and apportionments of PM2.5 and ozone over Japan via multiple numerical techniques. Atmospheric Chemistry and Physics, 20(17), 10311–10329. https://doi.org/10.5194/acp-20-10311-2020

Comprehensive Water Quality Survey, 2019. Ministry of the Environment, Japan. https://water-pub.env.go.jp/water-pub/mizu-site/mizu/kouiki/dataMap.asp

Deleersnijder, E., Campin, J.-M., & Delhez, E. J. M. (2001). The concept of age in marine modelling I. Theory and preliminary model results. In Journal of Marine Systems (Vol. 28). https://doi.org/https://doi.org/10.1016/S0924-7963(01)00026-4

Delhez, E., Deleersnijder, E., Mouchet, A., & Beckers, J.-M. (2003). A note on the age of radioactive tracers. https://doi.org/https://doi.org/10.1016/S0924-7963(02)00245-2

Delhez, E. J. M. (2006). Transient residence and exposure times. Ocean Science, 2, 1–9. https://doi.org/https://doi.org/10.5194/os-2-1-2006

Delhez, E. J. M., Campin, J.-M., Hirst, A. C., & Deleersnijder, E. (1999). Toward a general theory of the age in ocean modelling. https://doi.org/https://doi.org/10.1016/S1463-5003(99)00003-7

Delhez, É. J. M., & Deleersnijder, É. (2006). The boundary layer of the residence time field. Ocean Dynamics, 56(2), 139–150. https://doi.org/10.1007/s10236-006-0067-0

Delhez, É. J. M., Heemink, A. W., & Deleersnijder, É. (2004). Residence time in a semi-enclosed domain from the solution of an adjoint problem. Estuarine, Coastal and Shelf Science, 61(4), 691–702. https://doi.org/10.1016/j.ecss.2004.07.013

Egbert, G. D., & Erofeeva, S. Y. (2002). Efficient Inverse Modeling of Barotropic Ocean Tides. Journal of Atmospheric and Oceanic Technology, 19(2), 183–204. https://doi.org/https://doi.org/10.1175/1520-0426(2002)019%3C0183:EIMOBO%3E2.0.CO;2

Elliff, C. I., & Kikuchi, R. K. P. (2015). The ecosystem service approach and its application as a tool for integrated coastal management. In Natureza e Conservacao (Vol. 13, Issue 2, pp. 105–111). Elsevier. https://doi.org/10.1016/j.ncon.2015.10.001

Emery, C., Tai, E., & Yarwood, G. (2001). Enhanced Meteorological Modeling and Performance Evaluation for Two Texas Ozone Episodes. https://www.tceq.texas.gov/assets/public/implementation/air/am/contracts/reports/mm/EnhancedMetModelingAndPerformanceEvaluation.pdf

Encyclopedia of Applied and Computational Mathematics. (2015). In Encyclopedia of Applied and Computational Mathematics. Springer Berlin Heidelberg. https://doi.org/10.1007/978-3-540-70529-1

Haidvogel, D. B., Arango, H., Budgell, W. P., Cornuelle, B. D., Curchitser, E., Di Lorenzo, E., Fennel, K., Geyer, W. R., Hermann, A. J., Lanerolle, L., Levin, J., McWilliams, J. C., Miller, A. J., Moore, A. M., Powell, T. M., Shchepetkin, A. F., Sherwood, C. R., Signell, R. P., Warner, J. C., & Wilkin, J. (2008). Ocean forecasting in terrain-following coordinates: Formulation and skill assessment of the Regional Ocean Modeling System. Journal of Computational Physics, 227(7), 3595–3624. https://doi.org/10.1016/j.jcp.2007.06.016

Harada, K., & Tanda, M. (2011). Influence of the changes of the load inflow total nitrogen (TN) from rivers of Harima area in Hyogo Prefecture to the dissolved inorganic nitrogen (DIN) in Harima-nada. Bull. Hyogo Pref, Tech. Cent Agr. Forest. Fish. (Fish. Sec) (in Japanese), 42, 87–91.

Hersbach, H., Bell, B., Berrisford, P., Biavati, G., Horányi, A., Muñoz Sabater, J., Nicolas, J., Peubey, C., Radu, R., Rozum, I., Schepers, D., Simmons, A., Soci, C., Dee, D., & Thépaut, J.-N. (n.d.). ERA5 hourly data on single levels from 1940 to present. Copernicus Climate Change Service (C3S) Climate Data Store (CDS). 2023. Retrieved August 28, 2023, from https://cds.climate.copernicus.eu/cdsapp#!/dataset/reanalysis-era5-single-levels?tab=overview

Horstman, E. M., Wijnberg, K. M., Smale, A. J., & Hulscher, S. J. M. H. (2009). On the consequences of a long-term perspective for coastal management. Ocean and Coastal Management, 52(12), 593–611. https://doi.org/10.1016/j.ocecoaman.2009.08.009

Hyogo Prefectural Technology Center for Agriculture, F. and F. (n.d.). Harima Nada observatories. Https://Www.Hyogo-Suigi.Jp/Gj/.

Japan Meteorological Agency (JMA). (n.d.). Meteorological Observatories and Automated Meteorological Data Acquisition System (AMeDAS). https://www.data.jma.go.jp/gmd/risk/obsdl/

Metzger, E. J., Helber, R. W., Hogan, P. J., Posey, P. G., Thoppil, P. G., Townsend, T. L., Wallcraft, A. J., Smedstad, O. M., & Franklin, D. S. (2017). Global Ocean Forecast System 3.1 Validation Testing. https://www7320.nrlssc.navy.mil/pubs/2017/metzger-2017.pdf

Naval Research Laboratory. (2021). HYCOM - Hybrid Coordinate Ocean Model . https://www.hycom.org/dataserver/gofs-3pt1/analysis

Orlanski, I. (1976). A Simple Boundary Condition for Unbounded Hyperbolic Flows. In JOURNAL. OF COMPUTATIONAL PHYSICS (Vol. 21). https://doi.org/https://doi.org/10.1016/0021-9991(76)90023-1

Pintos Andreoli, V., Mori, M., Koga, Y., Shimadera, H., Suzuki, M., Matsuo, T., & Kondo, A. (2021). Numerical Assessment of Total Nitrogen (Tn) Load Discharged from Rivers into Harima-Nada, the Seto Inland Sea, Using A Numerical Coupled Hydrological-Water Quality Model. IOP Conference Series: Earth and Environmental Science, 801(1). https://doi.org/10.1088/1755-1315/801/1/012009

Powell, E. J., Tyrrell, M. C., Milliken, A., Tirpak, J. M., & Staudinger, M. D. (2019). A review of coastal management approaches to support the integration of ecological and human community planning for climate change. Journal of Coastal Conservation, 23(1), 1–18. https://doi.org/10.1007/s11852-018-0632-y

Shchepetkin, A. F., & Mcwilliams, J. C. (1998). Quasi-Monotone Advection Schemes Based on Explicit Locally Adaptive Dissipation. https://doi.org/https://doi.org/10.1175/1520-0493(1998)126%3C1541:QMASBO%3E2.0.CO;2

Shchepetkin, A. F., & McWilliams, J. C. (2003). A method for computing horizontal pressure-gradient force in an oceanic model with a nonaligned vertical

coordinate. Journal of Geophysical Research: Oceans, 108(3). https://doi.org/10.1029/2001jc001047

Shchepetkin, A. F., & McWilliams, J. C. (2005). The regional oceanic modeling system (ROMS): A split-explicit, free-surface, topography-following-coordinate oceanic model. Ocean Modelling, 9(4), 347–404. https://doi.org/10.1016/j.ocemod.2004.08.002

Skamarock, W. C., Klemp, J. B., Dudhia, J., Gill, D. O., Barker, D. M., Wang, W., & Powers, J. G. (2005). A Description of the Advanced Research WRF Version 2. https://doi.org/http://dx.doi.org/10.5065/D6DZ069T

Stein, B. A., Staudt, A., Cross, M. S., Dubois, N. S., Enquist, C., Griffis, R., Hansen, L. J., Hellmann, J. J., Lawler, J. J., Nelson, E. J., & Pairis, A. (2013). Preparing for and managing change: Climate adaptation for biodiversity and ecosystems. In Frontiers in Ecology and the Environment (Vol. 11, Issue 9, pp. 502–510). https://doi.org/10.1890/120277

Warner, J. C., Armstrong, B., He, R., & Zambon, J. B. (2010). Development of a Coupled Ocean-Atmosphere-Wave-Sediment Transport (COAWST) Modeling System. Ocean Modelling, 35(3), 230–244. https://doi.org/10.1016/j.ocemod.2010.07.010

Warner, J. C., Rockwell Geyer, W., & Arango, H. G. (2010). Using a composite grid approach in a complex coastal domain to estimate estuarine residence time. Computers and Geosciences, 36(7), 921–935. https://doi.org/10.1016/j.cageo.2009.11.008

Warner, J. C., Sherwood, C. R., Signell, R. P., Harris, C. K., & Arango, H. G. (2008). Development of a three-dimensional, regional, coupled wave, current, and sediment-transport model. Computers and Geosciences, 34(10), 1284–1306. https://doi.org/10.1016/j.cageo.2008.02.012

WRAP, 2013. Western Regional Air Partnership (WRAP) West-wide Jump-start Air Quality Modeling Study (WestJumpAQMS). Environ International Company, & Alpine Geophysics
https://www.wrapair2.org/pdf/WestJumpAQMS_FinRpt_Finalv2.pdf

Yoshida, M., Nakagawa, N., & Umemoto, S. (2010). Variation of nutrient salt concentration in rivers water flowing into Osaka Bay and Harima-Nada (in Japanese). http://www.eco-hyogo.jp/files/1813/8182/2580/notes201203.pdf

Zhang, W. G., Wilkin, J. L., & Schofield, O. M. E. (2010). Simulation of water age and residence time in New York Bight. Journal of Physical Oceanography, 40(5), 965–982. https://doi.org/10.1175/2009JPO4249.1

Chapter 4 - Numerical Assessment of Total Nitrogen (TN) Load Discharged from Rivers into Harima Nada, the Seto Inland Sea, Using a Numerical Coupled Hydrological -Water Quality Model

4.1 Introduction

As mentioned in Chapter 1, the Harima Nada region is very enclosed and strongly affected by river discharges. Because of the current oligotrophication problems and the sustained decrement in DIN concentration (Fig. 4), many efforts and research have been conducted to help with solutions for reverting the situation. Some previous approaches used to clarify nutrient loads and dynamics focused on numerical estimations, others based on empirical relationships from observed data series, and some used a combination of both techniques (Abo et al., 2018; Ikeno & Miwa, 2014; Kobayashi et al., 2019; Naito et al., 2011; Yanagi, 2015; Yanagi & Tanaka, 2013) However, a detailed assessment of the river's contributions is still challenging and a problem that needs to be addressed.

The previous estimations of river discharges and nutrient loads in Harima Nada used observed datasets in which the influence of the annual heavy rain events in the study region was not considered, representing the reality but up to a certain extent. During the rainy season (between June and July) and typhoon season (from late July to October), extreme meteorological events frequently happen all over Japan. As a consequence of heavy rain and flood episodes, soils' hydraulics change (due to the soil layers' oversaturation), which affects the processes and mechanisms in which nutrients are exported from land to superficial waters, causing in a short period the input of big nutrients loads into river mainstreams that are discharged into the sea.

There are ten rivers (besides the Kako River) that directly discharge their waters in the study area: four on the northern coast, two on the east side, and four on the southern side (Fig. 25. In this chapter, the same physically distributed Hydro-Chemical Model described in Chapter 2 and the methodology used for ECs determination in the Kako River were extended to these other rivers to calculate the total freshwater and TN loads riverine derived. Additionally, the estimation for discharged water and TN load was extended to the Yoshino River, the largest river of Shikoku Island, and discharges next to Harima Nada's southern border in the Naruto Strait

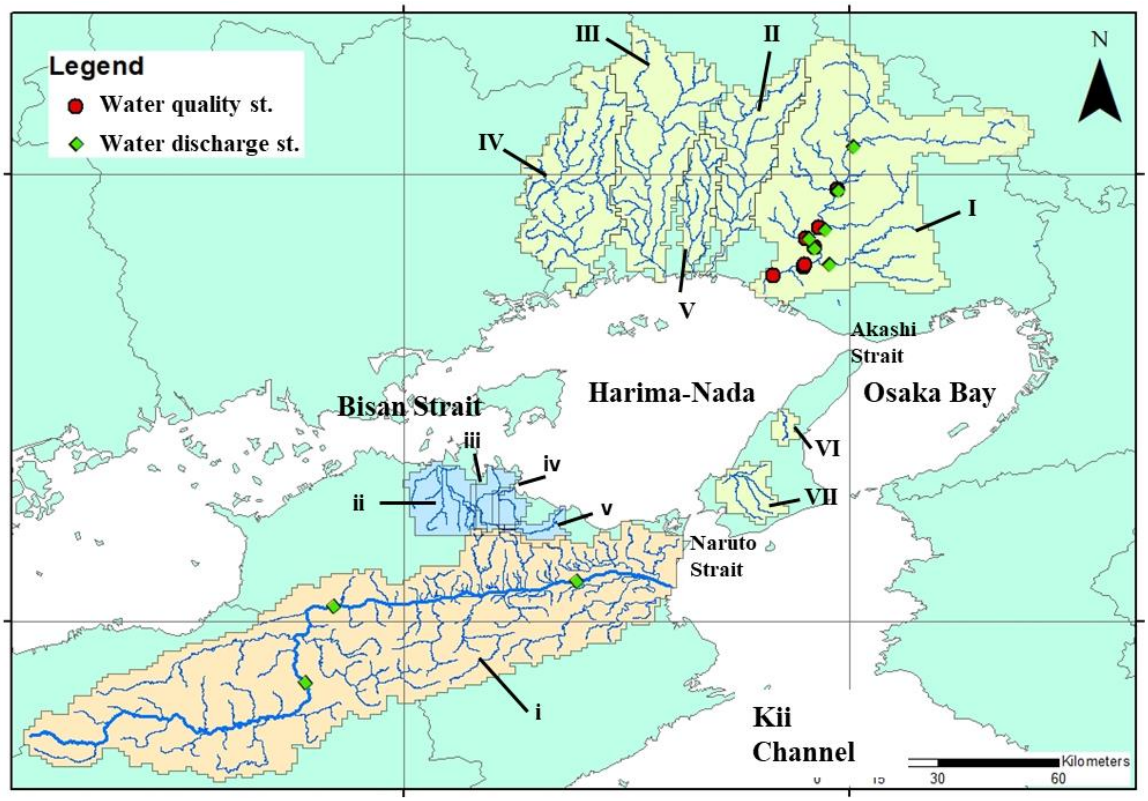

Hyogo Prefecture rivers

I) Kako River	II) Ichi River
III) Ibo River	IV) Chikusa River
V) Yumesaki River	VI) Gunge River
VII) Mihara river	

Shikoku Island rivers

i) Yoshino River	ii) Kasuga/Shin system
iii) Minato River	iv) Kamobe River
v) Tsuda River	

Fig. 25 - Rivers considered in this study

In addition to the approach used in Chapter 1, point source data was added to estimate TN loads in the northern and eastern coast of Harima Nada (Hyogo Prefecture rivers). For the southern area, no datasets were available, and the estimation was performed exclusively for nonpoint source TN loads.

The obtained results are expected to assist in identifying particularities in the area's rivers and their categorization as sources of nutrients and freshwater. In addition, the same as the results from Chapter 2 were used for forcing the Kako River in the atmospheric-marine model, the obtained results from this analysis aimed to be input datasets to complete the

analysis of freshwater discharge dynamics in the region, helping in the development of a future biogeochemical model for the area.

4.2 Methodology

4.2.1 Study site and modeling framework

The entire Harima Nada area was split into two sub-areas for this study: North - for all the Hyogo Prefecture rivers that discharge in the northern and eastern coasts, and South – for the rivers that discharge from Shikoku Island. Simulations were conducted between January 2009 and December 2016, giving the Hydro-Chemical Model 12 months of spin-up for discharged water and TN load.

4.2.1.1 Computational domains and datasets

For the eleven rivers that directly discharge into Harima Nada and the Yoshino River, the computational domains were defined in the same way and using the same considerations described in Chapter 2, section 2.2. The main characteristics of the rivers are summarized in Table 12, and the description of the datasets is presented in Table 13. Point source datasets were added to the Hydro-Chemical Model for six of the seven rivers of the northern region.

The computational domain of each river is shown in Figs. 26 and 27. In Fig. 26, point source information was provided for the HIES (unpublished data), and it corresponds with the economic activities and population density of each of the watersheds. The point source datasets include sewage and water treatment plants, and industrial and commercial waters, and their time resolution varied from daily to monthly or bimonthly. For the points where the time resolution was lower (monthly or bimonthly), values were considered constant for the periods between them for the entire study period.

Meteorological datasets from AMeDAS and JMA observatories were handled similarly to Chapter 2, section 2.2.2 described. The same correction by elevation (Eq. 2.1 and Eq. 2.2) was done on each of the studied watersheds for temperature and rainfall to consider the drop in temperature and the increase in rain with altitude.

Table 12 - Harima Nada Rivers and their most representative characteristics

	River name	Watershed area (km^2)	Average discharge (m^3/s)	Number of cells	Number of meteorological stations and observatories of the watershed	Number of point sources considered
North Region	Kako	1730.0	45.9	1852	20	165
	Ibo	810.0	21.4	777	14	67
	Chikusa	730.0	6.6	720	10	63
	Ichi	496.0	6.3	448	9	67
	Yumesaki	205.0	*	197	6	17
	Mihara (Awaji Island)	123.7	*	136	4	18
	Gunge (Awaji Island)	26.3	*	36	3	*
South Region	Yoshino	3750.0	107.7	3701	28	*
	Kasuga/Shin System	131.9	*	222	4	*
	Kamobe	68.0	*	87	5	*
	Minato	51.6	*	67	4	*
	Tsuda	43.7	*	55	5	*

* : No information available

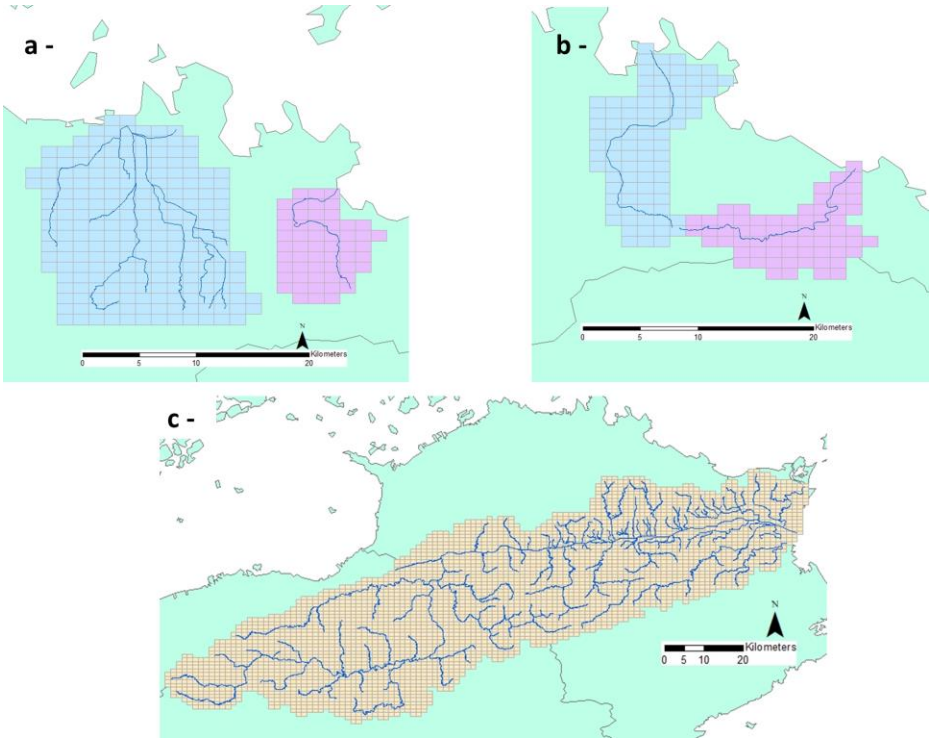

Fig. 26 – River domains in the south region of Harima Nada. a-Kasuga/Shin System and Tsuda River (from left to right), b- Kamobe and Minato Rivers (from left to right), and c- Yoshino River

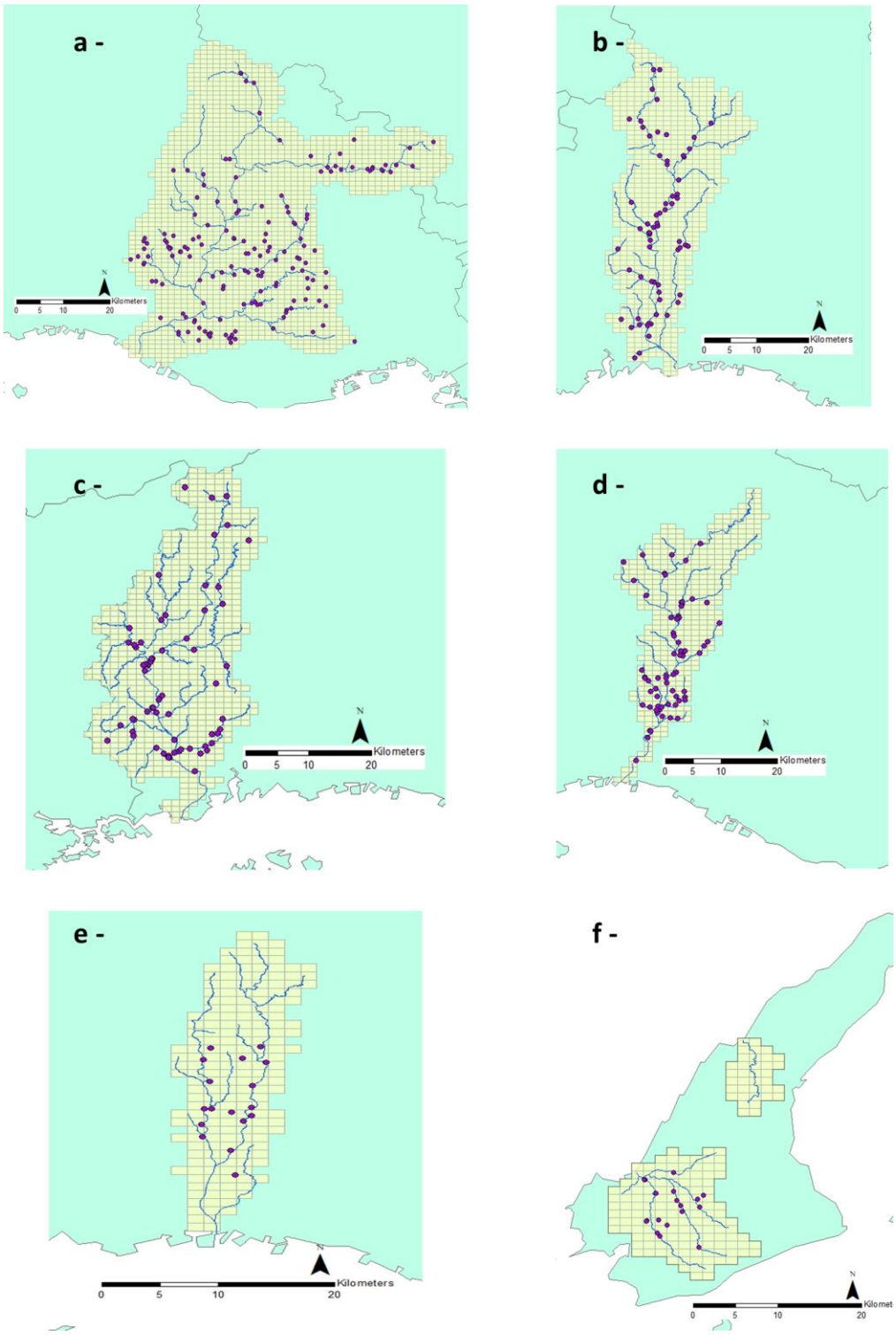

Fig. 27 - River domains in the north and east sides of Harima Nada and location of the considered point sources. a- Kako River, b- Ibo River, c- Chikusa River, d- chi River, e- Yumesaki River, f- Mihara and Gunge Rivers (from left to right)

Table 13 - Information on the input datasets used in the model simulation

	Dataset	Resolution	Source
Hydrological Module	Elevation	1 km	MLIT - 1
	Land Usage	1 km	MLIT – 1
	River's watershed boundary	100 m	MLIT – 1
	River's Channel	*	MLIT -1
	Forestation	1 km	Biodiversity Center of Japan
	Precipitation	Hourly	JMA
	Air temperature, wind speed, water-vapor pressure, atmospheric pressure, solar irradiance	10 - min	JMA
Chemical Module	Land Usage	1 km	MLIT -2
	Point source information (location, discharged volume, and load)	Monthly	HIES (Unpublished data)
	Nitrogen monthly wet-deposition	Monthly	Ministry of Environment of Japan (MOEJ)
Model Validation	Freshwater flow	Hourly	MLIT -2
	TN load	Monthly/seasonal	MLIT - 2
	TN load	Hourly	HIES (unpublished datasets)

(* - does not correspond)

The land use information from the MLIT (MLIT – 1) was standardized in the four main categories used in Chapter 2 (mountain, paddy, city, and farm), plus water bodies for all the watersheds studied. The ratios of occupation in each river domain are shown in Table 14. As was seen for the Kako River, the mountain land use is predominant in all the watersheds of the study region, representing around 60% or more, except for the Kasuga/Shin system in the wester-south area. Urban areas are primarily located near estuaries, and their ratio mainly varies with the population density of the particular place and its production activities. Paddy and farm land uses are more extended in the eastern and south river basins. As an additional observation, the Yoshino River watershed is mainly occupied by mountains (> 80%), while the rest of the land uses represent a very small part of it.

Table 14- Land usage distribution per river watershed

Region	River name	% Land use distribution				
		Mountain-forest	Paddy	Urban area	Farm	Water bodies
North (Hyogo Prefecture)	Kako	66.4	18.7	11.3	1.0	2.6
	Ibo	82.5	8.3	6.7	0.4	2.1
	Chikusa	85.0	8.0	4.7	0.7	1.6
	Ichi	77.2	11.0	8.5	0.3	3.0
	Yumesaki	74.9	6.6	16.6	0.3	1.6
	Mihara (Awaji Island)	54.6	2.3	12.3	28.2	2.6
	Gunge (Awaji Island)	44.6	44.4	5.0	4.4	1.7
South (Shikoku Island)	Yoshino	83.3	4.8	5.0	4.2	2.7
	Kasuga/Shin System	34.4	25.3	32.4	3.1	4.8
	Minato	83.1	9.4	4.6	0.5	2.4
	Kamobe	56.8	24.5	13.2	2.7	2.9
	Tsuda	65.7	21.1	9.0	2.1	2.1

4.2.2 Model description

The same Hydro-Chemical Model explained in Chapter 2, section 2.3, was used in this study's rivers. Additionally, the input of point source contributions for the North region was added, and Manning's or roughness coefficients were adjusted. Manning's coefficients significantly impact the numerical simulation of hydrological variables. These coefficients are strongly dependent on land use and soil coverage, and because the activities performed in the north and south regions of Harima Nada are considerably different, a literature review was conducted to set representative Manning values for Japanese land use classes (Bricker et al., 2018; Kimaro et al., 2004, 2005; Kometani et al., 2014, Ryuhey et al., 2012).

Coefficients were tuned during the validation of the hydrological module of the Hydro-Chemical Model in the Kako and the Yoshino rivers, which are the most representative of both regions. The fitting was made by adjusting the bibliography reported values by comparing the performance of the discharge simulation results with observed data. The better-fitting coefficients were extended in their use for the rest of the rivers of the corresponding region. Table 15 summarizes the values for each land use in the northern and southern areas.

Table 15 - Manning's Coefficients used for the north and south regions of Harima Nada

	Manning's coefficient for different soil usage			
Harima Nada Region	**Mountain-forest**	**Urban area**	**Paddy/farm**	**Water bodies**
North (Kako River)	0.030	0.060	0.020	0.025
South (Yoshino River)	1.00	0.010	3.50	0.020

4.3 Results and Discussion

4.3.1 Model validation

Model validation for discharged water and TN load was performed in the same manner and using the same statistics and benchmarks detailed in Chapter 2, subsections 2.2.4.4 (Table 3) and 2.4.1 (Table 4), respectively. Validation for stream flow was conducted in the Kako and Yolshino rivers since they are the most representative of both regions and the ones with long time series of observation datasets. The estimation of TN was previously validated in Chapter 2 for the Kako River, and it was extended to the rest of the rivers of the study area. Because datasets were unavailable to estimate different values of ECs, the values obtained in the Kako River were extended in this study for all the rivers that discharged in Harima Nada.

4.3.1.1 Mainstream discharge

Streamflow validation was performed jointly with Manning's coefficients adjustment in the north (Kako River) and south (Yoshino River) regions separately. Three stations with different catchment areas were used on each river's mainstream, as shown in Fig. 28. Daily and monthly average discharged water was calculated from the hourly datasets of the Water Information System of Japan (MLIT – 2) in the six chosen observatories for the period January 2009 – December 2012. In the case of the Kako River observatories, data for the year 2012 was unavailable, and that year is not represented. Daily and monthly charts of observed and simulated streamflow are presented in Fig. 29 for the Kako River and Fig. 30 for the Yoshino River in the corresponding validation points.

The results of the statistics showed that the hydrological model is effective in reproducing the trends at different time resolutions and catchment areas. RSR values, used

to quantify the simulation error, are for both regions in the benchmark of very good (<0.5), except for the daily values in the Funamachi station for the Kako River. In addition, from NSE values, it can be inferred that the model performs very well in reproducing observations, particularly for monthly time resolution in all the observatories in both rivers.

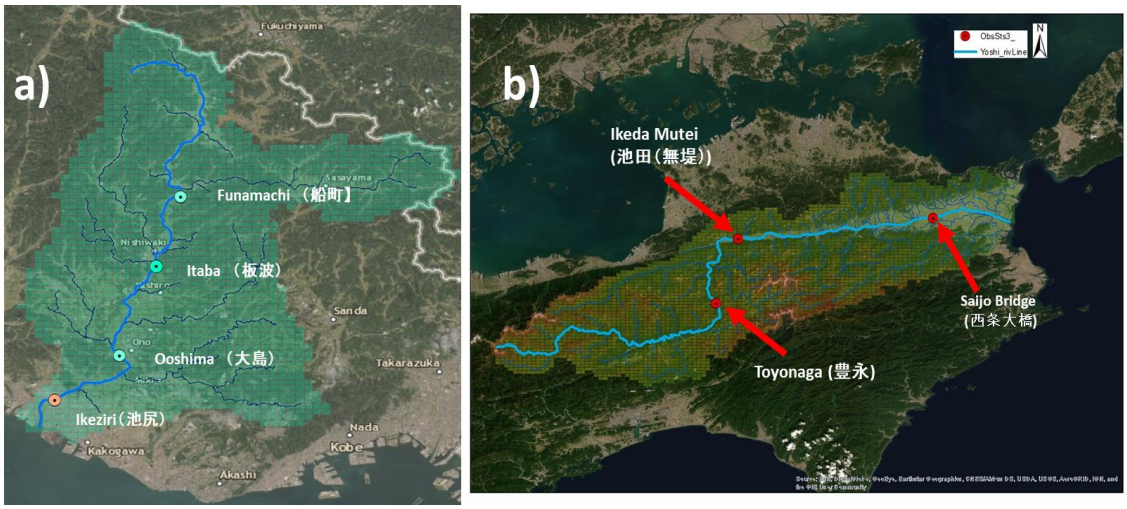

Fig. 28 - Monitoring stations from the MLIT- 2 used to validate discharged water in a) the Kako and b) the Yoshino rivers. (a) Funamachi, Itaba, and Ooshima are streamflow validation stations, and Ikeziri is the CO for TN validation (b)Toyonaga, Nakayabu, and Saijo Bridge are exclusively streamflow validation points

Table 16 – Performance validation and statistic results for the Kako and Yoshino rivers discharge

Monitoring Station	Time resolution	Average of observed data (m^3/s)	Average of simulated data (m^3/s)	R^2	RSR	NSE	pBIAS (%)
Kako River							
Funamachi	Daily	21.9	28.8	0.75	0.58	0.66	-31.5
	Monthly			0.88	0.45	0.79	-31.3
Itaba	Daily	36.0	43.9	0.67	0.63	0.61	-22.0
	Monthly			0.80	0.50	0.75	-22.0
Ooshima	Daily	48.6	60.4	0.85	0.55	0.83	-24.3
	Monthly			0.93	0.37	0.81	-24.3
Yoshino River							
Toyonaga	Daily	71.6	89.2	0.93	0.52	0.73	-24.4
	Monthly			0.97	0.40	0.87	+15.0
Ikeda Mutei	Daily	114.2	137.2	0.94	0.35	0.88	-20.1
	Monthly			0.98	0.27	0.93	-20.2
Saijo Bridge	Daily	152.6	187.6	0.91	0.46	0.79	-23.0
	Monthly			0.99	0.28	0.93	-23.6

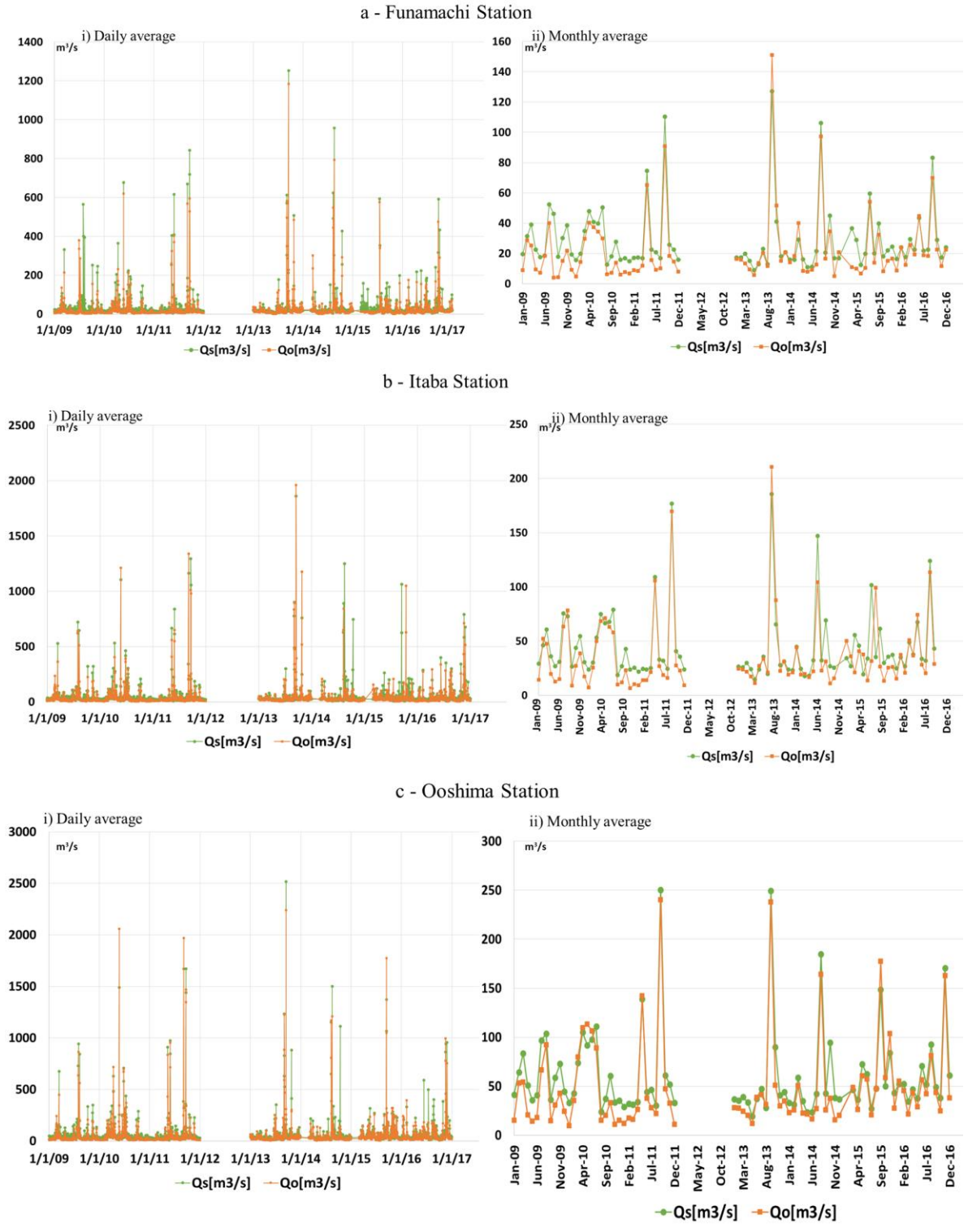

Fig. 29 - Daily and monthly averages for observed (orange) and simulated (green) values of discharged freshwater in the three monitoring stations of the Kako River

Fig. 30 - Daily and monthly averages for observed (orange) and simulated (green) values of discharged freshwater in the three monitoring stations of the Yoshino River

The obtained values of pBIAS showed that the model tends to overestimate streamflow discharge in both watersheds, but in particular, for the Kako River is more important in the smaller catchment area. The obtained values were in the range of satisfactory performance for this analysis at both time resolutions, indicating that the reproduction of average magnitudes is more sensitive than the other statistics. pBIAS values are easily affected by the quality of the observations and the associated uncertainty of the datasets. There were missing data for the datasets used in streamflow validation (from days to months or years in some cases), and since it does correspond to external data sources, the quality was considered unknown, which is the reason why pBIAS values were considered good enough to support the model's validation.

Daily time resolution shows lower performance for all the statistics, indicating that estimations are more easily affected by meteorological phenomena in both regions, in particular during rainy and typhoon seasons, an effect that is smoothed by monthly averages, same as it was observed during the model validation for the Kako River in Chapter 2.

4.3.1.2 TN loads

The results from Chapter 2, section 2.4.3.1, were used to validate the TN load in this study. Because of the lack of datasets in the other rivers with enough quality and a good time distribution, the transport model and the ECs calculated for the Kako River were considered representative of the region.

4.3.2 Total discharged freshwater

Total freshwater discharges are presented in Fig. 31 – a and b, for the northern and southern regions of Harima Nada, and the comparison between Yoshino River discharge and the entire Harima Nada is shown in Fig. 31 -c. Table 17 summarizes the obtained values for each river and the contribution ratios. Substantial differences in the discharged values between regions were found due to the differences in the river basins' size. South region discharges are in the order of 1/7 of the northern river ones (~1 mill vs ~ 7 mill. m^3/day).

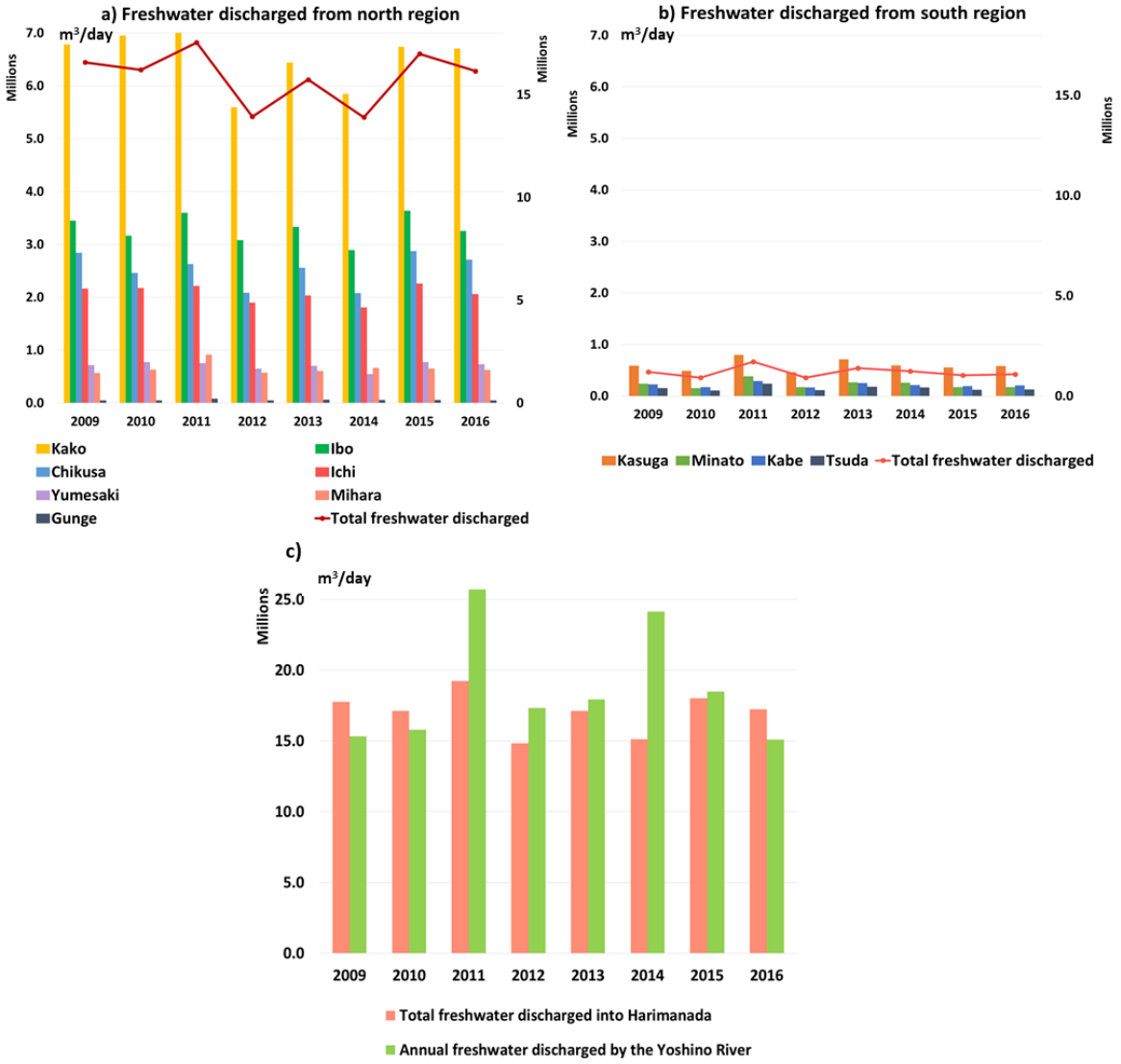

Fig. 31 -Annual average of TN load discharged into Harima Nada from the north (a) and south (b) regions, and (c) comparison between the Yoshino River and the entire Harima Nada's freshwater results

The Kako River was found to be the most significant contributor of the entire, accounting for approximately 40% of the entire freshwater discharged into Harima Nada, verifying the assumption made in Chapter 2 and the validation of the hydrological model. The correlation between river basin size and discharged water is direct for all the rivers in both regions. Some yearly variations in the discharge trend of the rivers in both areas can be associated with extreme rainfall events during the rainy and typhoon seasons during a particular year.

The results for the Yoshino River show that its average freshwater discharge is 1.1 times the volume of freshwater directly discharged into Harima Nada. The Yoshino River basin's size covers around 80% of the total river basins that directly discharge into the study region, which is why a comparatively significant discharge was expected. Yearly fluctuations in freshwater discharges are also more noticeable for the Yoshino River than for the entire Harima Nada, from which it can be inferred that meteorological characteristics vary between regions. The Yoshino River discharge estimation is important because it can help set boundary conditions for the southern border of Harima Nada.

Table 17 - Annual average discharged freshwater into Harima Nada (2009-2016)

Region	River name	Total cells	Average discharge ($x10^6$ m^3/day)	Total volume discharged into Harima Nada (%)
North	Kako	1852	6.55	38.3
	Ibo	777	3.30	19.3
	Chikusa	720	2.53	14.8
	Ichi	448	2.08	12.2
	Yumesaki	197	0.71	4.2
	Mihara (Awaji Island)	136	0.65	3.8
	Gunge (Awaji Island)	36	0.06	0.40
South	Kasuga/Shin System	222	0.60	3.5
	Kamobe	87	0.23	1.3
	Minato	67	0.22	1.3
	Tsuda	55	0.15	0.9
	Yoshino	3701	18.70	1.1 (respect the entire Harima Nada total)
Total volume discharged into Harima Nada ($x10^6$ m^3/day)			17.08	100%

4.3.3 Total discharged TN load

The estimated average TN load discharged from rivers into Harima Nada was estimated at 5000 tons/year for the study period. Because TN load is affected by river discharge, the higher contributions also corresponded to the northern area of Harima Nada. The Kako River discharges around 50% of the total, confirming the importance of its circulation water dynamics and nutrients transport inside Harima Nada.

TN loads are more associated with the type of land use, population density, and economic activities of the river basin than its size. Hence, the correlation between size and TN load was not found to be direct as in the case of discharged freshwater. In those watersheds where paddy and farm land uses are more extended (like the Mihara River in the north region and the Kasuga/Shin System in the south), TN loads showed to be comparatively high with respect to the watershed size, evidencing the fact that nutrients are exported in a more significant manner from those land uses in accordance with their ECs (see Table 5, Chapter 2).

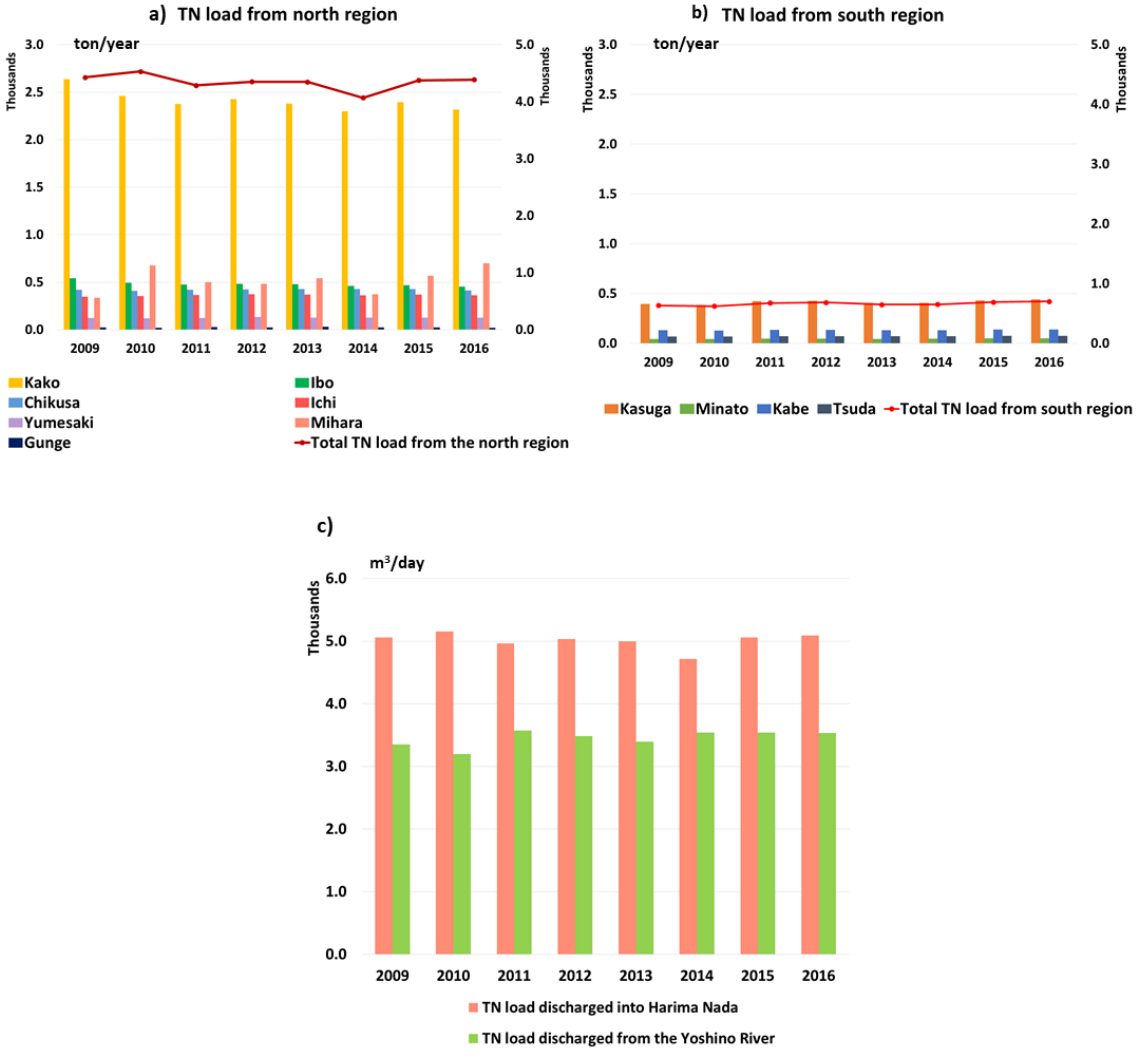

Fig. 32 - Annual average of TN load discharged into Harima Nada from the north (a) and south (b) regions, and (c) comparison between the Yoshino River and the entire Harima Nada's TN load results

Point source contributions were exclusively evaluated for the North region, and the extent of this contribution accounts for around 35 % of the estimated TN input. The northern area has a higher population density and is more industrialized, so it was expected that point source contribution loads per river were correlated with the size of the cities on their watersheds.

Table 18 - Annual average of TN load discharged into Harima Nada (2009-2016)

Region	River name	Total cells	Number of PS'	Land TN load (ton/year)	Land TN load+ PS (ton/year)	PS contribution to TN load (%)	Ratio of TN load discharged into Harima Nada (%)
North	Kako	1852	273	1748.5	2411.0	32.2	48.1
	Ibo	777	63	437.9	481.6	10.0	9.7
	Chikusa	720	63	386.3	420.0	8.8	8.4
	Ichi	448	67	305.4	362.0	18.6	7.2
	Yumesaki	197	17	120.8	125.6	4.0	2.5
	Mihara (Awaji Island)	136	18	517.2	521.6	<1.0	10.2
	Gunge (Awaji Island)	36	---	23.5	---	---	0.5
South	Kasuga/Shin System	222	---	414.4	---	---	8.3
	Kamobe	87	---	44.5	---	---	1.0
	Minato	67	---	132.9	---	---	2.7
	Tsuda	55	---	71.1	---	---	1.4
	Yoshino	3701	---	3451.0	---	---	69.0 (respect the entire Harima Nada total)
Total TN load discharged into Harima Nada (ton/year)				4202.5	5008.2	---	100%

The results obtained for the Yoshino River showed that only from nonpoint sources can its basin export almost 70% of the TN load (nonpoint + point source) discharged in Harima Nada. The Yoshino River watershed covers an extensive area in Shikoku Island, but

the main land use in the basin is mountains (Table 14), which has the smaller value of all the ECs and accounts for the minor nonpoint source contribution (Table 5). Additional information on point source contributions could not be integrated into this work for the Yoshino River, nor datasets on TN load in any particular mainstream observatory, but on its estuary is located one of the biggest cities of the Shikoku Island, which could provoke deviations from the estimated values. However, as a first approach to describe the capacity of the river basin to export TN, it was considered that the obtained results could be a realistic estimation of it.

Annual variations in the TN loads discharged per year in the entire Harima Nada and the Yoshino River seem to not vary much independently of the differences in the total annual discharges (Fig. 32). Same observation can be extended between regions in Harima Nada, which shows the capacity and availability of the rivers for exporting TN is limited.

4.4 Conclusions

The hydrological model could be effectively adjusted and validated in the Yoshino River as the representative river of the Shikoku island for estimating TN load and freshwater discharged from the rivers in the southern region of Harima Nada. The methodology for estimating TN from nonpoint sources, developed in Chapter 2, was reproduced in all the rivers of the study region and confirmed the importance of the Kako River as a source of freshwater and nutrients in Harima Nada. Substantial differences were found between the freshwater and TN loads discharged from the north and south regions, which is directly related to the size of the river watersheds and the population density. Differences in discharged freshwater were found to be significant between years and are affected by the climatological events that occur in the area, but TN loads seem to not follow the same trend. TN loads remain mostly unchanged for the study period, indicating that nutrients and their availability is limited. TN point source contribution from the northern region was 35% of the total contribution, showing that industrial and economic activities play a key role in the nutrient loads discharged into the sea. Validation of the TN load released for the Yoshino is necessary, as well as the extent of the point source contribution to its watershed TN load.

References – Chapter 4

Abo, K., Satoshi, A., Kazuhiro, H., Yoshiki, N., Hayashi, H., Murata, K., Wanishi, A., Ishikawa, Y., Masui, T., Nishikawa, S., Yamada, K., Noda, M., & Tokumitsu, S. (2018). Long-Term Variations in Water Quality and Causal Factors in the Seto Inland Sea , Japan. *Bulletin on Coastal Oceanography (in Japanese, English Abs.)*, *55*(2), 2101–2111.

Acid Rain Survey's Results published by the Ministry of Environment of Japan (MOEJ), http://www.env.go.jp/air/acidrain/monitoring/h27/post_24.html

Biodiversity Center of Japan. (n.d.). http://www.biodic.go.jp/dload/mesh_vg.html

Bricker J D, Gibson S, Takagi H and Imamura F, 2018 On the Need for Larger Manning's Roughness Coefficients in Depth-Integrated Tsunami Inundation Models, *Coastal Engineering* **57(2)**, 1550005-1-1550005-13, https://doi.org/10.1142/S0578563415500059

Ikeno, H., & Miwa, H. (2014). *Numerical analysis of tidal current and nutrient distribution in Harimanada*. *June*. 10.2208/prohe.52.1387

Japan Meteorological Agency (JMA). (n.d.). *Meteorological Observatories and Automated Meteorological Data Acquisition System (AMeDAS)*. https://www.data.jma.go.jp/gmd/risk/obsdl/

Kimaro T A, Tachikawa Y and Takara K; 2003 Evaluating land-use change effects on flood peaks using a distributed rainfall-runoff model in Yasu River, Japan; *Weather Radar Information and Distributed Hydrological Modelling – Proceedings of Symposium HS03- IUGG2003, Sapporo, Japan*; IASH Pub. Number 282.2003

Kimaro T A, Tachikawa Y and Takara K, 2005 Distributed hydrologic simulations to analyze the impacts of land use changes on flood characteristics in the Yasu River basin in Japan, *Journal of Natural Disaster Science* **27(2)**, 85-94

Kobayashi, S., Nakada, S., Futamura, A., Nagamoto, K., & Fujiwara, T. (2019). Observation and modeling of seawater exchange in a strait-basin system in the Seto Inland Sea, Japan. *Journal of Water and Environment Technology*, *17*(3), 141–152. https://doi.org/10.2965/jwet.18-042

Kometani S, Uotani T, Michioku K, Kanda K, Irie Y and Yanagida K, 2014 Equivalent manning roughness coefficient in an open channel of compound cross section with tree vegetation, *土木学会論文集 B1(水工学)* **70(4)**, 697-02 (in Japanese).

Ministry of Land Infrastructure Transport and Tourism of Japan (MLIT). (n.d.-a). *National land numerical information download service (国土数値情報ダウンロードサービス)*. https://nlftp.mlit.go.jp/ksj/

Ministry of Land Infrastructure Transport and Tourism of Japan (MLIT). (n.d.-b). *Water Information System*. http://www1.river.go.jp/

Naito, K., Tanabe, A., Itakura, S., Yamaguchi, M., & Imai, I. (2011). Evaluation of major nutrients regulating the growth of diatoms in Harima-Nada, the Seto Inland Sea, Japan. *Bulletin of Fisheries Sciences, Hokkaido University*, *61*(1), 5–12.

Ryuhey Y, Iizumi T, Nishimori M and Yokozawa M, 2012 Impacts of land-use changes on surface warming rates and rice yield in Shikoku, western Japan, *Geophysical Research Letters* 39, L22401, https://doi.org/10.1029/2012GL053711

Yanagi, T. (2015). Oligotrophication in the Seto Inland Sea. In *Eutrophication and Oligotrophication in Japanese Estuaries – The present status and future tasks* (pp. 39–67). Springer Netherlands.

Yanagi, T., & Tanaka, T. (2013). Origins of Phosphorus and Nitrogen in the Seto Inland Sea, Japan. *Reports of Research Insitute for Applied Mechanics, Kyushu University*, *144*, 13–18.

Chapter 5 - General Conclusions

5.1 General Conclusions

In the present work, one methodology for nonpoint source nutrients estimation, a physically distributed watershed Hydro-Chemical Model, and a coupled atmospheric-marine model based on the COAWST Model System were effectively developed and validated for the Harima Nada region of the Seto Inland Sea for the period between April 2010 and March 2012.

TN and TP nonpoint source estimations were successfully calculated and validated in the Kako River, one of the most important rivers in West Japan. The developed methodology for estimating ECs in the river watershed, which combines observed and simulated datasets discretized per rain event, was proven to reduce the number of necessary observation points to only one near the estuary. A robust regression method was applied to obtain an MLR in which the ECs for each land use corresponded with the regression coefficients. The chosen regression method effectively avoided data transformations and the significant problems derived from them and reduced the number of extreme rainfall events (outliers) filtered from the entire dataset population.

The obtained TN and TP ECs' performances were verified and validated, showing good reproducibility of the observations at different time resolutions, but it was found that they tend to underestimate the results due to the simplifications of the approach. The developed methodology requires careful consideration of its application because the applicability of the ECs estimated cannot be suitable in certain conditions. It was found that when deviations in the annual precipitation exceed 30%, ECs and the model performance are reduced, and the underestimation of nutrients occurs to a greater extent. The differences in rainfall affect nutrient exported loads to the mainstream differently, depending on the particular land use. Paddy ECs were shown to be more sensitive to rainfall variations for nitrogen and phosphorous, evidencing that operating conditions and the differences in the hydraulic model may affect the obtained values to a different extent than for the other land uses. The intercept of the MLR considered accounting for other types of contributions substantially varied under different rainfall conditions, showing that TP loads in the

mainstream are more sensitive to rainfall variations. Mechanisms of soil runoff, erosion, and damn operations that occur as a consequence of extreme rainfall events can significantly impact nutrients contribution, particularly TP loads.

The atmospheric-marine model described atmospheric and marine variables well at the selected horizontal and time resolutions. The previously calculated TN load and freshwater discharge were forced into the ROMS Model component, and it was found that seasonal mean residence times and circulation patterns agreed with the observations and previous research findings in biomass production, its growth rate, and its seasonal distributions.

The analysis of the results showed that tracer concentration and the magnitude of the horizontal speed decrease with depth, but no substantial differences in circulation patterns and tracer distribution were found between the surface and 10 m depth layers for the same season in Harima Nada, probably as a consequence of the shallow bathymetry and the enclosed geography of the region. On the contrary, between seasons, the mean residence times, water circulation patterns, and river waters distributions are strongly seasonally affected, and they govern many of the biogeochemical processes that occur in the study region.

To improve the estimation of freshwater and nutrient loads, the ECs estimated for the Kako River were used in the Hydro-Chemical model on the other 11 rivers that directly discharge into Harima Nada and in the Yoshino River, which discharges next to the southern border. Validation on the south coast of Harima Nada was effectively conducted for discharged water in the Yoshino River, showing very good agreement with the observations. Results showed that because of its extensive area, the Yoshino River discharges 1.1 times the total freshwater that Harima Nada receives, which can be significant in setting the boundary conditions for the study area and the exchange of water in the Naruto Strait.

It was found that the volume of freshwater discharged is directly correlated with the size of the watershed, which confirmed the importance of the Kako River and the northern rivers (bigger river basins) in the study area. Significant differences in the total discharged

water with years were found, evidencing that river discharges are similarly directly affected by rainfall variations. Meteorological events seemed to have a higher impact on Shikoku Island, where the annual variations seemed to be higher than in the northern region of Harima Nada. In the case of TN discharged loads, no direct correlation was found with the area of the watershed. However, TN loads are more sensitive to the population density and the activities performed in the watershed. Particularly in those river basins with a higher occupation of city-farm or paddy land uses, the TN loads did not follow a size-discharge direct relation. Point source contribution from the northern region of Harima Nada was estimated to be around 30% of the study region's total, representing more than the contribution from the southern rivers (~20% over the total TN load).

Annual fluctuations in TN load were found to be smaller than for discharged freshwater for Harima Nada and the Yoshino River, which evidences that land exported nutrients are limited by other physical and physicochemical processes not considered in this approach, and the extent of their direct correlation with direct runoff does not increase over a certain amount. Validation for TN load in the Yoshino River could not be performed, the same as for any of the other rivers in the south region, but previous research concluded that around 20% of the TN load of Harima Nada corresponds to Shikoku Island contributions, which agreed with the obtained results. The results for the Yoshino River reinforce the idea of considering it for better-defining boundary conditions in the southern region.

From the results obtained in Chapters 2 and 4, it can be concluded that the Kako River is the most important contributor to freshwater and TN load into Harima Nada waters, being responsible for 40% and 30% of the total contributions, respectively. The northern coasts of the study region directly received the maximum contribution of nutrients and fresh water, which makes it an area of higher biomass productivity, two premises confirmed by the obtained simulation results. Seasonal variabilities on the average circulation patterns and mean residence times were also consistent with the region's observations, showing that the developed coupled model effectively reproduces the conditions in the study area.

The presented approach has limitations in each of its components. The EC methodology has limitations that need to be considered when applying it to a river watershed in which the size, land use distribution, or geological characteristics are too different from the ones the Kako River has and may be unsuitable or need modifications. The underestimation of the TN and TP loads is directly linked with the simplifications made in the definition of the approach and the type of method used for obtaining the MLR models. Improving the transport model to consider point source contributions, physical, and physicochemical processes like soil runoff can increase performance, which is a task for future works. In addition, the performance of the ECs and the simulation results are lower, and they underestimate nutrient loads to a bigger extent when rainfall exceeds 30% or more of the conditions of their estimation, but for those years in which precipitation is considerably lower the quality of the results needs to be evaluated.

In principle, the horizontal resolution of the ROMS module in the coupled atmospheric-marine model needs to be increased to define the Kako River plume precisely and describe its dynamics. The model needs some adjustments in the conditions set up to boost its performance, particularly for river forcing (temperature series, more superficial stratification, etc.) and tracer experimental conditions. More freshwater and nutrients must be forced inside Harima Nada to effectively describe the region before setting up parameters for developing a biogeochemical model. Lastly, the estimation of TN needs to be validated in the southern region of Harima Nada, and representative export coefficients may be estimated in this area. This first approach tried to solve the lack of nutrient datasets for validation by improving the definition of the hydrological module of the river model and the discharge of freshwater, but as was previously mentioned, the relation between direct runoff and land-derived nutrients is not linear in all the range, and more research needs to be conducted.

The extent of this work sets an antecedent for a better understanding and more accurate description of the study area conditions, and it is the first step in developing a complete high-resolution model in the Harima Nada of these characteristics. The numerical tools presented in this work can potentially assess the influence of particular meteorological

events or environmental accidents in the area by modifying its configuration. They can also contribute to a better understanding of the biogeochemical processes of Harima Nada and many other places inside the Seto Inland Sea or Japan of similar characteristics.

Appendices

Appendix 1 - Hydrological Model Equations

A.1.1. Heat balance methodology

Surface energy balance model

The expression of the conservation of energy law,

$$R\downarrow + Q_a = \sigma T_s^4 + H + lE + G \quad (2.1)$$

$R\downarrow$: Net incoming radiation flux [J s-1 m-2], Q_a : Anthropogenic heat flux [J s-1 m-2],

σT_s^4 : Outgoing longwave radiation [J s-1 m-2], H : Sensible heat flux [J s-1 m-2],

lE : Latent heat flux [J s-1 m-2], G : Ground heat flux [J s-1 m-2],

σ : Stefan - Boltzman coefficient [J s-1 m-2 K-4], T_s : Surface temperature [K]

$R\downarrow$, H, and lE are calculated according to:

$$R\downarrow = (1-\alpha)S\downarrow + L\downarrow \quad (2.2)$$

$$H = c_P \rho_a C_H U(T_s - T_a) \quad 2.3)$$

$$l = 2.50 \times 10^6 - 2.4 \times 10^3 \times (T_s - 273.15) \quad 2.4)$$

$$E = l\rho_a \beta C_H U(q_{ssat} - q_a), \quad 2.5)$$

α : Albedo [-], $S\downarrow$: Incoming shortwave radiation [J s^{-1} m^{-2}],

$L\downarrow$: Incoming long-wave radiation [J s^{-1} m^{-2}],

c_P : Specific heat of air at constant pressure [J kg^{-1} K^{-1}], ρ_a : Air density [kg m^{-3}],

C_H : Bulk transfer coefficient [-],

U : Near-surface wind speed [m s^{-1}], l : Latent heat of vaporization [J kg^{-1}],

E : Rate of evaporation [kg s^{-1} m^{-2}], β : Evaporation efficiency [-],

q_{sSat} : Saturation-specific humidity [kg^{-}], q_a : Near-surface specific humidity [kg kg^{-1}]

The heat storage amount G is expressed using a force restore model [20]:

$$\mathrm{G} = \frac{C_g D_u}{2}\left[\frac{\partial T_s}{\partial t} + \frac{2\pi}{\tau_y}\left(T_s - T_{yM}\right)\right], D_u = \left[\frac{2k_g}{\omega}\right]^{\frac{1}{2}} \quad (2.6)$$

C_g : Volumetric heat capacity of soil [J m-3 K-1], D_u : Considered depth [m], τ_y : Period [s],

T_{yM} : Average soil temperature [K], k_g : Thermal diffusivity of the soil [m^2 s-1], ω : Angular frequency [s-1]

Saturated soil's specific humidity q_{sSat}:

The saturation vapor pressure e_{sSat} is calculated using Tetens' formula (2.7) to estimate the saturated specific humidity of the soil q_{sSat} as:

$$e_{sSat} = 6.1078 \times 10^{\frac{a_{Sat}(T_s - 273.15)}{(b_{Sat} + T_s - 273.15)}} \quad (2.7)$$

$$q_{sSat} = \frac{0.622\left(\frac{e_{sSat}}{p_a}\right)}{1 - 0.378\left(\frac{e_{sSat}}{p_a}\right)} \quad (2.8)$$

e_{sSat} : Saturation vapor pressure [hPa], p_a : Ground atmospheric pressure [hPa], a_{sat} : Tetens' constant [-], b_{sat} : Tetens' constant [K]

Air density ρ_a:

Air density distribution is expressed over the soil considering the water vapor pressure of it (e_a) as:

$$\rho_a = 1.293 \times \frac{273.15}{T_a} \times \frac{P_a}{1013.25}\left(1 - 0.378\frac{e_a}{P_a}\right) \quad (2.9)$$

e_a : water vapor pressure in the soil [hPa]

Specific soil's humidity q_a:

$$q_a \equiv \frac{0.622\left(\frac{e_a}{p_a}\right)}{1-0.378\left(\frac{e_a}{p_a}\right)} \quad 2.10)$$

Long-wave radiation flux$L\downarrow$:

$$L\downarrow = (0.74 + 0.19\log_{10}\omega_{TOP} + 0.07(\log_{10}\omega_{TOP})^2)\sigma T_a^4$$

$$\log_{10}\omega_{TOP} = 0.0315(T_{dew} - 273.15) - 0.1836 \text{ [21]}$$

$$T_{dew} = \frac{b_{Sat}\log_{10}\left(\frac{e_s}{6.1078}\right)}{a_{Sat} - \log_{10}\left(\frac{e_s}{6.1078}\right)} + 273.15 \quad 2.11)$$

ω_{top} : Effective amount of water vapor [m]、T_{dew} : Dew point temperature [K]

Snow-fall and snow-melting processes

When the air temperature (T_a) is lower than the defined snow-fall temperature T_c(2.12), the precipitation is considered snow. The equivalent water input w_{eqn} and the snow temperature T_{sn} are calculated using the air temperature (2.13)

$$T_c = (11.01 - 1.5e_a) + 273.15 \quad 2.12)$$

$$w_{eqn} = \rho_w r_s - w_{cn} \quad 2.13)$$

$$w_{cn} = \begin{cases} 0.05\rho_w r_s & \text{if } T_a \geq 273.15 \\ 0 & \text{otherwise} \end{cases}, T_{sn} = \begin{cases} 273.15 & \text{if } T_a \geq 273.15 \\ T_a & \text{otherwise} \end{cases} \quad 2.14)$$

T_c : Boundary temperature between rain and snow [K], w_{eqn} : Equivalent water as snow [kg m^{-2}],

ρ_w : Water density [kg m^{-3}], r_s : Precipitation volume [m],

w_{cn} : Water content in fresh snow [kg m^{-2}], T_{sn} : temperature of fresh snow [K]

The equivalent water expressed as fresh snow w_{eq}, the effective snow water content w_c, the snow surface temperature T_s and the snow height H_{ss}, are expressed for the equations (2.15) to (2.18) as follows:

$$\widetilde{w}_{eq} = w_{eq} + w_{eqn} \quad (2.15)$$

$$\widetilde{w}_c = w_c + w_{cn} \quad (2.16)$$

$$\tilde{T}_s = \frac{w_{eq}}{\widetilde{w}_{eq}} T_s + \frac{w_{eqn}}{\widetilde{w}_{eq}} T_{sn} + 273.15 \quad (2.17)$$

$$H_{ss} = \frac{w_{eq}}{\rho_n} \quad (2.18)$$

w_{eq} : *Equivalent amount of water in the snow layer [kg m-2],*

w_c : *Moisture content of the snow layer [kg m-2],*

H_{ss} : *Snow height [m]*

ρ_n : *Snow density [kg m-3],* $\sim$: *Superscript to indicate updated values*

The snow-melting heat Q_m it is calculated with the heat balance shown in equation (2.19):

$$Q_m = R\downarrow - \sigma {T_s}^4 - H - lE + Q_r,\ Q_r = c_w(T_a - T_s)\rho_w R_s \quad (2.19)$$

Q_m : Snow-melting heat [J s^{-1} m^{-2}], Q_r : Rain heat [J s^{-1} m^{-2}], R_s : Precipitation intensity [m s^{-1}],

c_w : Water's specific heat [J kg^{-1} K^{-1}]

Five different processes express snow accumulation/melting phenomena: (a) consolidation, (b) temperature rising, (c) snow-melting, (d) re-freezing, and (e) cooling. The following equations are the ones used to model all of them.

Consolidation Process

$$\widetilde{\rho_n} = \rho_n + \frac{w_{eq}}{\eta}\rho_n \Delta t \quad (2.20)$$

$$\eta = 3.44 \times 10^6 A_t exp\big(0.0253\rho_n - 0.0985(T_s - 273.15)\big) \quad (2.21)$$

$$A_t = \begin{cases} 10^{-(0.179(T_a - 273.15)+2.15)} + 0.0015 & \text{if } T_a \geq 261.25 \\ 1.0 & \text{otherwise} \end{cases} \quad (2.22)$$

η：Compressive viscosity coefficient [kg s m^{-2}]、Δt：Time step [s]

Temperature rising

$$Q_h = |T_s - 273.15| c_s w_{eq} \text{ if } Q_m \geq 0, \qquad T_s < 273.15 \quad (2.23)$$

$$\tilde{T}_s = \begin{cases} T_s + \dfrac{Q_m}{c_s w_{eq}} & \text{if } Q_m \leq Q_h \\ T_s + \dfrac{Q_h}{c_s w_{eq}} & \text{otherwise} \end{cases} \quad (2.24)$$

Q_h： Heat needed to keep snow temperature at 0°C (273.15 K) [J m^{-2}],

c_s：Ice's specific heat[J kg^{-1} K^{-1}]

When $Q_m > Q_h$ the heat balance change sign and $(Q_m - Q_h)$ becomes a snow-melting process

Snow-melting

$$H_t = \frac{Q_m - Q_h}{l_F}, \qquad l_F = 3.34 \times 10^5 + 2500.0 \times (T_s - 273.15)$$
$$\text{if } Q_m \geq Q_h, \qquad T_s = 273.15 \quad (2.25)$$

H_t： Amount of snow melted per unit area [kg m^{-2}], l_F： Ice's melting latent heat [J kg^{-1}]

The water content w_c and the equivalent water content w_{eq} change depending on the amount of snow melted as it is expressed in equations (2.26) and (2.27):

$$\begin{cases} \widetilde{w_c} = w_c + w_{eq} & \text{if } H_t \geq w_{eq} \\ \widetilde{w_c} = w_c + H_t & \text{otherwise} \end{cases} \quad (2.26)$$

$$\begin{cases} \widetilde{w_{eq}} = 0 & \text{if } H_t \geq w_{eq} \\ \widetilde{w_{eq}} = w_{eq} - H_t & \text{otherwise} \end{cases} \quad (2.27)$$

During the snow-melting process, the water excess that cannot be retained in the snow layer w_{cm} is percolated to the soil as:

$$P_r = w_c - w_{cm} \text{ when } w_c \geq w_{cm} \quad (2.28)$$

$$w_{cm} = w_{hc} w_{eq} \quad (2.29)$$

$$w_{hc} = \begin{cases} 0.111 \times 0.131\rho_n & \text{if } \rho_n > 0.4 \\ 0.025 \times 0.040\rho_n & \text{otherwise} \end{cases} \quad (2.30)$$

$$\widetilde{w} = w_c - P_r \quad (2.31)$$

w_{cm} : Possible amount of water that can be retained [kg m^{-2}], P_r: : Percolation amount [kg m^{-2}],

w_{hc} : Possible water retention rate [-]

Re-freezing

When the amount of snow-melting heat Q_m becomes negative, the amount of snow melted per unit area H_t also becomes negative. If additionally there is water presence in the snow layer (w_c), the amount of re-freezing snow can be calculated as:

$$H_t = \frac{Q_m}{l_F} \quad \text{if } Q_m < 0, \quad w_c > 0 \quad (2.32)$$

$$\begin{cases} \widetilde{w_c} = 0 & \text{if } H_t \geq w_c \\ \widetilde{w_c} = w_c + H_t & \text{otherwise} \end{cases} \quad (2.33)$$

$$\begin{cases} \widetilde{w_{eq}} = w_{eq} + w_c & \text{if } H_t \geq w_c \\ \widetilde{w_{eq}} = w_{eq} - H_t & \text{otherwise} \end{cases} \quad (2.34)$$

Cooling

In the same way, the re-freezing process occurs when the snow-melting heat Q_m becomes negative, but there is no presence of water in the snow layer ($w_c = 0$), there is a decrement in the temperature of the snow layer $\tilde{T}_s$ as:

$$\tilde{T}_s = T_s + \frac{Q_m}{c_s w_{eq}} \quad \text{if } Q_m - l_F H_t \leq 0, \quad w_c = 0 \quad (2.35)$$

A.1.2. Canopy interception for forest

When precipitation events occur in a forest area, a portion of the water reaches the soil directly, while trees' foliage retains another one and redistributes it to the different parts of the tree, or it re-evaporates to the atmosphere. Depending on the tree species of a forest, the type of phenomena that occurs in more significant extension to the water "retained" by canopy interception.

In this study, tree species are determined to the whole grid, and it is considered only one equivalent species (the dominant one) on each constituent square of the grid. The parameters a_I , b_I on the right side of the equation (2.36), used to estimate canopy interception P_I, are estimated depending on the dominant species and the presence or absence of foliage [22]. The model also assumes that all the amount of precipitation that exceeds canopy interception reaches the soil and infiltrates.

$$P_I = a_I \rho_w r_s + b_I \quad (2.36)$$

P_I : Canopy interception [kg m^{-2}], a_I, b_I : Breakage evaporation parameter [-]

A.1.3. Flow analysis model

For the soil layers considered in this model and the four different types of land usage considered in layer A (**Error! Reference source not found.**), the Kinematic Wave Model is u

sed on three of them (farming, urban, and mountain forest) to describe water flow in and between layers. Paddy soils are defined using a double tank model.

For the Kinematic Wave Model, the depth of layer A, the amount of intermediate runoff between different land-use types, and the water penetration in layer B are estimated using the amount of water entering the system. Paddy's double tank model estimates water exchange using paddy ridge paths' overflow and their lateral infiltration. The Linear Storage Method for groundwater is applied for layers B to D. However, when any of these layers reaches saturation, the water returns to the upper layers as an overflow flux (backflow shown in red in Fig.15. Evapotranspiration flux is calculated based on the amount of water entering the system on layer A, and any other shortfall in the total amount of water entering the system is considered in the layer B.

Kinematic Wave Model

$$\frac{\partial h_{al}}{\partial t} + \frac{\partial q_{al}}{\partial x} = r + u_b - q_v \quad (2.37)$$

$$q_{al} = \begin{Bmatrix} \alpha(h_{al} - d_a)^{\frac{5}{3}} + a h_{al} \\ a h_{al} \end{Bmatrix} \text{ when } h_{al} \begin{Bmatrix} \geq d_a \\ < d_a \end{Bmatrix} \quad (2.38)$$

$$d_a = \lambda_a D_a \quad (2.39)$$

$$\alpha = \frac{\sqrt{\sin\theta}}{n} \quad (2.40)$$

$$k_{heff} = \frac{k_h \sin\theta}{\lambda_a} \quad (2.41)$$

$$q_v = k_{va} h_{al} \quad (2.42)$$

h : Water depth [m], q : Outflow rate per unit width [$m^2\ s^{-1}$], r : Rain rate [$m\ s^{-1}$],

q_v : Penetration's speed into the lower layer [$m\ s^{-1}$]

θ：Slope angle[-], n：Equivalent slope's roughness[$m^{-1/3}$ s],

k_{va}： Vertical hydraulic conductivity [m s^{-1}]

k_{ha}：Horizontal hydraulic conductivity [m s^{-1}], λ：Porosity [-], D：Layer thickness [m],

d：Water storage's saturation height [m]

a：A subscript for layers, k_{heff}： Effective horizontal hydraulic conductivity [m s^{-1}]

l：Subscript depending on land usage (paddy, mountain forest, urban, and farming)

Paddy Double Tank Model

In this model, besides the tank structure, water from the river channel is provided as an input to maintain the paddy field's necessary depth.

$$\frac{\partial h_{ap}}{\partial t} = r + p_{qs} - q_{ap} \quad (2.43)$$

$$q_{ap} = \sum_j a_{pj} \max\left(h_{ap} - Z_{apj}, 0\right) \quad (2.44)$$

p：Subscript for paddy field, q_{ap}： Paddy water's outflow [m s^{-1}],

p_{qs}: Required supply inflow [m s^{-1}]

a_p： Constant outflow from the paddy [s^{-1}], Z_{ap}:： Limit height for the paddy outflow [m],

j：Subscript for tank's exchange hole

Linear Storage Model

$$\frac{dh}{dt} = r - q_i \quad (2.45)$$

$$q_i = q_h + q_v + u \quad (2.46)$$

$$q_h = k_h \max(h - Z, 0) \quad (2.47)$$

$$Z = D(\lambda - \lambda_w) \quad 2.48)$$

$$q_v = k_v h \quad 2.49)$$

$$u = \begin{Bmatrix} h - d \\ 0 \end{Bmatrix} \text{ when } h \begin{Bmatrix} \geq d \\ < d \end{Bmatrix} \quad 2.50)$$

$$d = \lambda D \quad 2.51)$$

q_i : Inflow rate [m s^{-1}], u : return flow rate [m s^{-1}], λ_w : Porosity that contributes to the inflow [-], Z : Apparent layer thickness

River Channel Model

The Kinematic Wave Model is applied to represent river channel hydrodynamics, considering that the river's cross-section is triangular, as shown in **Error! Reference source not found.** A.1.

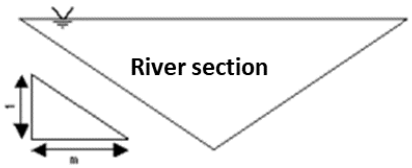

Fig. A. 1 - Scheme of the river cross-section geometry considered in the River Channel Model

$$\frac{\partial A_r}{\partial t} + \frac{\partial Q_r}{\partial x} = q_r \quad 2.52)$$

$$Q_r = \alpha_r A_r^{\frac{4}{3}} \quad 2.53)$$

$$\alpha_r = \left(\frac{\sqrt{I}}{n}\right)\left(\frac{m}{\left(2\sqrt{1+m^2}\right)^2}\right)^{\frac{1}{3}} \quad 2.54)$$

$$q_r = 2\frac{\sum_{l,l\notin p} q_{al}A_l}{\sum_{l,l\notin p} A_l} + \frac{q_{ap}A_p + (q_{hb} + q_{hc})\sum_l A_l}{bl} \quad (2.55)$$

A_r ： River channel cross-section area [m^2], Q_r:：Flow rate [m^3 s^{-1}],

q_r ： Lateral slope's inflow [m^2 s^{-1}], I ：River gradient [-]

n ：Equivalent roughness of the river channel [$m^{-1/3}$ s], m ：Slope angle of the river channel [-],

bl ：River channel length [m], A ：Watershed area[m^2]

b, c ：B, C layer's subscript

Appendix II – Supplementary materials to Chapter 3

Appendix III – Supplementary materials to Chapter 4

Table A3.1 – Monthly validation of WRF results in different AMeDAS stations of the domain for temperature, wind speed, and relative humidity

Temperature (°C)

Fukuoka								
	N	obs_ave	sim_ave	R	MBE	MAE	RMSE	IA
2010/03	744	10.8407	11.1955	0.9301	0.3548	1.157	1.5792	0.9596
2010/04	720	13.7851	14.456	0.9312	0.6709	1.2314	1.615	0.9481
2010/05	744	19.2297	20.2961	0.9081	1.0664	1.3965	1.9428	0.9261
2010/06	720	23.49	25.2251	0.8545	1.7351	1.9122	2.3202	0.8319
2010/07	744	27.6606	29.0387	0.8894	1.3781	1.5189	1.8938	0.8851
2010/08	744	30.3095	31.4481	0.866	1.1386	1.3517	1.7549	0.881
2010/09	720	26.3061	27.1081	0.9518	0.802	1.1819	1.5254	0.9629
2010/10	744	20.0118	20.5822	0.9387	0.5703	1.0866	1.3577	0.9598
2010/11	720	13.1989	13.7889	0.8954	0.59	1.1689	1.5297	0.9363
2010/12	744	8.7493	9.0553	0.9406	0.306	1.082	1.3632	0.9679
2011/01	744	3.7753	3.9477	0.8404	0.1724	0.8888	1.142	0.9134
2011/02	672	8.1749	8.4734	0.9468	0.2985	1.0151	1.3576	0.9696
all	8760	17.1786	17.9372	0.9884	0.7586	1.2498	1.6448	0.9918
Hiroshima								
	N	obs_ave	sim_ave	R	MBE	MAE	RMSE	IA
2010/03	744	9.0634	9.0106	0.9046	-0.0529	1.2827	1.6561	0.9501
2010/04	720	13.0058	13.0793	0.9329	0.0735	1.111	1.4062	0.9652
2010/05	744	18.47	18.542	0.9132	0.072	1.2438	1.5439	0.9546
2010/06	720	23.3139	23.5128	0.8841	0.1989	1.1214	1.3987	0.9367
2010/07	744	27.2352	26.8445	0.8489	-0.3907	1.2106	1.479	0.9119
2010/08	744	30.3329	29.1122	0.9146	-1.2207	1.3922	1.6018	0.9014
2010/09	720	26.1672	25.4344	0.9617	-0.7328	1.1717	1.4101	0.9687
2010/10	744	19.2515	19.2382	0.9478	-0.0133	0.9804	1.26	0.9731
2010/11	720	11.9494	11.9816	0.9156	0.0321	1.1961	1.4732	0.9541
2010/12	744	7.3008	7.1945	0.9199	-0.1063	1.3194	1.6385	0.9579
2011/01	744	2.8687	2.2801	0.9099	-0.5885	1.133	1.4012	0.9325
2011/02	672	6.6167	6.4204	0.9386	-0.1963	1.1522	1.4301	0.9679
all	8760	16.3522	16.1066	0.988	-0.2456	1.1937	1.4801	0.9937
Kagoshima								
	N	obs_ave	sim_ave	R	MBE	MAE	RMSE	IA
2010/03	744	9.9921	9.852	0.9339	-0.1401	1.1793	1.4901	0.963
2010/04	720	13.4388	13.4935	0.9354	0.0547	1.1084	1.3984	0.9648
2010/05	744	18.691	18.3638	0.906	-0.3272	1.2865	1.6023	0.9474
2010/06	720	23.4257	23.5542	0.9086	0.1285	1.0455	1.2878	0.9484

2010/07	744	27.1165	26.7843	0.8597	-0.3322	1.079	1.3254	0.916
2010/08	744	29.4478	28.7312	0.874	-0.7166	1.0984	1.2964	0.9053
2010/09	720	26.2022	25.6661	0.9529	-0.5361	1.2148	1.4346	0.9605
2010/10	744	19.6843	20.3608	0.9137	0.6765	1.2147	1.5726	0.9455
2010/11	720	13.0482	13.1609	0.8721	0.1127	1.2825	1.6089	0.9296
2010/12	744	9.0574	8.9053	0.8947	-0.1521	1.4878	1.8427	0.9439
2011/01	744	4.2582	3.8152	0.8279	-0.443	1.1502	1.3921	0.8953
2011/02	672	7.1874	7.232	0.946	0.0446	1.0644	1.3756	0.9723
all	8760	16.8503	16.7121	0.986	-0.1382	1.1855	1.4784	0.9928

Kochi

	N	obs_ave	sim_ave	R	MBE	MAE	RMSE	IA
2010/03	744	11.4407	11.4875	0.9154	0.0467	1.3174	1.6049	0.9559
2010/04	720	14.7792	14.7544	0.9101	-0.0247	1.2365	1.5494	0.9512
2010/05	744	19.3755	19.616	0.8535	0.2404	1.4614	1.8183	0.9138
2010/06	720	23.2818	23.7735	0.9151	0.4917	1.1254	1.4	0.9345
2010/07	744	27.0065	27.1375	0.8544	0.131	0.9386	1.1905	0.9108
2010/08	744	29.0664	28.8437	0.8652	-0.2227	1.0638	1.2392	0.9016
2010/09	720	26.425	26.3749	0.9189	-0.0501	1.2105	1.4472	0.954
2010/10	744	20.6676	21.0016	0.8789	0.334	1.3692	1.6617	0.9341
2010/11	720	13.5071	14.0022	0.8978	0.4952	1.4875	1.7643	0.9356
2010/12	744	8.7152	9.0489	0.9212	0.3337	1.5575	1.8827	0.9576
2011/01	744	4.2507	3.8262	0.933	-0.4244	1.2851	1.5209	0.9463
2011/02	672	8.9092	8.6604	0.9338	-0.2489	1.4243	1.6966	0.9619
all	8760	17.33	17.4231	0.9833	0.0931	1.2889	1.5778	0.9915

Nagoya

	N	obs_ave	sim_ave	R	MBE	MAE	RMSE	IA
2010/03	744	9.084	10.402	0.9424	1.318	1.4387	1.8232	0.9386
2010/04	720	13.2939	14.4682	0.9412	1.1743	1.3988	1.7824	0.9483
2010/05	744	18.6645	20.1528	0.9692	1.4883	1.5413	1.8177	0.9533
2010/06	720	23.9228	25.8141	0.9599	1.8913	1.9157	2.1393	0.9134
2010/07	744	27.8321	29.9264	0.9492	2.0943	2.1107	2.3658	0.8932
2010/08	744	29.3614	31.3064	0.9362	1.945	1.9845	2.1891	0.859
2010/09	720	26.0636	27.8868	0.9759	1.8232	1.8465	2.0923	0.9473
2010/10	744	19.4146	21.2389	0.9546	1.8242	1.8971	2.1421	0.9211
2010/11	720	12.0426	13.2416	0.9484	1.199	1.3723	1.5957	0.9409
2010/12	744	7.8526	8.3459	0.9621	0.4933	0.9677	1.2519	0.977
2011/01	744	2.7742	2.4667	0.9196	-0.3075	0.86	1.1162	0.9551
2011/02	672	6.6037	6.7166	0.9372	0.1129	1.1841	1.5109	0.966
all	8760	16.4632	17.7244	0.9924	1.2611	1.5451	1.8589	0.9909

Nobeoka								
	N	obs_ave	sim_ave	R	MBE	MAE	RMSE	IA
2010/03	743	11.1802	11.078	0.9123	-0.1022	1.4633	1.8332	0.9544
2010/04	720	14.1997	14.5013	0.9196	0.3016	1.3277	1.6575	0.9565
2010/05	744	18.8647	19.6277	0.8637	0.7631	1.6403	2.087	0.9083
2010/06	720	22.1306	23.4752	0.8965	1.3446	1.6	1.9866	0.905
2010/07	744	26.2079	27.4129	0.8612	1.205	1.4334	1.7581	0.8714
2010/08	744	27.9157	28.3856	0.7834	0.4699	1.3795	1.7083	0.8704
2010/09	720	25.2125	25.7847	0.9127	0.5722	1.3151	1.6036	0.9477
2010/10	744	19.5001	19.7307	0.861	0.2306	1.4987	1.8355	0.9248
2010/11	720	12.7678	13.4319	0.8951	0.6641	1.6435	1.9914	0.9253
2010/12	744	8.653	8.718	0.9116	0.065	1.5638	1.9349	0.9541
2011/01	744	4.1817	3.518	0.9215	-0.6637	1.2439	1.497	0.9477
2011/02	672	8.654	8.7563	0.9047	0.1023	1.6485	1.9551	0.9482
all	8759	16.667	17.0789	0.9786	0.4119	1.4785	1.8278	0.9883
Totori								
	N	obs_ave	sim_ave	R	MBE	MAE	RMSE	IA
2010/03	744	7.9973	8.1835	0.9437	0.1862	1.1548	1.5012	0.9635
2010/04	720	11.6389	12.1506	0.93	0.5117	1.4701	1.9453	0.9435
2010/05	744	17.0681	17.982	0.9148	0.9138	1.5707	2.1341	0.9423
2010/06	720	22.1056	23.4691	0.9009	1.3636	1.8012	2.2867	0.8945
2010/07	744	26.728	27.4627	0.9156	0.7347	1.2393	1.532	0.9331
2010/08	744	29.8306	30.0057	0.838	0.175	1.3938	1.7123	0.8988
2010/09	720	24.6797	25.438	0.953	0.7583	1.4713	1.7661	0.9597
2010/10	744	17.7598	18.7874	0.9266	1.0276	1.5079	1.8573	0.9363
2010/11	720	11.1808	12.0754	0.8957	0.8946	1.6578	1.9923	0.9158
2010/12	744	7.104	7.3314	0.8972	0.2274	1.6371	1.9572	0.9453
2011/01	744	1.5379	1.4271	0.6395	-0.1108	1.3444	1.7936	0.7957
2011/02	672	5.0402	5.529	0.8851	0.4888	1.5986	2.0602	0.9351
all	8760	15.2824	15.8778	0.9828	0.5954	1.4851	1.8887	0.9904
Wakayama								
	N	obs_ave	sim_ave	R	MBE	MAE	RMSE	IA
2010/03	744	9.9921	9.852	0.9339	-0.1401	1.1793	1.4901	0.963
2010/04	720	13.4388	13.4935	0.9354	0.0547	1.1084	1.3984	0.9648
2010/05	744	18.691	18.3638	0.906	-0.3272	1.2865	1.6023	0.9474
2010/06	720	23.4257	23.5542	0.9086	0.1285	1.0455	1.2878	0.9484
2010/07	744	27.1165	26.7843	0.8597	-0.3322	1.079	1.3254	0.916
2010/08	744	29.4478	28.7312	0.874	-0.7166	1.0984	1.2964	0.9053
2010/09	720	26.2022	25.6661	0.9529	-0.5361	1.2148	1.4346	0.9605
2010/10	744	19.6843	20.3608	0.9137	0.6765	1.2147	1.5726	0.9455
2010/11	720	13.0482	13.1609	0.8721	0.1127	1.2825	1.6089	0.9296

2010/12	744	9.0574	8.9053	0.8947	-0.1521	1.4878	1.8427	0.9439
2011/01	744	4.2582	3.8152	0.8279	-0.443	1.1502	1.3921	0.8953
2011/02	672	7.1874	7.232	0.946	0.0446	1.0644	1.3756	0.9723
all	8760	16.8503	16.7121	0.986	-0.1382	1.1855	1.4784	0.9928

Wind Speed (m/s)

Fukuoka

	N	obs_ave	sim_ave	R	MBE	MAE	RMSE	IA
2010/03	744	3.5372	3.8966	0.691	0.3593	1.2247	1.5719	0.8193
2010/04	720	3.1307	3.4932	0.7519	0.3625	1.0796	1.4125	0.8571
2010/05	744	2.9976	3.1499	0.7608	0.1523	0.9962	1.2868	0.8664
2010/06	720	2.3182	2.5981	0.5356	0.2799	1.0085	1.3093	0.7275
2010/07	744	2.5168	2.6898	0.5693	0.173	1.0119	1.3219	0.7546
2010/08	744	2.8968	3.0274	0.6078	0.1306	1.1103	1.4354	0.7829
2010/09	720	2.8299	3.1812	0.698	0.3514	1.0811	1.4196	0.8249
2010/10	744	2.6901	3.0978	0.743	0.4078	1.0354	1.3156	0.8468
2010/11	720	2.5117	2.6942	0.7639	0.1825	0.8656	1.1663	0.8688
2010/12	744	3.3001	3.932	0.7695	0.6319	1.256	1.654	0.8542
2011/01	744	3.1616	4.0465	0.7968	0.885	1.2646	1.6154	0.8498
2011/02	671	2.7508	2.8448	0.8187	0.094	0.9175	1.1975	0.8993
all	8759	2.89	3.2266	0.7321	0.3366	1.0729	1.4026	0.8465

Hiroshima

	N	obs_ave	sim_ave	R	MBE	MAE	RMSE	IA
2010/03	744	3.8493	3.1181	0.5234	-0.7312	1.6309	2.0465	0.6979
2010/04	720	3.6426	2.8964	0.5229	-0.7462	1.5538	1.9535	0.6865
2010/05	744	3.4406	2.8494	0.3003	-0.5911	1.6493	2.0957	0.5807
2010/06	720	2.9443	2.3652	0.2105	-0.5791	1.3412	1.7803	0.5368
2010/07	743	2.9027	2.8174	0.5239	-0.0853	1.1192	1.4673	0.7273
2010/08	744	3.2078	2.7909	0.624	-0.4169	1.106	1.3712	0.7691
2010/09	719	3.8127	3.032	0.6266	-0.7806	1.3151	1.6475	0.7355
2010/10	744	3.9327	2.7737	0.5678	-1.159	1.5298	1.9047	0.6728
2010/11	720	3.9799	2.4662	0.3382	-1.5137	2.019	2.4715	0.5569
2010/12	744	3.7672	2.7049	0.3315	-1.0623	1.9484	2.4314	0.5829
2011/01	744	2.9824	2.5471	0.1855	-0.4353	1.5846	1.9556	0.5129
2011/02	672	3.7266	2.4838	0.5618	-1.2428	1.6238	2.0626	0.6838
all	8758	3.5132	2.7396	0.4411	-0.7735	1.5342	1.9576	0.6487

Kagoshima

	N	obs_ave	sim_ave	R	MBE	MAE	RMSE	IA
2010/03	743	3.3903	3.5056	0.7054	0.1153	1.2172	1.5358	0.8367
2010/04	720	3.3472	3.468	0.5378	0.1208	1.2451	1.5907	0.7346
2010/05	744	3.0698	3.1034	0.5555	0.0337	1.1693	1.4747	0.7467
2010/06	720	3.026	3.0925	0.4983	0.0665	1.2436	1.614	0.692

2010/07	744	2.7789	3.0595	0.6517	0.2806	1.0232	1.2688	0.7916
2010/08	744	3.3757	3.5701	0.716	0.1944	1.0344	1.317	0.8422
2010/09	720	3.0989	3.079	0.6984	-0.0199	1.067	1.3319	0.8303
2010/10	744	3.345	3.1103	0.5854	-0.2347	1.2244	1.551	0.7569
2010/11	720	3.1121	2.587	0.5044	-0.525	1.1677	1.4398	0.6954
2010/12	732	3.4148	3.1773	0.6175	-0.2375	1.3168	1.7058	0.7816
2011/01	739	3.5277	3.1158	0.6185	-0.412	1.2383	1.5657	0.7727
2011/02	671	3.1861	2.6896	0.4284	-0.4966	1.3929	1.6964	0.6486
all	8741	3.2234	3.1342	0.5986	-0.0892	1.1933	1.5122	0.7728

Kochi

	N	obs_ave	sim_ave	R	MBE	MAE	RMSE	IA
2010/03	744	1.7458	3.3087	0.3014	1.5629	1.8818	2.7716	0.4118
2010/04	720	1.7992	3.1324	0.4135	1.3333	1.6177	2.3522	0.4827
2010/05	744	1.745	2.5454	0.442	0.8004	1.1804	1.6575	0.5374
2010/06	720	1.6276	2.2762	0.3937	0.6486	1.0538	1.4744	0.5505
2010/07	744	1.5313	2.2509	0.3878	0.7196	1.0451	1.5047	0.5039
2010/08	744	1.7329	2.3519	0.4501	0.619	0.9693	1.2617	0.5982
2010/09	720	1.7706	2.5868	0.3918	0.8163	1.3256	1.9835	0.4754
2010/10	744	1.603	3.0069	0.3502	1.4039	1.704	2.381	0.3986
2010/11	720	1.7121	2.5043	0.3414	0.7922	1.2273	1.7504	0.4738
2010/12	743	1.7734	2.722	0.3964	0.9487	1.3304	1.9844	0.5108
2011/01	744	1.7337	2.6592	0.5122	0.9254	1.2777	1.667	0.6174
2011/02	672	1.6071	2.7419	0.4109	1.1347	1.3687	1.848	0.5018
all	8759	1.6989	2.6739	0.388	0.975	1.3318	1.9328	0.4929

Nagoya

	N	obs_ave	sim_ave	R	MBE	MAE	RMSE	IA
2010/03	743	3.2637	3.4462	0.7512	0.1825	1.0949	1.4318	0.8607
2010/04	720	3.4068	3.5777	0.7673	0.1709	1.0217	1.3428	0.8727
2010/05	744	3.4784	3.6268	0.7988	0.1485	0.9406	1.2326	0.8911
2010/06	720	2.5772	2.7291	0.6691	0.1519	0.8843	1.1336	0.8139
2010/07	744	2.704	2.9769	0.6575	0.2729	0.9138	1.184	0.8025
2010/08	744	2.7034	2.7451	0.6531	0.0417	0.8153	1.0985	0.8094
2010/09	720	2.726	2.8959	0.6992	0.1699	0.8682	1.1065	0.8291
2010/10	744	2.387	2.6603	0.697	0.2733	0.9311	1.1863	0.8242
2010/11	720	2.5987	2.7954	0.7668	0.1967	0.9002	1.1707	0.8712
2010/12	744	2.9187	3.2437	0.7016	0.325	1.1691	1.5519	0.8265
2011/01	744	3.1694	3.4788	0.6558	0.3095	1.1112	1.462	0.8015
2011/02	672	2.9153	2.7707	0.8222	-0.1446	0.8877	1.1479	0.9035
all	8759	2.9047	3.0822	0.7383	0.1775	0.9626	1.2643	0.8551

Nobeoka								
	N	obs_ave	sim_ave	R	MBE	MAE	RMSE	IA
2010/03	742	3.0655	3.728	0.4828	0.6625	1.7965	2.4113	0.6825
2010/04	720	2.7399	3.2265	0.4768	0.4866	1.5487	2.0328	0.6843
2010/05	744	2.3031	2.9369	0.425	0.6338	1.2374	1.6669	0.6505
2010/06	720	1.8507	2.6761	0.3954	0.8254	1.353	1.738	0.6047
2010/07	744	1.6634	2.56	0.2051	0.8966	1.3276	1.74	0.4778
2010/08	744	2.3656	2.9792	0.5058	0.6136	1.1048	1.4368	0.6895
2010/09	720	2.331	3.0192	0.6115	0.6883	1.2203	1.6639	0.7369
2010/10	744	2.7371	3.4616	0.6602	0.7245	1.4228	1.8569	0.7935
2010/11	720	2.7144	2.5688	0.3058	-0.1457	1.3782	1.877	0.5857
2010/12	744	3.4449	2.661	0.2991	-0.7839	1.7642	2.3946	0.56
2011/01	744	3.5163	2.8056	0.5135	-0.7106	1.6276	2.1909	0.6703
2011/02	672	2.7967	3.1399	0.5789	0.3431	1.292	1.6638	0.7558
all	8758	2.6283	2.9799	0.4539	0.3516	1.4243	1.9149	0.6772
Totori								
	N	obs_ave	sim_ave	R	MBE	MAE	RMSE	IA
2010/03	742	3.6704	4.5191	0.7079	0.8487	1.5521	1.9922	0.8146
2010/04	720	3.2003	3.9325	0.649	0.7322	1.3391	1.767	0.776
2010/05	744	3.234	3.5923	0.6475	0.3583	1.2429	1.6	0.7945
2010/06	719	2.4922	2.2573	0.3796	-0.2349	1.1229	1.4137	0.6256
2010/07	744	2.6758	2.5773	0.538	-0.0985	1.0933	1.4013	0.7357
2010/08	744	3.246	3.2163	0.6489	-0.0297	1.0753	1.3825	0.8
2010/09	719	2.8243	3.1676	0.6188	0.3432	1.1267	1.4717	0.7733
2010/10	744	2.3755	2.9895	0.6092	0.6139	1.2193	1.6298	0.7435
2010/11	719	2.9229	3.4769	0.5649	0.5539	1.2775	1.7033	0.7327
2010/12	744	3.4739	4.1475	0.5758	0.6736	1.4823	1.9204	0.7413
2011/01	744	2.8741	3.7583	0.5138	0.8843	1.5226	1.9977	0.6794
2011/02	672	2.7808	3.4497	0.6045	0.6689	1.2701	1.6721	0.7428
all	8755	2.9837	3.4257	0.6172	0.442	1.2777	1.6772	0.7714
Wakayama								
	N	obs_ave	sim_ave	R	MBE	MAE	RMSE	IA
2010/03	744	4.4499	4.8283	0.7215	0.3784	1.4471	1.8335	0.842
2010/04	720	3.8989	4.0614	0.6483	0.1626	1.3654	1.7868	0.7972
2010/05	744	3.9958	3.9678	0.6557	-0.028	1.276	1.7088	0.8048
2010/06	720	3.5344	3.3673	0.6798	-0.1671	1.2473	1.6835	0.8185
2010/07	744	3.8728	4.0833	0.7233	0.2104	1.433	1.8399	0.8382
2010/08	744	3.7638	3.6748	0.6936	-0.0891	1.2448	1.5687	0.8234
2010/09	720	3.5947	3.4202	0.6207	-0.1745	1.329	1.6296	0.7794
2010/10	744	3.1617	3.3751	0.5746	0.2134	1.1505	1.4636	0.7587
2010/11	720	3.5453	3.3863	0.5397	-0.1589	1.3725	1.7219	0.7406

2010/12	744	4.6579	4.8997	0.6947	0.2418	1.5326	1.9511	0.8286
2011/01	744	4.5517	5.0916	0.7091	0.5398	1.3639	1.7477	0.828
2011/02	672	3.6668	3.7127	0.6105	0.0459	1.3055	1.62	0.7823
all	8760	3.8957	3.996	0.6808	0.1003	1.3394	1.7185	0.822

Realtive Humidity (%)

Fukuoka

	N	obs_ave	sim_ave	R	MBE	MAE	RMSE	IA
2010/03	744	5.2744	5.1721	0.9521	-0.1023	0.4685	0.6383	0.975
2010/04	720	6.144	6.0729	0.9502	-0.0711	0.5717	0.7614	0.9723
2010/05	744	8.9012	8.4724	0.8992	-0.4288	0.8653	1.2036	0.9378
2010/06	720	13.3451	12.9555	0.9172	-0.3896	0.991	1.3719	0.9433
2010/07	744	16.9123	16.7089	0.6095	-0.2034	0.9644	1.2331	0.7473
2010/08	744	17.699	17.2972	0.6838	-0.4018	1.1929	1.6024	0.8038
2010/09	720	14.4601	13.9724	0.9117	-0.4878	1.0113	1.4851	0.9476
2010/10	744	9.5416	9.3118	0.9127	-0.2299	0.7921	1.0494	0.9525
2010/11	720	5.5896	5.5749	0.8887	-0.0147	0.4801	0.6036	0.9417
2010/12	744	4.5972	4.5553	0.9577	-0.042	0.4159	0.513	0.9775
2011/01	744	2.9164	2.9917	0.8453	0.0753	0.3288	0.4206	0.9013
2011/02	672	4.4124	4.304	0.9213	-0.1084	0.4132	0.5747	0.9575
all	8760	9.1803	8.9796	0.982	-0.2007	0.7097	1.0367	0.9906

Hiroshima

	N	obs_ave	sim_ave	R	MBE	MAE	RMSE	IA
2010/03	744	4.5805	4.7353	0.8845	0.1548	0.5934	0.8909	0.9321
2010/04	720	5.7161	5.7554	0.9289	0.0393	0.6623	0.8868	0.9629
2010/05	744	7.7473	7.9221	0.8834	0.1748	0.8997	1.2913	0.9373
2010/06	720	12.3129	12.5249	0.9433	0.212	0.9574	1.1879	0.9642
2010/07	744	16.2432	16.7318	0.72	0.4887	0.9478	1.1423	0.7919
2010/08	744	16.7945	17.5397	0.7118	0.7451	1.0502	1.2381	0.7718
2010/09	720	13.4219	13.5381	0.9406	0.1163	0.9754	1.2512	0.9658
2010/10	744	8.9617	8.7019	0.9025	-0.2598	0.7735	1.0407	0.9466
2010/11	720	5.3533	5.2249	0.8646	-0.1284	0.5733	0.7663	0.9241
2010/12	744	4.2468	4.2361	0.9198	-0.0108	0.4613	0.5964	0.9583
2011/01	744	2.8421	2.7748	0.7447	-0.0673	0.3009	0.3912	0.8541
2011/02	672	3.7847	3.9622	0.9167	0.1775	0.4088	0.5726	0.9396
all	8760	8.5315	8.6689	0.9843	0.1374	0.7187	0.9838	0.9913

Kagoshima

	N	obs_ave	sim_ave	R	MBE	MAE	RMSE	IA
2010/03	744	6.8565	6.4862	0.951	-0.3702	0.7347	0.9692	0.9699
2010/04	720	7.9552	7.4484	0.963	-0.5067	0.7599	0.9756	0.9729
2010/05	744	10.6956	9.9315	0.88	-0.7641	1.1138	1.5829	0.918
2010/06	719	14.6765	14.6151	0.9477	-0.0614	0.8073	1.0519	0.973

2010/07	744	18.4681	17.924	0.7324	-0.5441	0.8886	1.1895	0.8167
2010/08	744	19.1944	18.5132	0.6515	-0.6813	1.0191	1.3148	0.7568
2010/09	720	16.8315	15.5368	0.9154	-1.2947	1.4429	1.9021	0.9067
2010/10	744	11.2317	10.3923	0.9342	-0.8394	1.0913	1.393	0.9475
2010/11	720	6.9747	6.2596	0.8879	-0.7152	0.9089	1.1561	0.9093
2010/12	744	5.7888	5.1701	0.9477	-0.6188	0.7557	0.9417	0.9539
2011/01	743	3.3228	2.8735	0.7762	-0.4493	0.5018	0.6507	0.7971
2011/02	672	5.5984	5.056	0.9324	-0.5424	0.6992	0.9169	0.9476
all	8758	10.6639	10.0479	0.9833	-0.616	0.8943	1.2152	0.9887

Kochi

	N	obs_ave	sim_ave	R	MBE	MAE	RMSE	IA
2010/03	744	5.8645	5.3967	0.9043	-0.4678	0.912	1.2046	0.942
2010/04	720	7.2923	6.4436	0.9234	-0.8488	1.115	1.4178	0.9399
2010/05	744	9.7174	8.7925	0.9105	-0.9249	1.2128	1.6292	0.9336
2010/06	720	14.5781	13.5853	0.9533	-0.9928	1.2049	1.4613	0.9556
2010/07	744	18.5064	17.4447	0.7275	-1.0617	1.2302	1.5395	0.7483
2010/08	744	19.496	18.4669	0.7121	-1.0291	1.2152	1.4898	0.7459
2010/09	720	15.844	14.3512	0.9339	-1.4928	1.6101	1.9929	0.9265
2010/10	744	10.7371	9.4673	0.8939	-1.2698	1.4617	1.8337	0.9001
2010/11	720	6.3883	5.3776	0.8599	-1.0107	1.1299	1.4222	0.8392
2010/12	744	4.7063	4.3467	0.9073	-0.3596	0.668	0.924	0.9402
2011/01	744	2.6221	2.5342	0.7883	-0.0879	0.2998	0.3982	0.8735
2011/02	672	4.4786	4.1669	0.9083	-0.3117	0.6448	0.8372	0.9451
all	8760	10.0538	9.231	0.9823	-0.8227	1.0598	1.4132	0.9858

Nagoya

	N	obs_ave	sim_ave	R	MBE	MAE	RMSE	IA
2010/03	744	4.4463	4.5166	0.9264	0.0703	0.5252	0.7574	0.9555
2010/04	720	5.5798	5.3921	0.94	-0.1877	0.5606	0.7832	0.967
2010/05	744	7.7594	7.3079	0.9257	-0.4514	0.7935	1.0211	0.953
2010/06	720	12.3655	12.2317	0.9437	-0.1338	0.9005	1.1784	0.9685
2010/07	744	15.9381	15.5878	0.6858	-0.3503	1.1206	1.4117	0.7965
2010/08	744	17.0994	16.8185	0.6456	-0.2809	1.0092	1.2768	0.7801
2010/09	695	13.5338	13.1863	0.9149	-0.3476	0.9605	1.2512	0.9512
2010/10	744	10.0538	8.8109	0.8967	-1.2429	1.3003	1.5931	0.8762
2010/11	720	5.5966	4.8815	0.9011	-0.7152	0.7719	0.9517	0.8902
2010/12	744	4.4493	4.0648	0.931	-0.3845	0.5259	0.667	0.9479
2011/01	744	3.0627	2.6618	0.6806	-0.4009	0.4952	0.6127	0.7356
2011/02	672	3.7679	3.5338	0.9443	-0.234	0.4597	0.5693	0.9648
all	8735	8.6569	8.2668	0.9821	-0.3901	0.7873	1.059	0.9895

Nobeoka								
	N	obs_ave	sim_ave	R	MBE	MAE	RMSE	IA
2010/03	743	5.9112	5.6263	0.9467	-0.2849	0.6681	0.8665	0.9684
2010/04	720	7.4669	6.8903	0.9588	-0.5766	0.833	1.0276	0.9682
2010/05	744	9.907	8.9575	0.9258	-0.9494	1.1964	1.5217	0.9373
2010/06	720	14.737	13.5856	0.9166	-1.1513	1.3601	1.6737	0.9218
2010/07	744	18.6586	17.129	0.5231	-1.5296	1.6594	2.001	0.583
2010/08	744	19.783	17.9471	0.6341	-1.8359	1.8774	2.2131	0.595
2010/09	720	16.3714	14.555	0.9344	-1.8163	1.8454	2.1993	0.8982
2010/10	744	10.9551	9.9956	0.911	-0.9595	1.2529	1.5647	0.928
2010/11	720	6.5495	5.9134	0.9166	-0.6361	0.8092	1.0156	0.9311
2010/12	744	4.9393	4.6277	0.9505	-0.3116	0.5537	0.7171	0.9685
2011/01	744	2.7301	2.5804	0.8136	-0.1497	0.3114	0.4206	0.8875
2011/02	672	4.8353	4.5383	0.9273	-0.297	0.6107	0.7869	0.9553
all	8759	10.2705	9.3927	0.9835	-0.8778	1.084	1.4595	0.9843
Totori								
	N	obs_ave	sim_ave	R	MBE	MAE	RMSE	IA
2010/03	743	4.6247	4.6401	0.9244	0.0154	0.4626	0.6002	0.9583
2010/04	720	5.5081	5.4894	0.9382	-0.0187	0.5317	0.6873	0.9675
2010/05	744	8.0541	7.9154	0.9071	-0.1387	0.7126	0.9816	0.9503
2010/06	720	12.2979	12.163	0.9338	-0.1349	0.9255	1.2007	0.9626
2010/07	744	16.1616	16.2361	0.7331	0.0745	0.8242	1.0312	0.841
2010/08	744	17.4807	17.55	0.7486	0.0693	0.8835	1.1704	0.8595
2010/09	717	14.4585	13.6619	0.9222	-0.7966	1.1735	1.4757	0.9444
2010/10	697	10.055	9.4721	0.8954	-0.5829	0.8958	1.1413	0.9278
2010/11	720	5.8707	5.3995	0.8412	-0.4712	0.6866	0.8686	0.885
2010/12	744	4.5154	4.5011	0.9021	-0.0143	0.4941	0.6353	0.9478
2011/01	744	3.4205	3.3443	0.641	-0.0762	0.3337	0.4265	0.7957
2011/02	672	3.9888	4.0012	0.8739	0.0124	0.471	0.6022	0.9249
all	8709	8.8949	8.726	0.984	-0.1689	0.6988	0.9503	0.9917
Wakayama								
	N	obs_ave	sim_ave	R	MBE	MAE	RMSE	IA
2010/03	744	4.7932	5.2347	0.9352	0.4415	0.6175	0.8636	0.9547
2010/04	720	5.6975	6.0071	0.9548	0.3096	0.5843	0.7531	0.9719
2010/05	744	8.7525	8.7011	0.9208	-0.0514	0.8119	1.0721	0.9587
2010/06	720	13.0965	13.07	0.9478	-0.0264	0.9756	1.2409	0.9645
2010/07	744	16.5179	17.0903	0.6947	0.5724	1.0054	1.2198	0.7925
2010/08	744	17.4943	18.1982	0.5997	0.7039	1.2019	1.433	0.7306
2010/09	720	13.826	14.4631	0.9361	0.6371	1.1638	1.4068	0.9558
2010/10	744	9.6269	9.7921	0.9277	0.1652	0.6555	0.8707	0.9603
2010/11	720	5.7547	5.8457	0.8165	0.091	0.6735	0.8897	0.9012

2010/12	744	4.3911	4.8626	0.9167	0.4715	0.6583	0.8657	0.9354
2011/01	744	2.7575	3.2131	0.793	0.4556	0.4965	0.5655	0.7496
2011/02	672	3.7834	4.2097	0.9289	0.4263	0.5469	0.7421	0.9416
all	8760	8.9082	9.2584	0.9845	0.3501	0.7838	1.0296	0.991

N : Number of observations

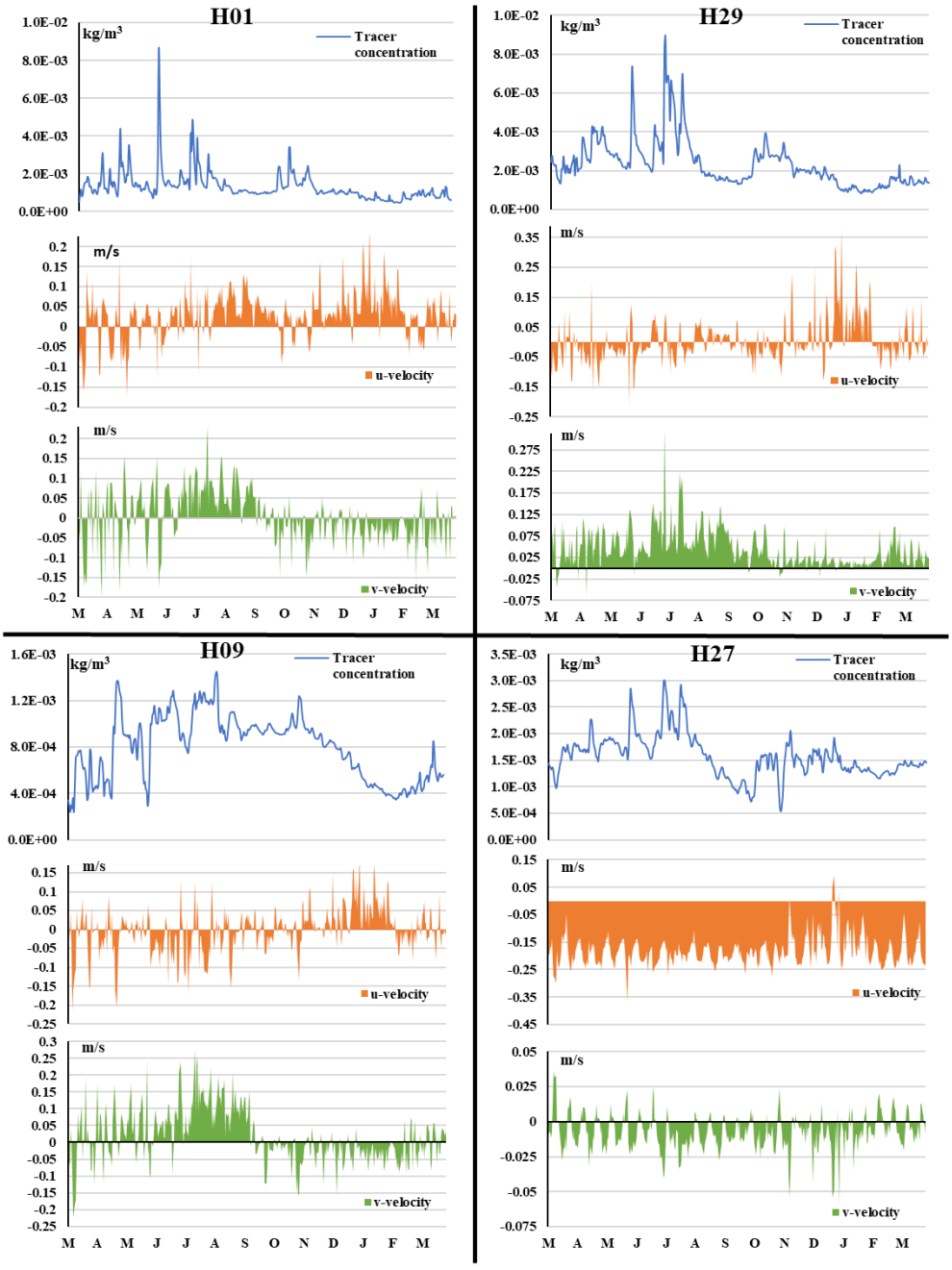

Fig. A3. 1 - Daily variations in concentration, u-velocity, and v-velocity in the surface layer for points H01, H09, H29, and H27 between March 2010 and February 2011